AN INVESTIGATION ON PRESSURE DROP FOR GAS-SOLIDS FLOW THROUGH BENDS

A thesis submitted in fulfilment

of the requirement for the award of the degree of

DOCTOR OF PHILOSOPHY

Submitted by

ATUL SHARMA

Registration No.: 951308001

THAPAR INSTITUTE
OF ENGINEERING & TECHNOLOGY
(Deemed to be University)

MECHANICAL ENGINEERING DEPARTMENT

THAPAR INSTITUTE OF ENGINEERING AND TECHNOLOGY, PATIALA-147004,

PUNJAB, INDIA

January 2020

This thesis is dedicated to my parents and wife for their love, support, and patience.

THESIS CERTIFICATION

I, Atul Sharma, declare that the work presented in this thesis report entitled, **"AN INVESTIGATION ON PRESSURE DROP FOR GAS-SOLIDS FLOW THROUGH BENDS"** submitted in fulfilment of requirement for the award of degree of Doctor of Philosophy in Mechanical Engineering Department, Thapar Institute of Engineering and Technology, Patiala, is an authentic record of my work carried out under the supervision of Dr S.S. Mallick (Associate Professor, Mechanical Engineering Department, Thapar Institute of Engineering and Technology, Patiala) from July 2013 to January 2020. The matter presented in this thesis has not been submitted either in part or full to any other University or Institute for the award of any other degree.

Atul Sharma Date: January 13, 2020

Registration No.: 951308001

It is certified that the above statement made by the student is correct to the best of my knowledge and belief.

Dr S.S. Mallick, PhD Supervisor Date: January 13, 2020

Associate Professor

Mechanical Engineering Department, Thapar Institute of Engineering and Technology, Patiala

ACKNOWLEDGEMENTS

At this moment of accomplishment, I am greatly indebted to my research guide, Dr S.S. Mallick, who accepted me as his PhD student and offered me his mentorship, professional guidance, and endless support. This work would not have been possible without his guidance and involvement, his support and encouragement daily from the start of my work to date. Under his guidance, I successfully overcame many difficulties and learnt a lot. His zeal for perfection, passion, unflinching courage and conviction has always inspired me to do more. His continuous support and back-up made this thesis as one of the most important things to be treasured throughout my life. He has taught me another aspect of life, that, "goodness can never be defied and good human beings can never be denied". For all these, I sincerely thank him from the bottom of my heart and will be truly indebted to him throughout my lifetime.

I am grateful to Prof. Dr Peter Wypych for arranging a large amount of raw data from conveying trials conducted at the University of Wollongong and for his valuable guidance at times and support. I thank him wholeheartedly for his invaluable suggestions and continuous encouragement throughout my journey.

I am also grateful to Dr Rehnu Pan, Vice General Manager, Fujian Longking Co., Ltd., China; for his valuable inputs and discussions during his visits India for short courses and conferences.

I express my sincere gratitude to my colleagues Dr Anu Mittal and Dr Gautam Setia, who helped me several times throughout my PhD. I am thankful to my lab mates, Mr Kapil Sharma and Mr Gourav Saluja for their lively company, support, and ever willingness to help as friends.

I acknowledge the people who mean a lot to me, my parents, for showing faith in me, giving me the liberty to choose what I desired, and for supporting me emotionally and financially. Thank you for raising me to be happy, healthy, motivated, and loved. I would not be here without your support and guidance. I salute you for the selfless love, care, pain and sacrifice you did to shape my life. This triumph is yours as much as it is mine. I would never be able to pay back the love and affection you showered upon me.

I owe thanks to a very special person, my wife, Preeti for her continued and unfailing love, support and understanding during my pursuit of PhD degree that made the completion of this thesis possible. She was always around at times I thought that it is impossible to continue; she helped me to keep things in perspective. I greatly value her contribution and deeply appreciate her belief in me. My heartfelt regard goes to my father in law and mother in law for their love and moral support.

I am highly indebted to the Department of Science and Technology (DST), Council for Scientific and Industrial Research (CSIR), and National Thermal Power Corporation Limited (NTPC) for providing the financial support to pursue the research work.

I thank the Thapar Institute of Engineering and Technology, Patiala, for providing me with such a great atmosphere to learn and perform my research. I greatly appreciate and acknowledge the support received from the Mechanical Engineering Department Laboratories and Central Workshop Staff. Most of the results described in this thesis would not have been obtained without their support.

Finally, I thank the Almighty for giving me the strength and patience to work through all these years so that today I can stand proudly with my head held high.

ABSTRACT

This thesis presents the results of an ongoing investigation into the modelling of pressure drop in bends due to the pneumatic conveying of fine powders. Two grades of cement and fly ash have been pneumatically conveyed from fluidised dense- to dilute-phase through three different radii of curvature (1000, 800, 600 mm), two different bend diameters (53 and 42 mm) and two different locations of test bend in the pipe loop. Six existing bend pressure drop models have been investigated for their prediction accuracy by comparing the predicted versus experimental bend pressure drop values. Based on the conveying data of different products, bend diameters, radius of curvature of bends, a new model for bend loss has been developed, which included physical properties of particles, parameters of gas flow, and the ratio of the radius of curvature of bends to pipe diameter and bend diameter. The new model was validated by using it to predict for bend losses for the experimental data provided in Pan (1992) and by comparing the predicted versus experimental values. The new model was able to predict the pressure loss in bend for fine powder consistently in the range of relative error of 4 to 32%.

In another approach, the total pressure drop due to the bend has been divided into its constituent parts, such as due to change in momentum of solids and air through the curvature zone, frictional pressure drop due to solids and air flows through the curvature zone and straight section of pipe (reacceleration zone) after the curvature zone and reacceleration of slow-moving particles at the end of curvature zone to their steady-state velocities. It has been estimated that the average particle velocity at the exit to the curvature zone of bend lies in the range of 73 % to 77% to the steady-state particle velocity values when the flow is fully developed. The pressure losses in the reacceleration zone were typically 4 to 8 times larger than that occurred in the curvature zone. The pressure drop characteristics in the curvature zone show a slightly drooping tendency with an increase in air mass flow rates. However, pressure

drop characteristics rose sharply in the reacceleration zone. The product with the largest particle size provided the maximum pressure drop. With an increase in the radius of curvature of bend, the bend pressure drop values got increased. Bend pressure drop was increased sharply with an increase in the conveying air amount, and with a decrease in the pipeline diameter.

Bend loss models have also been developed by separately considering the different components of the overall bend loss, such as momentum change of solids and air through the curvature zone, solids-air-wall friction through the curvature and reacceleration zone, and reacceleration of particles in the reacceleration zone. The new models have been evaluated by using it to predict for bend loss for a fly ash sample conveyed through a longer pipeline length, larger pipe diameter, and for larger solids flow rates. The results of validation have shown promising outcomes with the model predicting within 12.2% error, which has been considered to be acceptable.

TABLE OF CONTENTS

LIST OF FIGURES

LIST OF TABLES

LIST OF SYMBOLS AND ABBREVIATIONS

a_b	Constant in Singh and Wolfe equation (3.3)
a_c	Bend pressure loss under air-only conditions in Singh and Wolfe equation (3.3) [Pa]
Ar	Archimedes number ($Ar = \rho_f(\rho_s - \rho_f)gd^3/\mu^2$)
a_s	Constant in Singh and Wolfe equation (3.3)
B	Bend constant in Chambers–Marcus equation (3.5)
C	Particle velocity [m/s]
D	Internal diameter of pipe [m]
d_{10}	Particle diameter corresponding to 10% of cumulative undersize distribution [μm]
d_p, d_{50}	Median particle diameter [μm]
d_{90}	Particle diameter corresponding to 90% of cumulative undersize distribution [μm]
e	Mathematical constant (2.718)
Fr	Froude number based on superficial air velocity and pipe diameter ($Fr = V/(gD)^{0.5}$)
Fr_s	Particle Froude number based on single-particle terminal velocity and pipe diameter ($Fr_s = w_{fo}/(Dg)^{0.5}$)
g	Acceleration of gravity [m/s^2]
k_1, k_2, k_3	Constants in the new model equation (5.13)
L	Total length of the pipe [m]

L_t	The total length of the curvature and reacceleration zone of a bend [m]
L_v	Length of a vertical section of pipe [m]
m_a , m_f	Mass flow rate of air [kg/s]
m_s	Mass flow rate of solids [kg/s]
m^*	Solids loading ratio (m_s/m_a) or (m_s/m_f)
Δp	Pressure drop through a straight horizontal pipe or pipe section [Pa]
Δp_{acc}	Pressure drop due to initial acceleration [Pa]
Δp_b	Pressure drop due to solid-air mixture through bend [Pa]
Δp_{bs}	Bend pressure drop due to the solids only [Pa]
Δp_v	Pressure drop due to verticals [Pa]
Δp_{zs}	Pressure drop due to the solids for an equivalent length of straight pipe (having the same length as the arc length of the bend) [Pa]
$\Delta p_{f\_\Delta mv}$	Pressure drop due to the momentum change of air in the curvature zone [Pa]
Δp_{fr}	Pressure drop due to air and solids friction in the curvature and reacceleration zone [Pa]
Δp_{ra}	Pressure drop due to acceleration of the solids [Pa]
$\Delta p_{s\_\Delta mc}$	Pressure drop due to the momentum change of solids in the curvature zone [Pa]
R_b, r	Radius of curvature of bend [m]
Re	Reynolds number of gas
U_a	Actual air or gas velocity [m/s]
U_s	Actual particle velocity [m/s]
V, V_f	Superficial air or gas velocity [m/s]

VLR	Volumetric loading Ratio (*VLR*= (m_s/ρ_s)/(m_f/ρ_s))
w_{fo}	Single particle settling (or terminal) velocity [m/s]
Y_1, Y_2, Y_3	Constants in Pan equation (3.10)

Greek symbols

α	Constant in the Itō equation (4.3)
β_a	Bend angle in Singh and Wolfe equation (3.2)
λ_{bf}	Air alone friction factor through a bend
λ_{bs}	Friction factor due to solids through a bend
λ_f	Air/gas-only friction factor
λ_s	Solids friction factor through a straight pipe
μ	Air dynamic viscosity [Pa.s]
π	Mathematical constant (3.14)
ρ_f, ρ_a	Fluid or air density [kg/m^3]
ρ_b	Loose-poured bulk density [kg/m^3]
ρ_s	Particle density [kg/m^3]
τ_s	Shear stress on the pipe wall due to solids [kPa]
τ_a	Shear stress on the pipe wall due to fluid or air [kPa]
τ_1	Shear stress on the pipe wall due to the non-suspension layer in dense-phase regime [Pa]
τ_2	Shear stress on the pipe wall due to suspension layer in dense-phase regime [Pa]
ε	Pipe roughness [m]
ε_a	The volume fraction of air

ε_s	The volume fraction of solids
λ_{bsc}	Solids friction factor through the curvature zone of a bend
λ_{bsr}	Solids friction factor through the reacceleration zone after a bend

Abbreviations

ID	Internal Diameter

Subscripts

b	Bend
i	Value at the inlet of bend
o	Value at the outlet of bend
θ	Along θ direction
r	Along r direction

CHAPTER 1

INTRODUCTION AND OBJECTIVES

1.1 Introduction

Pneumatic conveying is the process of conveying bulk solids using a gas as the transport medium through pipes. A pneumatic conveying system offers many advantages over the mechanical conveying systems such as dust-free transportation, relatively high levels of safety, low routine maintenance and manpower costs, layout flexibility, and ease of automation, thereby making it suitable for a variety of industrial use. Some of the disadvantages of pneumatic conveying systems include high power consumption, pipe blockage, system wear, and product attrition (Frye & Peukert, 2004). Some of the industries in which bulk materials are conveyed include agriculture, power plant, cement, mining, chemical, pharmaceuticals, paint manufacture, metal refining, and processing. Pneumatic conveying systems are becoming popular due to stringent environmental and safety constraints(Tripathi et al. 2018). Pneumatic conveying is broadly divided into two categories: dilute and dense phase. In the dilute phase, the particles remain suspended in the high-velocity carrier gas during the conveying process.In contrast, the particles in the dense phase do not remain fully suspended in the gas stream and are conveyed at a low velocity (Ebrahimi, Crapper, & Ooi, 2014). Designing a pneumatic conveying system include determining the minimum transport boundary and total pipeline pressure drop as key parameters. Incorrect estimation of these parameters may result in serious operating problems such as more power consumption, system wear, line blockage, inadequate throughput, and product degradation (Molerus, 1996; Wypych, 1999). Hence an accurate prediction of these parameters is required for smooth, trouble-free, and optimum working of the pneumatic conveying system.

In a pneumatic conveying system, the total pipeline pressure drop comprises of four components. These are losses in the straight pipe, bend, vertical pipe, and losses due to the initial acceleration (Mallick, 2009). The use of bends in pneumatic conveying pipelines

provides the option of a flexible and compact layout. However, the bends also add to the pressure drop in the pipeline. The pressure drop through the bends in pneumatic conveying systems can be quite significant and is generally several times higher than that of a single fluid flow of a similar volumetric flow rate. For a typical industrial system, horizontal straight pipe and bend losses are more critical areas of concern as they form a significant share of total pipeline drops. Over the last decade, relatively more efforts have been made towards understanding the flow mechanism and modelling of pressure drop for straight pipes compared to that through the bends (Mallick, 2009; Gautam Setia, 2016). Conveying through a bend involves vortex flow, direction and momentum change of particles and gas through the bend and reacceleration of particles at the exit to the bend (Venkatasubramanian, Tashiro, Klinzing, & Mykelbust, 2000). Flow through bends results in a roping phenomenon where most of the moving particles are concentrated into a small portion of the cross-sectional area of the pipe due to centrifugal forces (Yan, Byrne, & Coulthard, 1994). A combination of these phenomena, occurring simultaneously, makes it challenging to model the pressures drop and flow situation (Bilirgen & Levy, 2001). There exist some models for bend pressure drop, such as Schuchart (1968), Singh and Wolfe (1972), Rossetti (1983), Chambers and Marcus (1986), Westman et al. (1987), Pan (1992), Pan and Wypych (1998). More recent models include that of Chunhui et al. (2012) and Cai et al. (2014). All these existing models are empirical and have provided reliable results for bend pressure drop predictions when used with the researchers' data. However, their accuracy and reliability have not been adequately examined for different products and setup conditions. Existing models have used mainly gas parameters for the pressure drop predictions and have not adequately addressed the particle parameters. It is quite evident that the particle properties can significantly affect the flow behaviour and pressure drop during the conveying. Hence, particle parameters must be considered while modelling bend pressure drop.

A larger radius of curvature of bend creates a gradual change in the flow direction, which can be imagined to be favourable to get a reduced pressure drop across the bend compared to a bend having a shorter radius of curvature. A gradual change in flow direction would not allow the particles to come to a sudden stoppage due to an abrupt change in the flow direction, thus limiting the requirement of reacceleration of particles at the exit to the bend and the associated losses. However, on the contrary, a larger bend radius increases the overall length of the arc that the particles must go through compared to the shorter radius of curvature of bends. Thus, increasing more distance through the bend resulting in increased length of bend experiencing particle-particle-wall friction. In the work of Pan (1992), Pan and Wypych (1998), Chunhui et al. (2012), and Cai et al. (2014), they have modelled bend loss using a particular location of the test-bend. It would be interesting to carry out an investigation at two different locations of test bend (i.e., different locations of tapping points) in the pilot plan and to examine the effects of conveying velocity on bend pressure drop for the same mass flow rate of air. Such tapping location or prevailing conveying velocity dependency of models has been found to exist in case of straight pipe pressure losses (Mallick, 2009). In an attempt to enhance the understanding of the effect of particle properties, bend, and pipeline configurations on the pressure drop through the bends, the following areas of concerns were identified where it was considered necessary to carry out a detailed experimental study. These areas are relative share of pressure losses within the bend (curvature zone) and after the bend (reacceleration zone); effect of change of powder properties on the pressure drop of bends; effect of different radius of curvature on the bend pressure drop; effect of different pipe diameters on bend pressure drop; effect of conveying velocity on bend pressure drop. Therefore, a detailed study is required to be carried out to address the above areas of concern that will examine the applicability and reliability of the existing bend models and to develop an improved bend loss model. The ultimate aim is to

provide the industry with an accurate modelling and scale-up procedure to predict the bend pressure loss, which will lead to the accurate prediction of total pipeline pressure drop.

In the "component" approach to modelling and scale-up procedure (Mallick, 2009), the pressure drop of each section of straight pipes and bends are calculated separately and are added sequentially to generate information about predicted total pipeline pressure drop. Therefore, even if an accurate straight-pipe pressure drop model is selected, the selection of the bend loss model can potentially alter the predicted total pipeline pressure drop values. Moreover, it can generate a significantly inaccurate prediction of total pipeline pressure drop in case an inappropriate or incorrect bend model is selected. Furthermore, typically, the bend pressure drop models use a conveying gas velocity corresponding to that at the exit to the bend. The accuracy of the prediction of conveying gas velocity at the outlet of bend depends on the reliability of the straight pipe pressure drop model that has been used to estimate pressure drop in the straight pipe section after the bend. Therefore, it is likely that the choice of a straight pipe model would also impact on the bend loss prediction provided by the bend pressure drop model. Studies need to be carried out in assessing the mutual influence of the straight pipe and bend models towards predicting total pipeline pressure drop.

1.2 Objectives

In view of the above, the specific objectives undertaken in this study are:

(1) To develop pneumatic conveying pilot plant with pipeline inner diameters of 42 and 53 mm with 69 m length, two test bend locations (horizontal-horizontal), radius of curvatures of bends of 600 mm, 800 mm and 1000 mm and different fine powders (such as power plant fly ash and cement) having pressure transducers installed at strategic locations.

(2) To carry out extensive pneumatic conveying trials for a wide range of flow conditions of different powders, pipeline diameters, radius of curvature of bends and test bend locations.

(3) To develop bend loss characteristics to evaluate the effects of different powders, pipeline diameters, radius of curvature of bends and conveying velocities on pressure drop through the bends and to assess the interdependency of predictions obtained from bend and straight-pipe models towards accurately estimating total pipeline pressure drop.

(4) To evaluate the accuracy of existing bend loss models under different conditions of product properties and bend configurations and to develop reliable model for pressure drop through bend.

(5) To validate the new developed bend model under the scale-up conveying condition of higher mass flow rate of solids.

1.3 Thesis outline

Chapter-wise distribution of the contents of the thesis is as follows:

Chapter 1 outlines the importance of accurately modelling pressure drop through bends, the limitations of the existing state of research and objectives of the present study.

Chapter 2 includes the description of test facilities (pneumatic conveying pilot plant) and the conveying programs that were developed and carried out under the scope of the present study.

Chapter 3 includes a comprehensive listing of the various existing bend models and their evaluation against experimental data. The chapter also shows the effect of the selection of different bend models on the predicted total pipeline pressure drop characteristics.

Chapter 4 includes the development of new empirical models for bend loss using dimensionless numbers and validation of the same. This chapter also shows the dependency "equivalent length" of a bend with mass flow rates of solids and air. The interdependencies of the predictions of straight-pipe and bend pressure drop models towards reliably estimating the total pipeline pressure drop has been assessed.

Chapter 5 describes the different components of total bend pressure drop through the bend and their trends with respect to other conveying parameters. This chapter also includes a new expression for total pressure drop through the bend having separate models for different bend loss components.

Chapter 6 includes the conclusion and some future suggestions for further research on modelling bend losses.

In this thesis, no separate "Literature Review" chapter has been included. However, a review of previous research on bend loss has been provided in the adequate detail in several chapters to maintain the compactness of the thesis, lucidness of reading without conceding the comprehensives of critical review.

CHAPTER 2

EXPERIMENTAL WORK

2.1 Introduction

This chapter's primary purpose is to describe the test rig, instrumentation, and test materials. A brief description of some of the key features is also given where required. In order to evaluate existing correlations and to develop new empirical correlations, a sequence of pneumatic conveying trials on the actual product must be performed in a test rig of appropriate size. The pneumatic conveyor research facilities located in the Particle and Bulk Solids Technology Laboratory of Thapar Institute of Engineering and Technology, Patiala, were used for the experimental study with new pipeline configuration and additional instruments to achieve the research objectives. A new large-scale pneumatic conveying test facility was also built in the laboratory to generate a data set with high mass flow rates of solids.

2.2 Pilot plant development with test bends and experimental program

The pneumatic conveying test facility has been developed at Thapar Institute of Engineering & Technology, Patiala (India). A typical schematic of the test set up used is shown in Figure 2.1. Kirloskar made electric-powered Model KES 18-7.5 rotary screw compressor was used, having the capacity of 3.37 m^3/min of free air delivery and maximum delivery pressure of 750 kPa. The airflow control valve was installed in the compressed air line upstream of the blow tank to vary the conveying airflow rates over a wide range of airflows. A vortex flow meter was installed in the compressed air line for the measurement of airflow rates. Bottom discharge type blow-tank of capacity 0.2 m^3 capacity of water fill volume was used to feed bulk solids into the pipeline in pressure conveying. The blow tank was mounted with solenoid operated dome-type material inlet, outlet and vent valves. A receiver bin of 0.7 m^3 capacity was installed on top of the blow tank and was fitted with bag filters having a pulse jet cleaning mechanism.

A	Blow Tank
B	Receiver Bin
C	Bag Filter
D	Compressed Air
B1-B6	90°Bends
B1	Location 1 Test Bend (R_b = 1.0/0.8/0.6 m)

B4	Location 2 Test Bend (R_b=1 m)
P1-P11	Pressure Transducers
Pipe Diameter	42/53 mm
Loop Length	69 m
All dimensions shown in the figure are in meters	

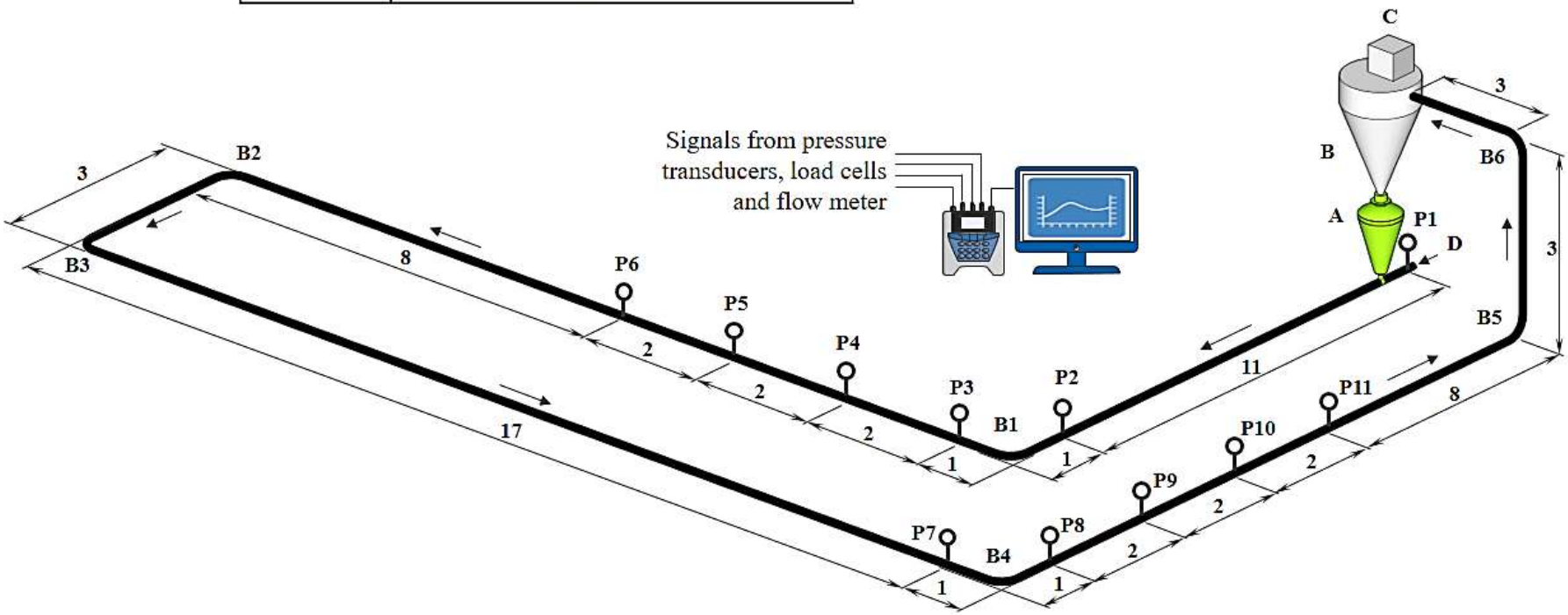

Figure 2.1: Schematic layout of test rig with 42/53 mm I.D. × 69 m length having test bends

The blow tank and receiver bin were supported by shear beam load cells (accuracy ±0.1%) to measure solids flow rates. Two mild steel pipelines of 42 mm I.D. × 69 m length and 53 mm I.D. × 69 m length were used as the test pipelines. The test loops included a 3 m vertical lift and 4 × 90^{o} bends having 1 m radius of curvature in addition to the test bends. A picture of the blow tank, receiver bin, bag filter, pneumatic panel, and programmable logic controller (PLC) panel is shown in Figure 2.2.

Figure 2.2: Blow tank, receiver bin, bag filter, pneumatic panel, and programmable logic controller (PLC) panel

A part of the pneumatic conveying line, which extends outside the Particle and Bulk Solids Technologies Laboratory is shown in Figure 2.3.

Figure 2.3: A part of the pneumatic conveying test loop

The selection of the test bends was done to fulfil the following two criteria: (a) an adequate amount of length upstream of the bend to allow a fully developed flow at the bend entry, (b) a considerable length downstream of the bend (5-6 m) for the particles to re-accelerate and to reach their steady state condition. In the present test loop both of the above conditions were being satisfied by the bends B1 and B4 and therefore are selected as the test bends. Various static pressure measurement points were installed along the pipeline across the test bends, where the P1 transmitter was used to measure the total pipeline pressure drop. P2 to P6 transmitters and P7 to P11 transmitters were used in test bend locations 1 and 2, respectively

(see Figure 2.1). Transmitters P2 and P7 were used to measure pipeline static pressures just at the beginning of bends, whereas P3 to P6 and P8 to P11 were used to measure static pressure after the bends at 2 m interval distance from each other to capture losses at the bend and just after the bend caused by the reacceleration of powders. Specification of static pressure transducers: manufacturer: Endress & Hauser, model: Cerabar PMC131, pressure range: 0-2 bar, maximum pressure: 3.5 bar (absolute), current signal: 4-20 mA. All other required instruments, such as PRV (pressure reducing valve), flow meter, NRV (non-return valve), blow off valve, pressure gauge, and load cells (shear beam type) were suitably placed. Calibration of the pressure transducers, load cells, and a flow meter was performed using a standardised calibration procedure (Mallick, 2009; Gautam Setia, 2016). A portable PC compatible data logger was used to record the electrical output signals from the load cells, pressure transducers, and flow meter. The data logger had 16 different channels with 14-bit resolution.

Figure 2.4 shows the piping and instrumentation diagram (P&ID) of the test facility. Compressed air from the dryer is fed to the air receiver tank from where it is further supplied to the test rig through a series of valves that distribute and control the air supply as per the experimental requirements. The compressed air from the air receiver is divided into two branches: instrument air line and transport air line. The instrument air line supplies the compressed air to the pneumatic panel for blow tank operation whereas the transport air line supplies the air to a 50 mm air header for pneumatic conveying of the test product. The valve G3 controls the amount of air being fed to the transport air line, and the valve G4 controls the air supply to the instrumentation line. Air pressure in the transport air line can be varied from 2-4 bar by using a pressure regulator valve, PR1, which is a manually operated valve, and the pressure in the instrumentation line is maintained at 5 bar by using PR2.

The air of the transport air line is passed through a vortex air flow meter and further distributed into 3 branches i.e. top air, fluidisation air and conveying air by using a 50 mm air header. Manually operated valves G5, G6, and G7 are used to control the air supply to the different regions of the blow tank as per the conveying requirements. These valves provide a wide range of flow conditions in the conveying pipeline.

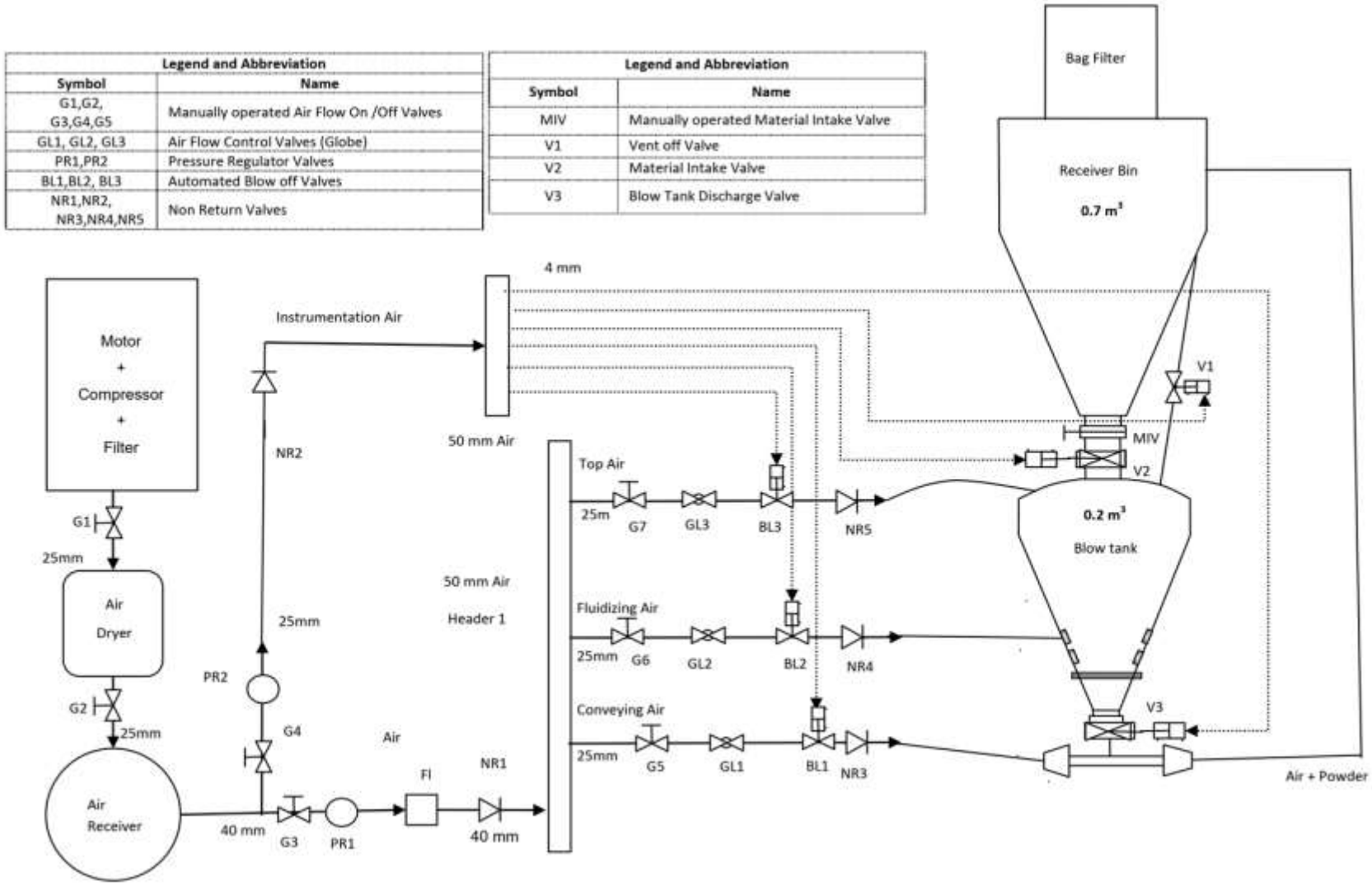

Figure 2.4: P&I Diagram of the compressed air system of test rig with 42/53 mm I.D. × 69 m length having test bends

During a conveying cycle, the automatic control valves BL1, BL2, and BL3 control the operation according to values set in the PLC control panel. A material inlet valve, V2 (automatic control), is used between the receiver bin and blow tank to feed the test material to the blow tank. A material discharge valve, V3 (automatic control), is used between the blow tank and the conveying line to feed the test material to the conveying line. To release the residual pressure of the blow tank after each conveying trial, an automatic control valve V1 is used on the pressure equalisation line.

Grey cement, fly ash, and white cement were initially used in the test program. These powders were conveyed through 2 different pipelines (or bends) diameters: 53 and 42 mm, respectively. Two test locations were used: B1 bend at location 1 and B4 bend at location 2 (Figure 2.1). Three different radii of curvature of bends were used: 1000, 800, and 600 mm (Figure 2.5).

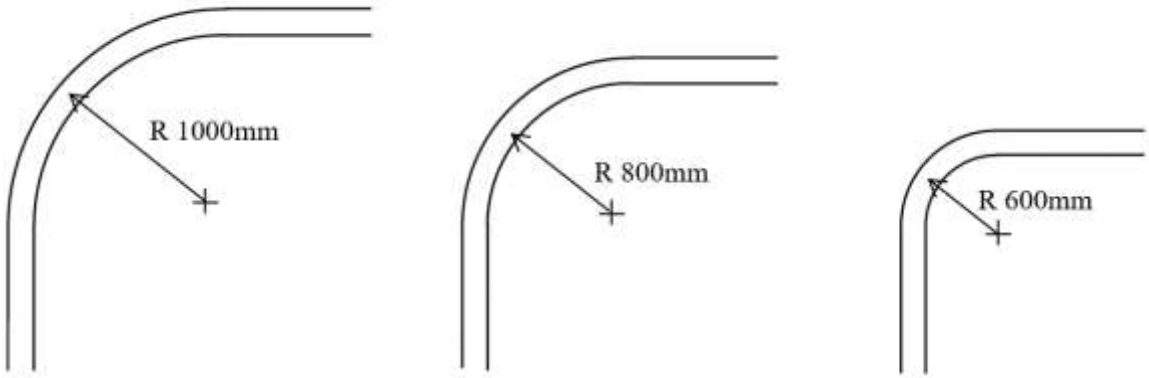

Figure 2.5: Different radius of curvature for test bends

As regards to the location of transmitters before and after the bend, Tripathi et al. (2018), Hall (2012) and Akilli et al. (2001) suggested that the initial acceleration length or the minimum straight length required for the powders to achieve developed flow (or steady flow condition is 30D, where D is the inner diameter of pipeline). In the experimental set-up (Figure 2.1), the

first pressure transmitter in the solid-gas line is located after 200D from the product feed point. Regarding reacceleration length after the bend, the work of previous researchers, such as Maynard (2006), Vásquez et al. (2008), Meloy and Hoff (2002), Laín and Sommerfeld (2013), Hyder et al. (2000), Hettiaratchi et al. (1998), Hastie et al. (2001), Bradley et al. (2001a), Bradley et al. (2001b), and Dhodapkar et al. (2009) suggested that the reacceleration length after the bend is limited between 30D to 100D and 2 m to 6 m. The maximum reported length for dense phase is 6 m, till which the transient effects have been reported. Nonetheless, the effects of transients were verified using an established technique mentioned in Pan (1992). Based on the above, the location of the first transmitter after 11 m from the blow tank and measurement of static pressure after up to 6 m of the test bends were considered appropriate. The location of pressure transducers across the test bend used in the test loop is shown in Figure 2.6.

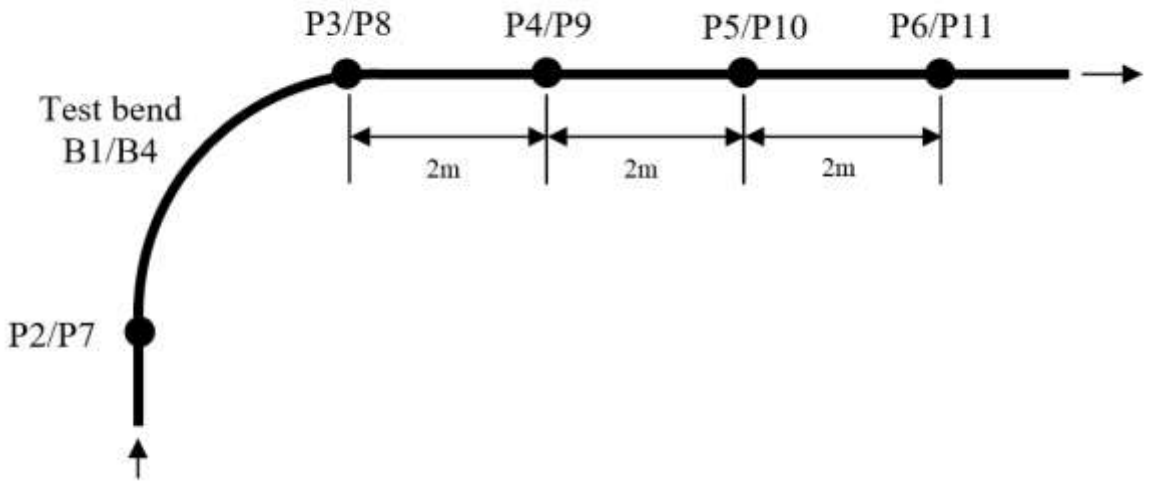

Figure 2.6: Location of pressure transducers across the test bend

The physical properties of the products are provided in Table 2.1. Details of different combinations of choice of products, pipe (or bend) diameters, test bend locations, and radius of curvature of bends are provided in Table 2.2

Table 2.1: Physical properties of powders conveyed

Product	**d_{10} (µm)**	**d_{50} (µm)**	**d_{90} (µm)**	**ρ_b (kg/m^3)**	**ρ_s (kg/m^3)**
Grey Portland Cement	3	18	53	1020	2680
White Portland Cement	3	19	50	1028	2720
Fly Ash	9	65	206	884	2000

Table 2.2: Different bend locations, bend radius of curvatures, bend diameters and products

Case no.	**Product**	**R_b (mm)**	**D (mm)**	**R_b/D**	**Location**
1	Grey Portland cement	600	53	11	B1
2	Grey Portland cement	800	53	15	B1
3	Grey Portland cement	1000	53	19	B1
4	Grey Portland cement	1000	53	19	B4
5	Fly ash	1000	53	19	B1
6	White Portland cement	1000	53	19	B1
7	White Portland cement	1000	42	24	B1

2.3 New large-scale test facility development and experimental program

A new pneumatic conveying test facility was built at the Particle and Bulk Solids Technologies Laboratory of Thapar Institute of Engineering & Technology to generate data set with high mass flow rates of solids. Figure 2.7 shows a schematic of the new facility. The new facility comprised of a multistage screw compressor (equipped with air receiver and drier) having the maximum delivery pressure of approximately 700 kPa-g having a capacity of 605 m^3/hr (Free Air Delivery). A bottom-discharge type blow-tank (A) having 0.8 m^3 empty volume was used to feed the product into the pipeline. On the top of the blow tank, a receiver bin (B) with an insertable pulse jet dust filter of capacity 2.5 m^3 capacity was installed. The test rig is of 128 m of length and having 105 mm pipeline bore and includes 12 number of bends (90^o bends of 1 m radius of curvature) and a vertical lift of 5 m. To measure static pressure in the horizontal straight sections of the pipeline, five static pressure transducers were employed along with all the pipelines, i.e., P2 to P6 (see Figure 2.7). The static pressure transducers had the following specification: manufacturer: Wika, model: S-20, pressure range: 0-2.5 bar-g, current signal: 4 to 20 mA. All other necessary instrumentation, such as the pressure-reducing valve, flow meter, non-return valve, flow-control valve, were installed in suitable locations. The receiver bin and blow tanks were supported on load cells (shear beam type) to determine mass flow rates of solids. To achieve a wide range of airflow rates; a flow control valve was used to change the air mass flow rate. A portable PC compatible data logger (Data Taker 80 and CEM20 channel expansion module) was used to record the electrical output signals from the load cells, static pressure transducer, and airflow meters. A part of the new large scale test facility is shown in Figure 2.8.

A	Blow Tank
B	Receiver Bin
C	Bag Filter
D	Compressed Air
P1-P6	Pressure Transducers

No. of Bends	12
Bend Radius	1 m
Pipe Diameter	105 mm
Loop Length	128 m
All dimensions shown here are in meters	

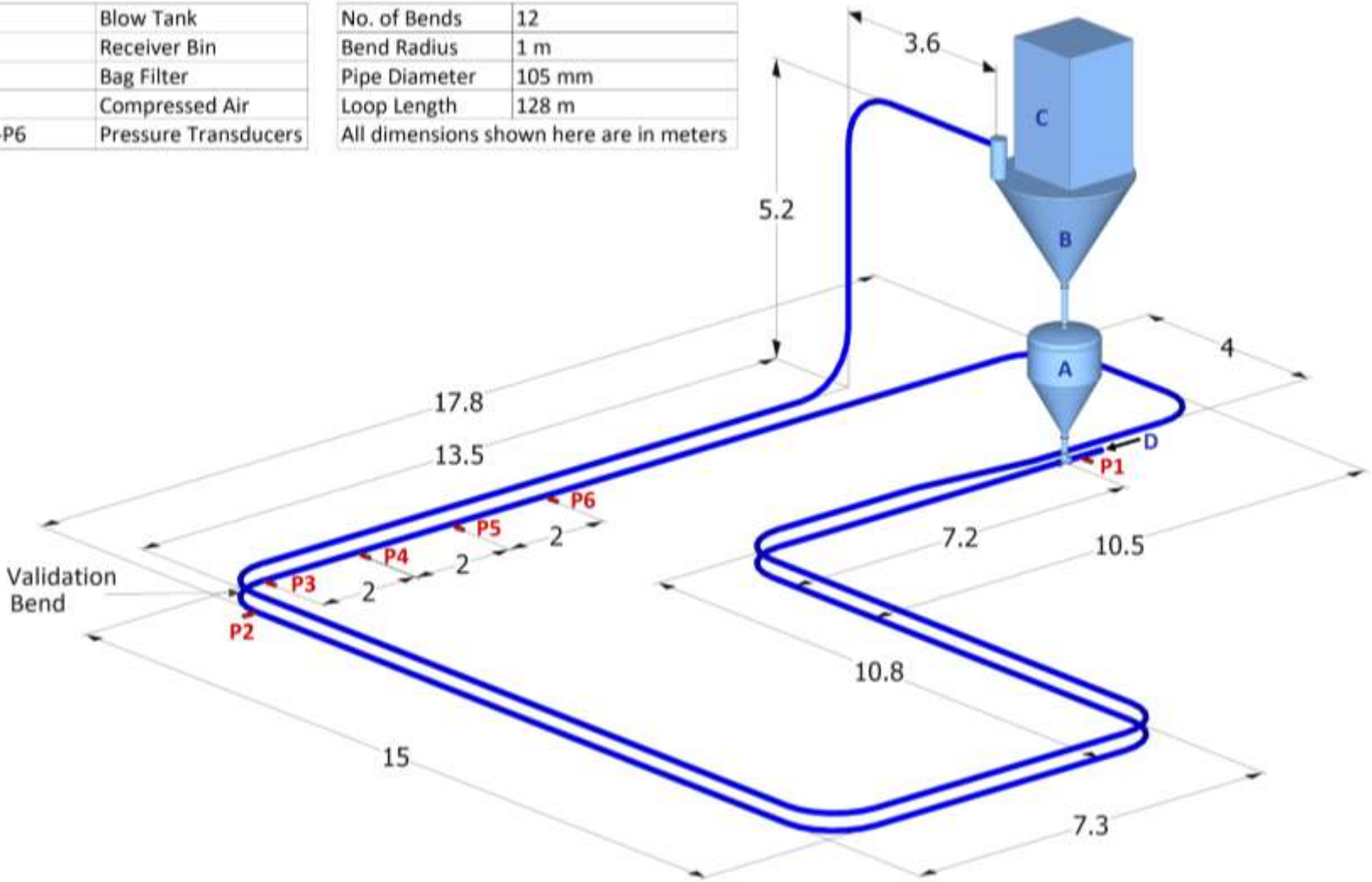

Figure 2.7: Schematic layout of new test rig with 105 mm I.D. × 128 m length having test bend

Figure 2.8: A part of the new large scale test facility

One sample of fly ash from a thermal power station was conveyed through this test rig. The test bend had a 1000 mm radius of curvature with a 105 mm pipeline inner diameter. This new rig was used to validate the bend loss model developed from the smaller rig (Figure 2.1) to a larger rig (Figure 2.7). The new test rig provides industry scale data in terms of higher m_s and subsequent high m*. Therefore, the new setup could validate the new model on account of higher m_s and higher m*.The smaller rig could convey fly ash or cement to a maximum of 10 t/h, whereas the new rig could convey up to 55 t/h. The test bend in the new rig is between P2 to P3. The physical properties of the fly ash samples are provided in Table 2.3. The standard calibration procedure was used to calibrate the pressure transducers, load cells, and flow meter (Mallick, 2009). P&I diagram for the new pneumatic conveying pilot plant is provided in Figure 2.9.

Table 2.3: Physical properties of products conveyed through new larger test rig

Powder	$\boldsymbol{d_{10}}$ **(µm)**	$\boldsymbol{d_{50}}$ **(µm)**	$\boldsymbol{d_{90}}$ **(µm)**	$\boldsymbol{\rho_s}$ **(kg/m^3)**	$\boldsymbol{\rho_b}$ **(kg/m^3)**
Fly ash	5	44	171	2104	1000

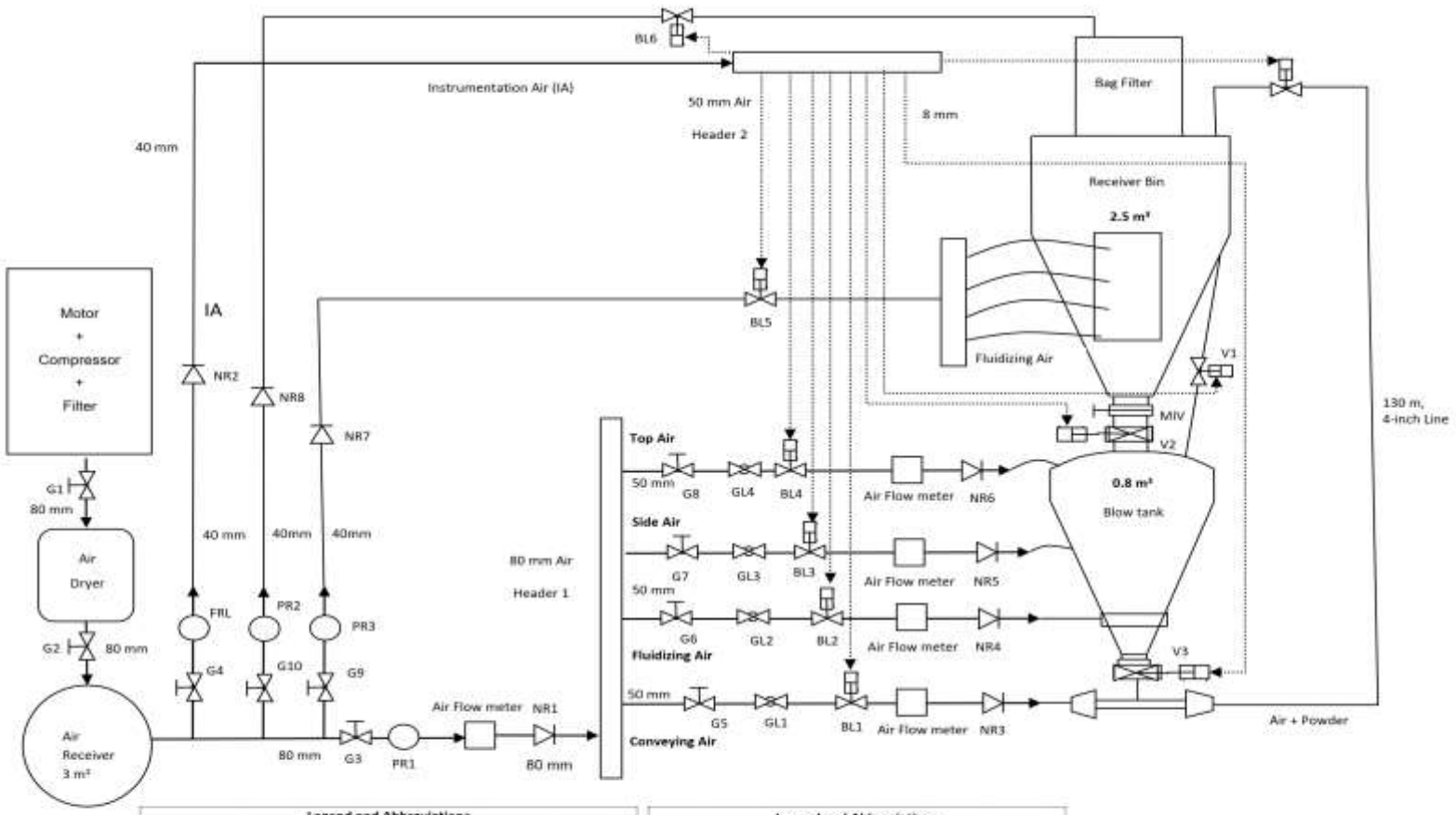

Legend and Abbreviations	
Symbol	**Name**
G1, G2.....	Manually operated Air Flow On /Off Valves
GL1, GL2.....	Air Flow Control Valves (Globe)
PR1, PR2.....	Pressure Regulator Valves
BL1, BL2.....	Automated Blow off Valves
NR1, NR2.....	Non Return Valves

Legend and Abbreviations	
Symbol	**Name**
MIV	Manually operated Material Intake Valve
V1	Vent off Valve
V2	Material Intake Valve
V3	Blow Tank Discharge Valve

Figure 2.9: P&ID for the newly developed pneumatic conveying test rig

2.4 Test data of other researchers used for modelling and scale-up purpose

Pneumatic conveying test data provided in Mallick (2009) and Pan (1992) for two samples of fly ash have been used in this thesis for assessing the interdependency of prediction of bend and straight-pipe models towards reliably estimating the total pipeline pressure drop and for validation of bend model developed. The physical properties and pipeline conditions of these products are provided in Table 2.4. Detail description of the experimental test set-ups are described in Mallick (2009) and Pan (1992). In Mallick (2009), all bends were 90^o and having a radius of curvature of 1 m. A schematic of the test set-up for the 69 mm I.D. × 168 m long and 69 mm I.D. × 554 m long pipelines are shown in Figures 2.10 and 2.11, respectively. The 105 mm I.D. × 168 m long pipeline had the same loop as Figure 2.10, except the pipeline diameter was raised to 105 mm.

Table 2.4: Physical properties of products and pipeline configurations

Product	**Origin of data**	**d_{50} (µm)**	**ρ_s (kg/m^3)**	**ρ_b (kg/m^3)**	**D (mm)**	**L (m)**	**No. of Bends**
Fly ash (Mallick, 2009)	University of Wollongong	30	2300	700	69 105 69	168 168 554	5 5 17
Fly ash (Pan, 1992)	University of Wollongong	16	2197	634	69	172	5

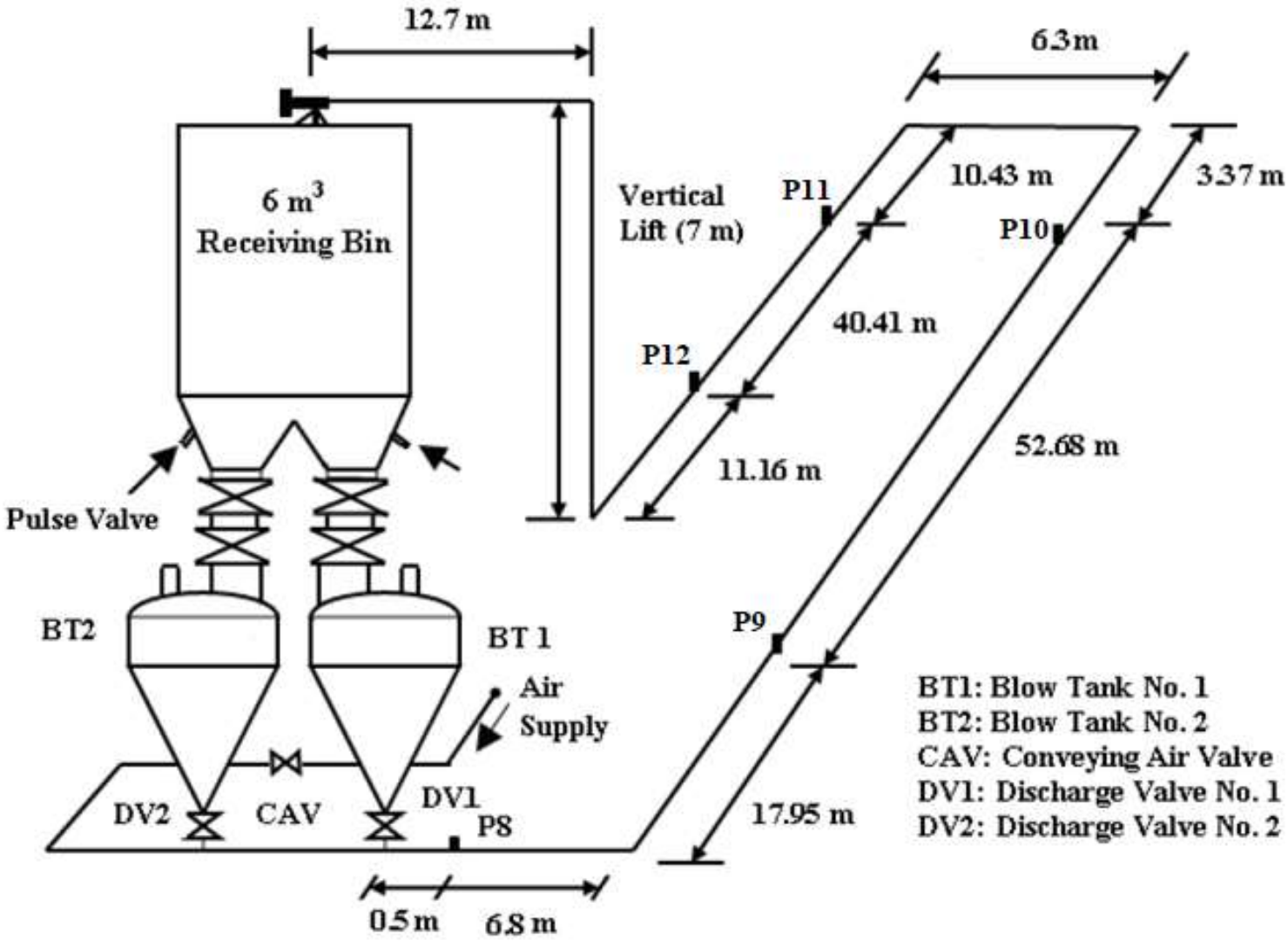

Figure 2.10: Layout of the 69 mm I.D. × 168 m test rig (Mallick 2009)

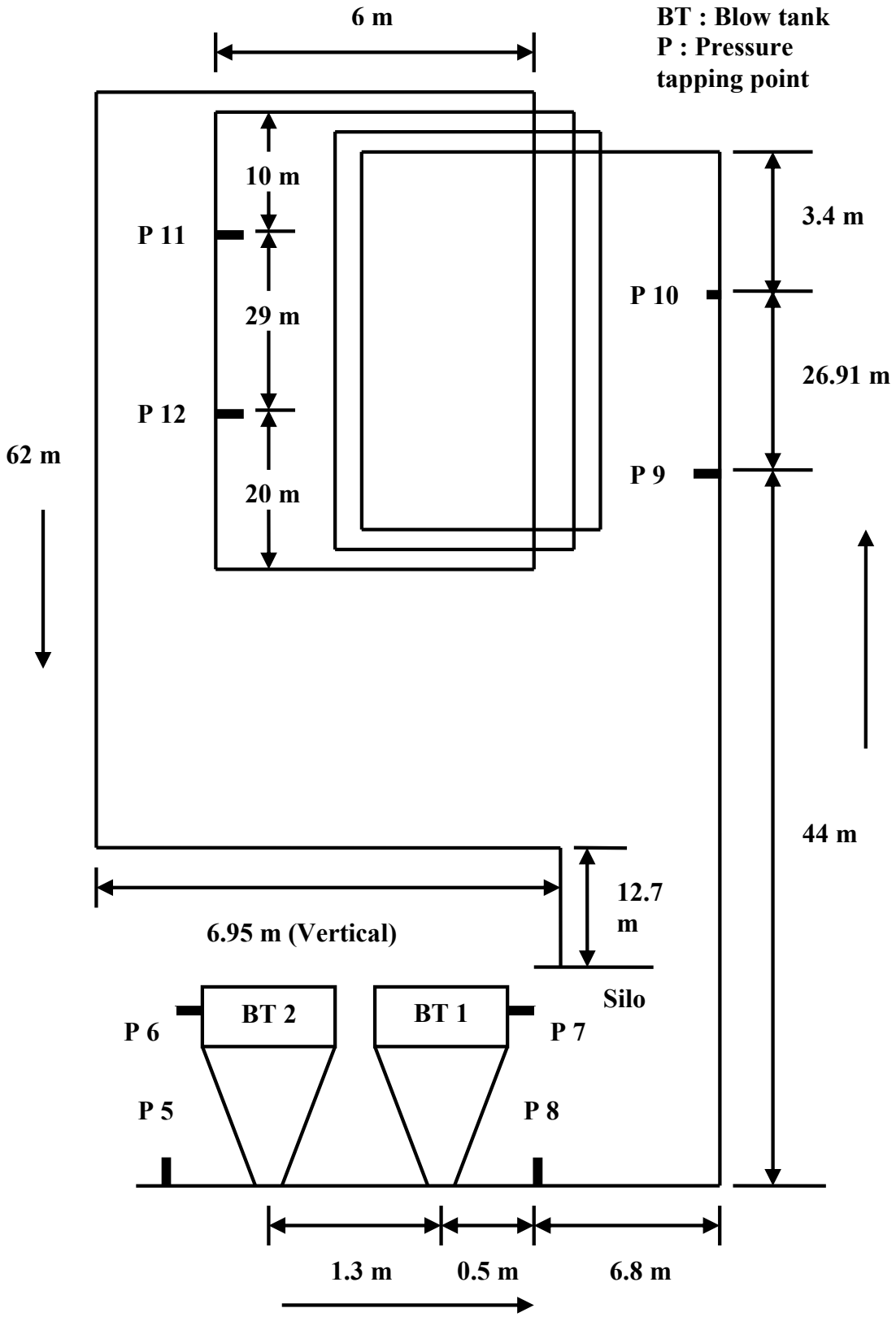

Figure 2.11: Layout of the 69 mm I.D. × 554 m test rig (Mallick 2009)

Due to the turbulent nature of a gas solids flow, the pressure readings obtained from the various pressure transmitters do not give stable readings under the steady state conditions. These signal fluctuations become more intense when the mixture flows through a curved pipe section such as bend (Mallick, 2009). In some cases, these fluctuations may be of the order of 0.1 bar; and thus, indicate that an average of the readings over a timespan would be needed to obtain useful data (Bradley, 1990). Table 2.5 provides typical standard deviations (expressed as % age of average value) for the different pressure tapings across the test bend. Pressure values of two specific experiments (of case 1 and case 2) along with their respective standard deviations (indicated by error bars) are shown in Figure 2.12.

Table 2.5: Standard deviations (expressed as % of average value) for the different pressure tapings across the test bend.

Standard deviation (as % of average value) for the different pressure tapings					
Case	**P2**	**P3**	**P4**	**P5**	**P6**
1	15.8	15.8	17.0	17.5	18.6
2	15.6	15.7	15.8	15.6	15.9
3	16.8	16.4	16.6	17.6	18.1
4	23.8	25.0	24.9	25.7	26.6
5	15.7	15.3	16.1	17.2	17.1
6	16.3	16.8	19.1	19.2	19.7
7	10.1	10.2	10.1	10.5	10.3

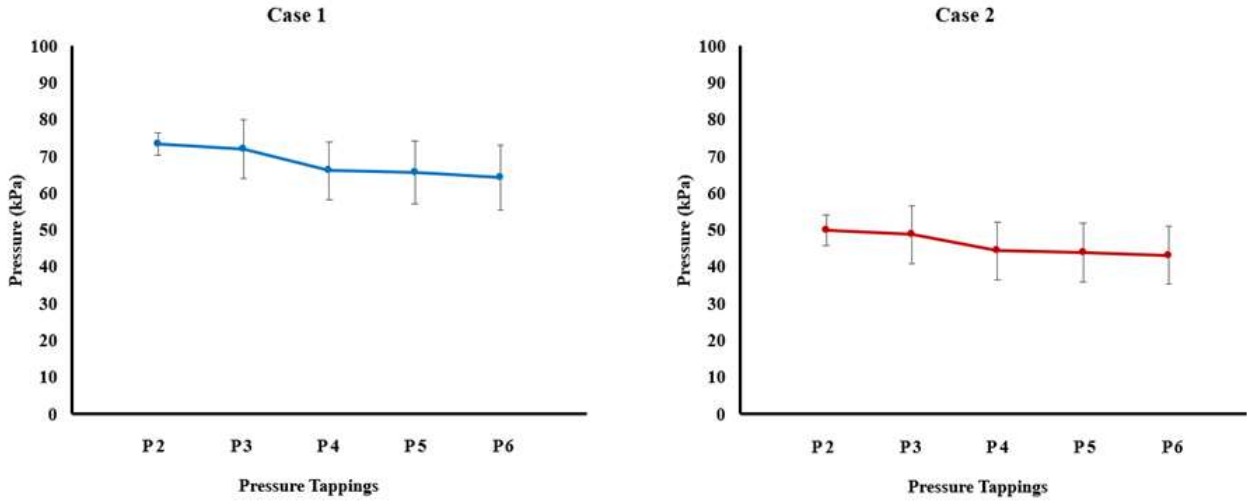

Figure 2.12: Pressure values along with standard deviations (indicated by error bars)

It can be seen from the Table 2.5 that the Case 4 records a high value of deviations in comparison with the other cases. The flow velocity in the case 4 (at test bend B4) is high as compared to all the other cases (at test bend B1), thus resulting in a high pressure drop and a high value of the signal fluctuation, and thereby causing a higher deviation.

A portable PC compatible data logger was used to record the electrical output signals from the pressure transducers. Pressure signals were recorded at a rate of 2 readings/sec for a period of two minutes or more (during the steady-state condition) and are averaged to remove the pressure fluctuations.

CHAPTER 3

EVALUATION OF EXISTING BEND PRESSURE DROP MODELS

3.1 Introduction

In a pneumatic conveying system, the total pipeline pressure drop comprises four components, i.e., losses in a straight pipe, bend, vertical lift, and losses due to the initial acceleration (Bansal, 2012). Horizontal line pressure loss and bend loss are the critical areas of concern for a typical industrial pneumatic conveying system because they form a significant proportion of total pressure loss in the pipeline. Conveying through a bend involves vortex flow, direction, and momentum change of particles and gas, reacceleration at its exit, and may even cause phase separation (Venkatasubramanian et al., 2000). Due to particle-particle and particle-wall friction through the bend (due to rope formation or particles pushed to the outer bend radius), particles leave the bend at a velocity significantly less than their steady state velocity. It takes considerable length downstream of the bend (6 m) for the particles to re-accelerate and to reach their steady state velocity condition. The energy needed for this re-acceleration is an extra pressure loss after the bend and is quite significant. Flow through bends also results in a roping phenomenon where most of the moving particles are concentrated into a small portion of the cross-sectional area of the pipe due to centrifugal forces (Yan et al. 1994). A combination of these phenomena, occurring simultaneously, makes it difficult to estimate the pressures drop due to bend in a gas-solids flow (Bilirgen & Levy, 2001). There exist various models such as Chambers and Marcus (1986), Westman et al. (1987), Pan (1992), Pan and Wypych (1997), Chunhui et al. (2012), for pressure drop estimation due to a bend. This chapter includes a comprehensive listing of these bend loss models and their evaluation against experimental data. The effect of the choice of different bend models on the predicted total pipeline pressure drop characteristics is also presented in this chapter.

3.2 Existing bend loss models

An early comprehensive study of pressure drop caused by bends was done by Schuchart (1968) using glass (size: 1500 to 3000 μm, particle density: 2610 kg/m^3) and plastic (size: 2180 μm, particle density: 1140 kg/m^3) as the test materials (as reported by Klinzing et al. 2010). A wide range of bend radius of curvatures ranging from 60 mm to 350 mm and pipe I.D.: 34.35 mm, were explored and the solids' contribution of the pressure drop due to solids-gas flow through a bend was expressed as:

$$\frac{\Delta p_{bs}}{\Delta p_{zs}} = 210 \left(\frac{2R_b}{D}\right)^{-1.15} \tag{3.1}$$

Where Δp_{bs} is the bend pressure drop due to the solids only, Δp_{zs} is the pressure drop due to the solids for an equivalent length of straight pipe (having the same length as the arc length of the bend), and R_b is the radius of curvature of the bend.

Singh and Wolfe (1972) used dimensional analysis to model the bend pressure drop (as reported by Pan 1992). They conveyed granular material through bends having a different radius of curvature (381, 762, and 1220 mm), all having an internal diameter of 150 mm. They conducted 108 experiments and expressed the seven essential variables in the following dimensionless ratios:

$$\frac{\Delta p_b}{\rho_{fo} V_{fo}^2} = f\left(\frac{R_b}{D}, \frac{m_s}{\rho_{fo} V_{fo} D^2}, \beta_a\right) \tag{3.2}$$

Where β_a is the bend angle. It was assumed that a generalised power function law would be valid; a relationship was developed between $\frac{\Delta p_b}{\rho_{fo} V_{fo}^2}$ and $\frac{m_s}{\rho_{fo} V_{fo} D^2}$, resulting in the following model for bend pressure drop:

$$\Delta p_b = a_c + a_S \frac{m_S V_{fo}}{D^2} \left(\frac{R_b}{D}\right)^{a_b} \quad (3.3)$$

Where a_c represents the bend pressure loss under air-only conditions. Using the least square method and a large number of experimental data, the following expression was obtained:

$$\Delta p_b = 0.13 + a_s \frac{m_s . V_{fo}}{D^2} \left(\frac{R_b}{D}\right)^{-0.18} \quad (3.4)$$

Chambers and Marcus (1986) proposed a correlation for predicting pressure loss in bends. The correlation is given as follows (equation 3.5). Chambers and Marcus (1986) recommended the use of the following values given in Table 3.1.

$$\Delta p_b = B(1 + m^*) \frac{\rho_f V_f^2}{2} \quad (3.5)$$

Table 3.1: Bend constant B or various bends

R_b/D	**B**
2	1.5
4	0.75
≥6	0.50

The values in the table indicate that for a small radius bend, the pressure drop will be more as compared to a long radius pipe under the same operating parameters. This model does not take into account particle properties and the location of bends in the pipeline.

Westman et al. (1987) conveyed four polymers with bulk densities ranging from 572 to 824 kg/m^3, particle densities from 877 to 1320 kg/m^3 of equivalent particle diameter from 3.40 to 3.51 mm using a vacuum system. They studied the bend pressure loss in dilute-phase flow through 90° bends of various geometries ($2R_b/D$ = 3, 10, 24). They concluded that the total pressure loss due to bend could be expressed as a sum of air and solids only pressure drop. The correlation is given as follows:

$$\frac{\Delta p_b}{0.5\rho_f V_f^2} = \lambda_{Total} = \lambda_{bf} + \lambda_{bs} \tag{3.6}$$

$$\lambda_{bf} = 0.167\left[1 + 17.062\left(\frac{2R_b}{D}\right)^{-1.219}\right] Re^{-0.17}\left(\frac{2R_b}{D}\right)^{0.84} \tag{3.7}$$

$$\lambda_{bs} = \frac{5.4\, m^{*1.293}}{Fr^{0.84}\left(\frac{2R_b}{D}\right)^{0.39}} \tag{3.8}$$

Pan (1992) tried to improve the scale-up procedures for the design of pneumatic conveying systems. Based on mathematical and dimensional analysis, semi-empirical correlations were derived predicting the solids' friction through bends. He performed experiments on five types of bends: one blinded-tee and four radius bends (R_b: 100, 254, 450 and 1000mm) and used fly ash as the conveying material with properties: ρ_s: 2197 kg/m^3**;** ρ_b: 634 kg/m^3**;** mean d_p: 15.5 μm. In order to investigate into the bend pressure drop, he used a test bend between two long horizontal straight pipes sections and derived the following bend model:

$$\Delta p_{bs} = 0.5\, m^* \lambda_{bs} \rho_{fo}\, V_{fo}^2 \tag{3.9}$$

Where, $\lambda_{bs} = Y_1\,(m^*)^{Y_2}\,(Fr)^{Y_3}$ (3.10)

Based on his empirical data, Pan (1992) proposed the values of Y_1, Y_2, and Y_3 (for 90° bend angle) as 0.0052, 0.49, and 1.1182, respectively.

Pan and Wypych (1998) derived a bend pressure loss model by conveying four different fly ash samples with median particle size ranging from 3.5 - 58 μm, particle density, and loose poured bulk density ranging from 2180-2540 kg/m^3 and 634-955 kg/m^3, respectively. The model was derived from a wide range of flow conditions (estimated air velocity range at pipe inlet: 3-25 m/s). The bend pressure loss due to solids only was expressed as:

$$\Delta p_{bs} = 0.5\, m^* \lambda_{bs} \rho_{fo}\, V_{fo}^2 \tag{3.11}$$

Where, $\lambda_{bs} = 0.0097\ (m^*)^{0.5676}\ (Fr)^{0.9647}\ \left(\rho_{fo}\right)^{-0.6232}$ (3.12)

Chunhui et al. (2012) conducted the dense phase pneumatic conveying trials on rice husk powder and different mixtures of the rice husk and coal (mass ratio of rice husk to coal = 3:0, 2:1 and 1:2) at a pressure of up to 4.0 MPa. The particle density and mean particle size of these three bulk materials were 1015, 1144, 1272 kg/m^3, and 67.81, 65.21, 62.61 μm, respectively. The solids pressure drop for the bend was given by:

$$\Delta p_{bs} = m^* \lambda_{bs} \pi \left(\frac{R_b}{2D}\right) \rho_f \frac{V_f^2}{2} \tag{3.13}$$

The following correlation was derived for solids friction factor of rice husk conveying through a bend:

$$\lambda_{bs} = (e)^{3.41}\ (Fr)^{-0.66} \left(\frac{\rho_s}{\rho_f}\right)^{-1.30} \tag{3.14}$$

Solids friction factor for coal conveying through a bend was given by:

$$\lambda_{bs} = (e)^{7.46}\,(Fr)^{-0.91}\left(\frac{\rho_s}{\rho_f}\right)^{-1.95} \tag{3.15}$$

The model given by equation (3.15) has been evaluated in this chapter as it is related to fine powder conveying.

Cai et al. (2014) studied the effect of material property, bend geometry, and location on pressure drop due to bends in dense-phase pneumatic conveying. They conveyed petroleum coke (two types: mean diameter of 163 μm and 56.69 μm; bulk density of 616 kg/m^3 and 475 kg/m^3 respectively) and anthracite powder (two types: mean diameter of 139.9 μm and 52.78 μm, and a density of 736 kg/m^3 and 588 kg/m^3, respectively) using nitrogen as the conveying gas. For horizontal bends, three radii of curvatures (120 mm, 200 mm, and 300 mm) were examined. Using Barth's additional pressure theory (pressure drop is considered as the sum of gas and solids pressure drop components) (Mallick, 2009) and multi-variable linear regression, they derived the empirical correlations of pressure drop through the bend. The bend pressure drop due to solids is given by:

$$\Delta p_{bs} = 0.5\, m^* \lambda_{bs} \pi \left(\frac{R_b}{D}\right) \rho_f \, \frac{V_f^2}{2} \tag{3.16}$$

Where,

$$\lambda_{bs} = (e)^{-0.126}\,(m^*)^{-0.961}\,(Fr)^{0.9647}\left(\frac{d_p}{D}\right)^{0.072}\left(\frac{R_b}{D}\right)^{-0.634} \tag{3.17}$$

Table 3.2 lists the different bend models developed by previous researchers.

Table 3.2: Summary of existing bend models

Authors	**Model**
Chambers and Marcus (1986)	Pressure drop due to bend: $\Delta p_b = B(1+m^*)\frac{\rho_f V_f^2}{2}$
Westman et al. (1987)	Solids contribution of pressure drop due to bend: $\frac{\Delta p_b}{0.5\rho_f V_f^2} = \lambda_{bs}; \lambda_{bs} = \frac{5.4\, m^{*1.293}}{Fr^{0.84}\left(\frac{2R_b}{D}\right)^{0.39}}$
Pan (1992)	Solids contribution of pressure drop due to bend: $\Delta p_{bs} = 0.5\, m^* \lambda_{bs} \rho_{fo}\, V_{fo}^2 \;\; ; \lambda_{bs} = 0.0052\, (m^*)^{0.49}\, (Fr)^{1.1182}$
Pan and Wypych (1998)	Solids contribution of pressure drop due to bend: $\Delta p_{bs} = 0.5\, m^* \lambda_{bs} \rho_{fo}\, V_{fo}^2 \; ; \lambda_{bs} = 0.0097 (m^*)^{0.567} (Fr)^{0.964} \left(\rho_{fo}\right)^{-0.623}$
Chunhui et al. (2012)	Solids contribution of pressure drop due to bend: $\Delta p_{bs} = m^* \lambda_{bs} \pi \left(\frac{R_b}{2D}\right) \rho_f \frac{V_f^2}{2} \; ; \lambda_{bs} = (e)^{7.46}\, (Fr)^{-0.91} \left(\frac{\rho_s}{\rho_f}\right)^{-1.95}$
Cai et al. (2014)	Solids contribution of pressure drop due to bend: $\Delta p_{bs} = 0.5\, m^* \lambda_{bs} \pi \left(\frac{R_b}{D}\right) \rho_f \frac{V_f^2}{2}$ $\lambda_{bs} = (e)^{-0.126}\, (m^*)^{-0.961}\, (Fr)^{0.9647} \left(\frac{d_p}{D}\right)^{0.072} \left(\frac{R_b}{D}\right)^{-0.634}$

3.3 Evaluation of bend loss models

All the previously discussed models have been evaluated in the following for their accuracy. Experimental conditions provided in Tables 3.3 and 3.4 are typical of that were used for the investigation for higher and lower solids loading ratio, respectively. Similar results were also generally found in other experiments. Higher and lower ranges have been considered to be from 63 to 21 and 39 to 10, respectively.

Table 3.3: Selected experimental condition for an investigation into bend models' accuracy for higher solids loading ratio range (63 to 21)

Case no.	**Product**	**R_b (mm)**	**D (mm)**	**R_b/D**	**Location**	**m_f (kg/s)**	**m_s (kg/s)**
1	Grey Portland cement	600	53	11	B1	0.039	2.15
2	Grey Portland cement	800	53	15	B1	0.038	1.66
3	Grey Portland cement	1000	53	19	B1	0.039	1.99
4	Grey Portland cement	1000	53	19	B4	0.039	2.09
5	Fly ash	1000	53	19	B1	0.036	1.67
6	White Portland cement	1000	53	19	B1	0.039	2.03
7	White Portland cement	1000	42	24	B1	0.045	0.96

Table 3.4: Selected experimental condition for an investigation into bend models' accuracy for lower solids loading ratio range (39 to 10)

Case no.	**Product**	**R_b (mm)**	**D (mm)**	**R_b/D**	**Location**	**m_f (kg/s)**	**m_s (kg/s)**
1	Grey Portland cement	600	53	11	B1	0.06	0.21
2	Grey Portland cement	800	53	15	B1	0.054	0.51
3	Grey Portland cement	1000	53	19	B1	0.042	1.56
4	Grey Portland cement	1000	53	19	B4	0.042	1.59
5	Fly ash	1000	53	19	B1	0.047	0.56
6	White Portland cement	1000	53	19	B1	0.047	1.23
7	White Portland cement	1000	42	24	B1	0.06	2.1

The results of the evaluation of the existing models are provided in Figures 3.1 and 3.2 for higher and lower ranges of solids loading ratio, respectively.

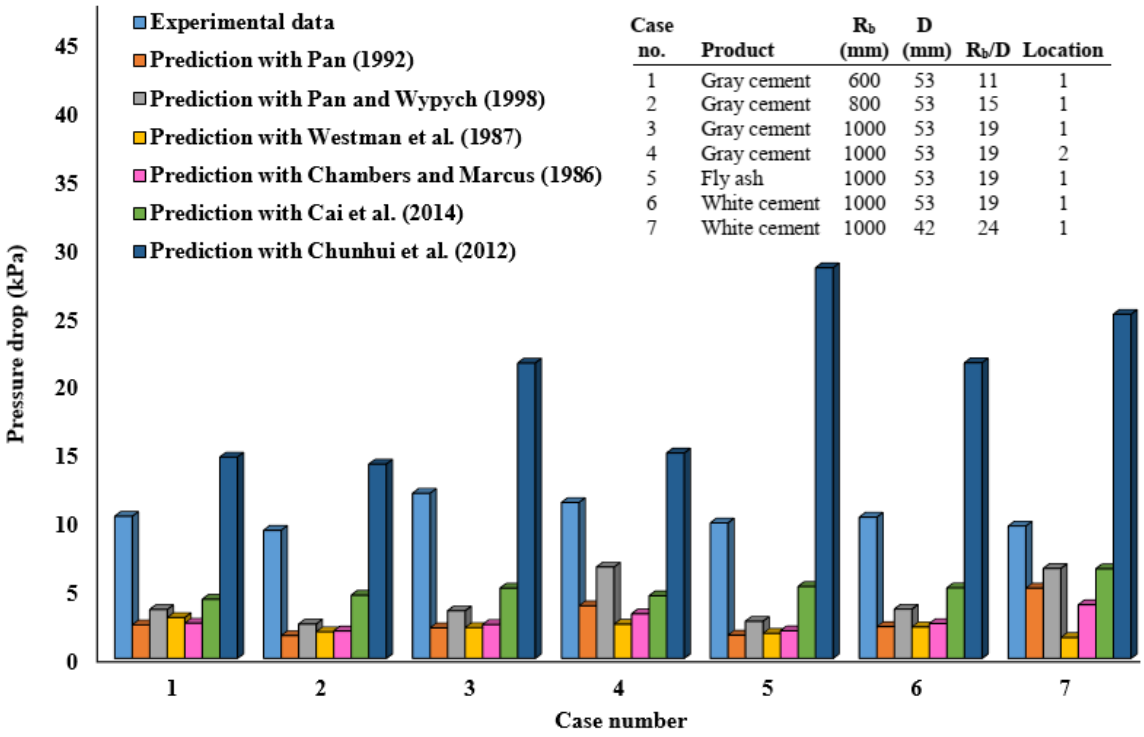

Case no.	Product	R_b (mm)	D (mm)	R_b/D	Location
1	Gray cement	600	53	11	1
2	Gray cement	800	53	15	1
3	Gray cement	1000	53	19	1
4	Gray cement	1000	53	19	2
5	Fly ash	1000	53	19	1
6	White cement	1000	53	19	1
7	White cement	1000	42	24	1

Figure 3.1: Comparison between experimental data and predicted bend pressure drop using different existing models and product, pipelines, bend configurations for high solids flow rates and low superficial gas velocities (m*: 63 – 21)

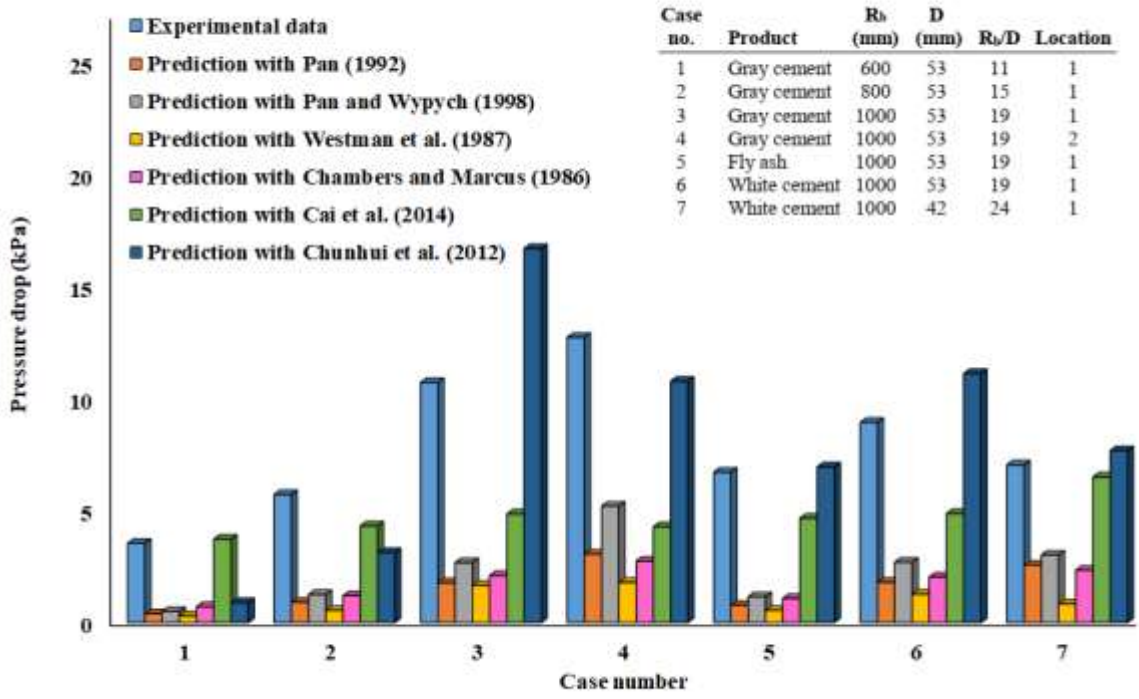

Case no.	Product	R_b (mm)	D (mm)	R_b/D	Location
1	Gray cement	600	53	11	1
2	Gray cement	800	53	15	1
3	Gray cement	1000	53	19	1
4	Gray cement	1000	53	19	2
5	Fly ash	1000	53	19	1
6	White cement	1000	53	19	1
7	White cement	1000	42	24	1

Figure 3.2: Comparison between experimental data and predicted bend pressure drop using different existing models and product, pipelines, bend configurations for low solids flow rates and high superficial gas velocities (m*: 39 – 10)

Figures 3.3 and 3.4 show the relative errors in the percentage of the experimental data derived from Figures 3.1 and 3.2, respectively (for higher and lower conveying velocities, respectively).

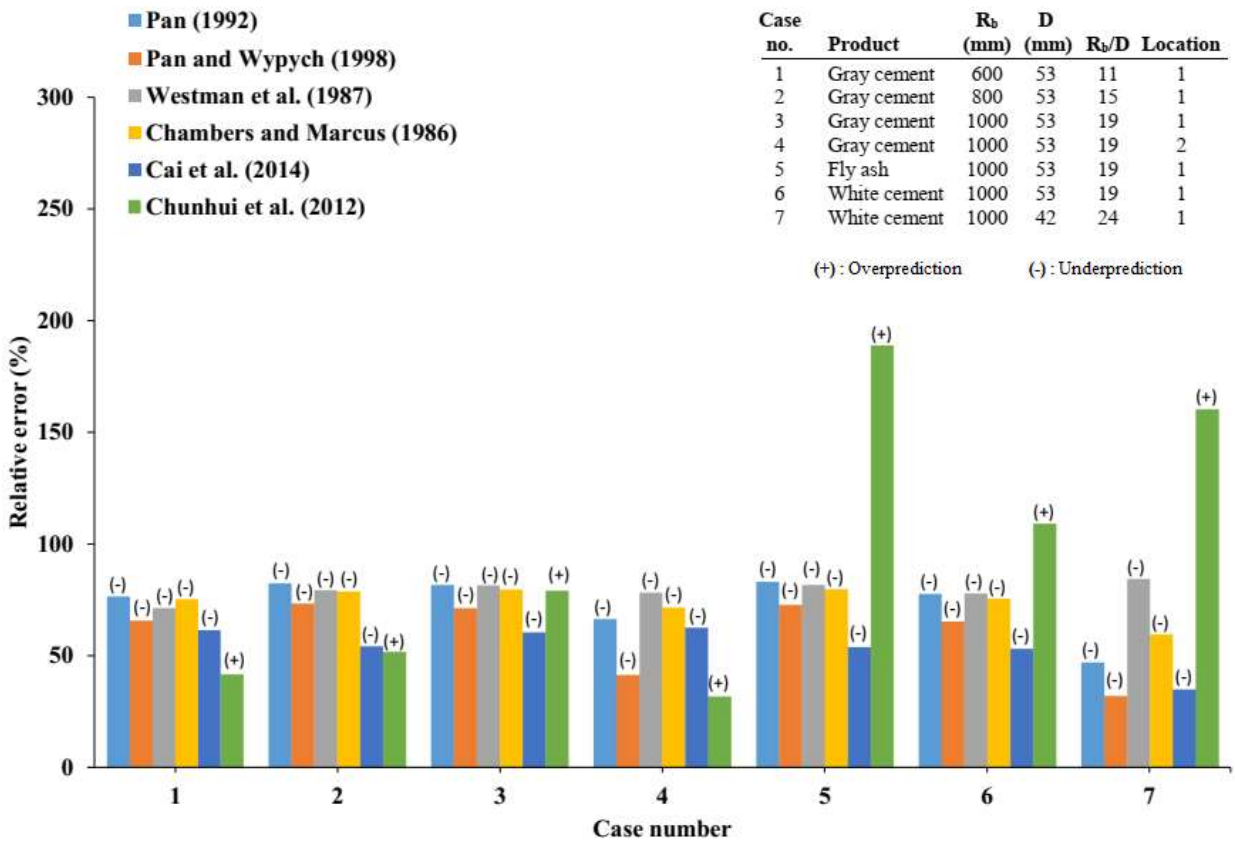

Case no.	Product	R_b (mm)	D (mm)	R_b/D	Location
1	Gray cement	600	53	11	1
2	Gray cement	800	53	15	1
3	Gray cement	1000	53	19	1
4	Gray cement	1000	53	19	2
5	Fly ash	1000	53	19	1
6	White cement	1000	53	19	1
7	White cement	1000	42	24	1

(+) : Overprediction (-) : Underprediction

Figure 3.3: Relative error (%) of the predicted values in comparison to experimental data of bend pressure drop for high solids flow rates and low superficial gas velocities and higher solids loading ratio

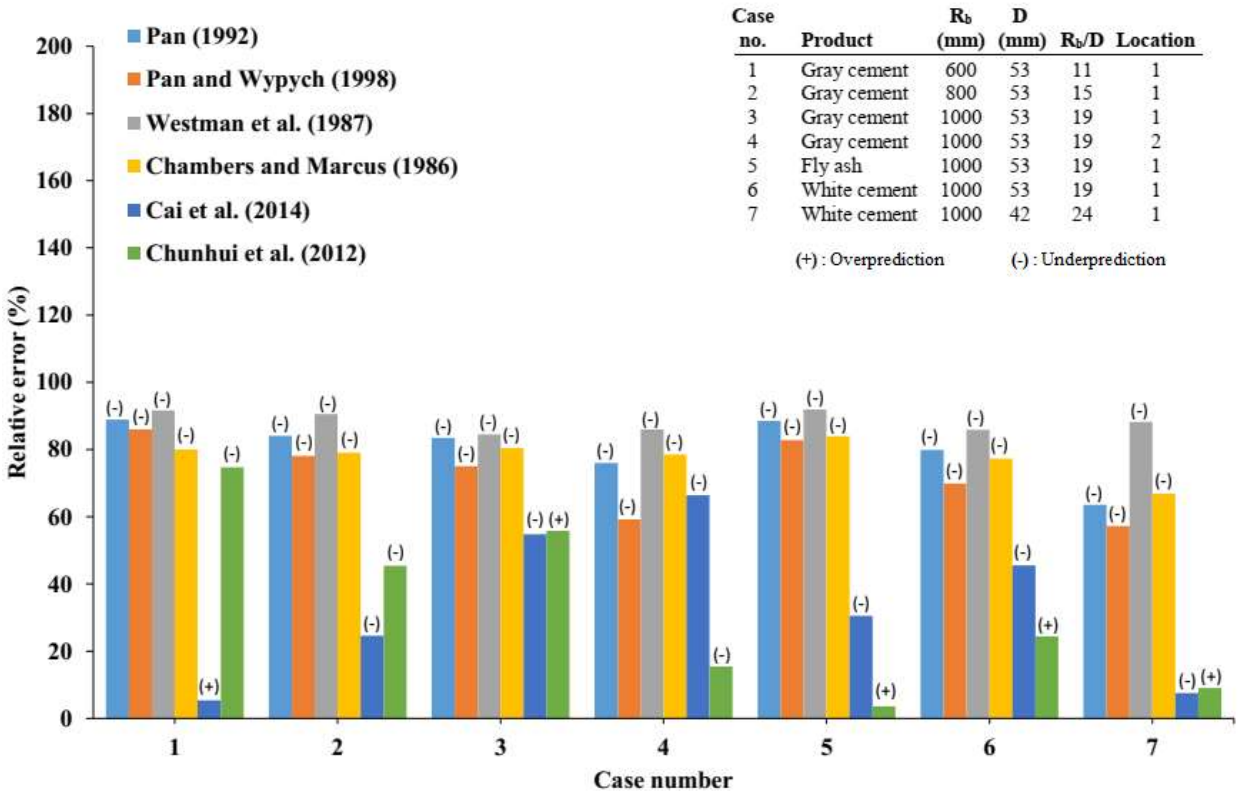

Case no.	Product	R_b (mm)	D (mm)	R_b/D	Location
1	Gray cement	600	53	11	1
2	Gray cement	800	53	15	1
3	Gray cement	1000	53	19	1
4	Gray cement	1000	53	19	2
5	Fly ash	1000	53	19	1
6	White cement	1000	53	19	1
7	White cement	1000	42	24	1

Figure 3.4: Relative error (%) of the predicted values in comparison to experimental data of bend pressure drop for low solids flow rates and high superficial gas velocities and lower solids loading ratio

Figures 3.1 to 3.4 show that none of the existing models could consistently provide accurate predictions covering both high and low solids loading ratio. Models tend to overall predict better in dilute-phase (lower solids loading ratio) compared to dense-phase (higher solids loading ratio). As an example, Cai et al. (2014) and Chunhui et al. (2012) models have only provided about 10 and 3% inaccuracy respectively, in cases 1 and 5 in low solids loading conveying (see Figures 3.2 and 3.4). However, the same models have provided 40 to 180% inaccuracies respectively for higher solids loading ratio regime of conveying (see Figures 3.1 and 3.3). In Chunhui et al. (2012) model, the particle related parameters, such as d_p/D and R/D are not present. The test material used by Chunhui et al. (2012) were rice husk and coal.

Therefore, Chunhui et al. (2012) attempted an ambitious task of modelling based on the data of two different bulk solids which have very different flow mechanisms (rice husk and coal). Moreover, Chunhui et al. (2012) did not use particle to pipe diameter and radius of curvature of pipe to pipe diameter terms in his model, which are believed to be important terms to capture particle and bend properties. It is thought that as a combination of these reasons, Chunhui et al. (2012) model provided high relative error. Pan (1992), Pan and Wypych (1998), Westman (1987), and Chambers and Marcus (1986) models have provided consistent deviation ranging from 30 to 80% in both high and low solids loading ratio regimes of conveying. Considering cases 3 and 4 in Figures 3.1 to 3.4, it can be inferred that the models generally tend to provide better predictions in location 2 (B4) than location 1 (B1); i.e., the models seem to predict somewhat better at higher velocities. This also shows that the prediction capability of models differs depending on the location of bend in the pipeline. Models of Pan (1992), Pan and Wypych (1998), Westman et al. (1987), and Chambers and Marcus (1986) have provided similar levels of accuracy with respect to change in the bend radius of curvature for both high and low solids loading ratio. The Chunhui et al. (2012) model seems to provide relatively higher accuracy at a lower radius of curvature at a higher solids loading ratio. The test bend at location 1 (B1) will experience low flow velocity as compared to the test bend at location 2 (B4). The existing bend models capture the effect of reacceleration losses that occur downstream of the bend (in the reacceleration length). In the case of test bend B1, the flow velocity is less, and the suspension density is high. Under these conditions, the contribution of the straight pipe losses (in reacceleration length) is more as compared to the reacceleration losses. On the other hand, the flow velocity occurring in the test bend B4 is high with a low value of suspension density. These conditions result in a higher contribution of the reacceleration losses as compared to the straight pipe losses (in reacceleration length). Hence the existing models have captured the bend pressure drop of B4 more accurately than the bend

B1. These results demonstrate the challenge of developing a reliable bend loss model. Such challenges include: (a) having transmitters installed in the pipeline that are accurate to register losses across bends; (b) defining the reacceleration length after the bends uniformly across the research community; (c) complex flow phenomenon within and just after the bend (such as roping effect).

3.4 Effect of bend pressure loss on total pipeline pneumatic conveying characteristics

It can be seen from Figures 3.1 to 3.4 that each of the bend models can provide substantially different predictions under different combinations of powders, bend, and pipeline configurations. In order to investigate the effects of the selection of the bend loss model on the prediction of total pipeline pressure drop, the following exercise has been carried out. A known reliable straight-pipe model has been used to estimate the straight-pipe losses, and different bend pressure drop models were used to predict the bend losses. The total pipeline pneumatic conveying characteristics (by adding the predicted straight and bend losses) were compared with the experimental pneumatic conveying characteristics. From the straight pipe data obtained from P11-P12 static pressure measurements for a wide range of dilute- to dense-phase conveying conditions of fly ash (see Figure 2.10), a two-layer based model for solids friction factor has been derived for straight pipe loss (Setia et al. 2016). Along with this common straight pipe model, five different bend models were applied to calculate the total pipeline pneumatic conveying characteristics using an MS EXCEL based program containing different straight pipeline sections and bends. Subsequently, the predicted total pipeline pneumatic conveying characteristics were compared with the experimental plots to evaluate the influence of the selection of the bend model on the total pipeline pressure drop. The two-layer model for solids friction through a straight pipe is provided by equation (3.18).

$$\lambda_s = \tau_1 [8.04 (VLR)^{-0.22} (w_{fo}/V_f)^{1.48}] + \tau_2 [0.0043 (C/V_f) + 2(w_{f0}/V_f)/\{(C/V_f) Fr^2\}] \quad (3.18)$$

$$\text{Where, VLR } (volumtric\ loading\ ratio) = \{(m_s/\rho_s)/(m_f/\rho_f)\} \quad (3.19)$$

τ_1 and τ_2 represent the relative contributions of the shear stress on the pipe wall due to non-suspension and suspension layers, respectively, based on the Froude number criteria. The first term in equation (3.18), τ_1 $(8.04 (VLR)^{-0.22} (w_{fo}/V_f)^{1.48})$, represents the solids friction contribution of the non-suspension flow, whereas the second term, τ_2 $(\lambda_s * C/V_f + 2\ w_{f0}/V_f /[(C/V_f) Fr^2])$, represents the suspension flow contribution. From a knowledge of λ_s, the pressure loss for a straight horizontal section of pipe for the solids-gas mixture can be calculated using equation (3.20), as given by Barth (1954). The straight-pipe model format of Setia et al. (2016) was proposed after a comprehensive validation for fly ash, ESP dust, and cement conveyed through 69 mm and 105 mm diameter and 168 m, 407 m, and 554 m long pipelines. Guan et al. (2017) independently validated the accuracy of the two-layer modelling procedure of Setia et al. (2016) and found reliable agreements with experimental data.

$$\Delta p = (\lambda_f + m*\lambda_s).L.\ \rho\ .V_f^2/2D \quad (3.20)$$

The effect of selecting a particular bend model on the prediction of total system pressure loss was evaluated by estimating the total pipeline conveying characteristics for fly ash for different solids throughput ranges for the 69 mm I.D. × 168 m and 105 mm I.D. × 168 m long test rigs by using several of the existing bend models separately and comparing the predicted PCC thus obtained (with themselves and with the experimental PCC). Losses due to initial acceleration and vertical pipe were estimated as per Chambers and Marcus (1986) as given by equations (3.21) and (3.22), respectively. Equations (3.18) to (3.20) were used to estimate the straight pipe pressure drop.

Acceleration Loss: $\Delta p_{acc} = \rho_f V^2 \left(1 + 2m^* C/V_f\right)/2$ (3.21)

Vertical loss: $\Delta p_v = m^* \rho_f g L_v \; V_f/C$ (3.22)

Since the same set of models were used to estimate losses occurring in horizontal pipe lengths, verticals and for initial acceleration and that the straight-pipe model is a validated, reliable model (Setia et al. 2016 and Guan et al. 2017); therefore any variation in magnitude (and trend) of the predicted total pipeline pneumatic conveying characteristics should occur only because of the choice of different bend models. Results are shown in Figures 3.5 and 3.6 for 69 mm I.D. and 168 m long pipeline for 19 t/h of ash-flow rate and 105 mm I.D. and 168 m long pipeline for 28 t/h ash-flow rate, respectively.

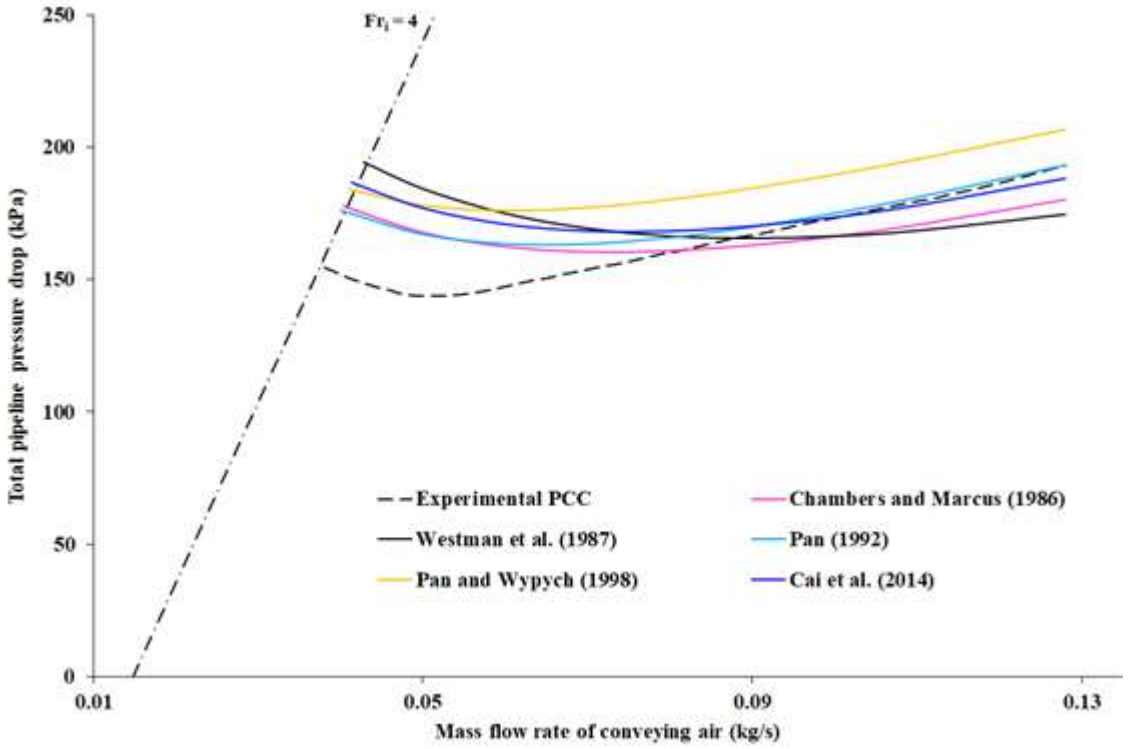

Figure 3.5: Comparison of experimental and predicted values of the total pressure drop using different bend models in a pipeline (fly ash, D = 69 mm, L = 168 m, m_s = 19 t/h)

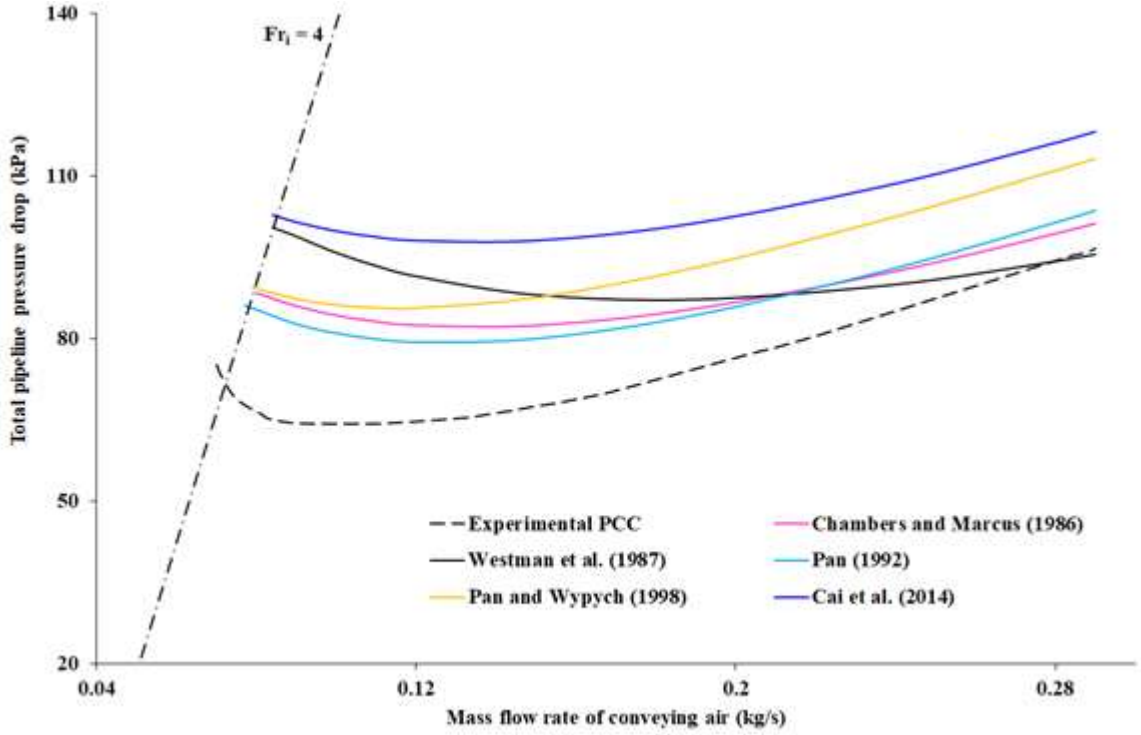

Figure 3.6: Comparison of experimental and predicted values of the total pressure drop using different bend models in a pipeline (fly ash, D = 105 mm, L = 168 m, m_s = 28 t/h)

The above comparison plots show that the selection of different bend models can generate significantly different predicted conveying characteristics (even though they all use the same solids friction factor model to calculate pressure drop in straight horizontal runs). The Westman et al. (1987) model has generated large over-prediction in the dense-phase region, and the predicted trends did not comply with the trends of experimental plots. Pan and Wypych (1998) model has provided desirable (but somewhat over-predicted) trends for both the pipelines. Perhaps this is because this model was developed specifically using fly ash data. The Chunhui et al. (2012) model provided large over-predictions; hence, predictions using the same have not been included in Figures 3.5 and 3.6.

CHAPTER 4

DEVELOPMENT OF EMPIRICAL MODELS FOR BEND PRESSURE DROP

4.1 Introduction

The use of bends in pipeline provides the option of a flexible and compact layout. However, the bends also add to the pressure drop in the pipeline. The pressure drop through the bends in pneumatic conveying systems can be quite significant and is generally several times higher than that of a single fluid flow of a similar volumetric flow rate. While relatively more research has been carried out in recent times the modelling of solids friction for straight pipes (Mallick 2009; Setia 2016), modelling of pressure drop through bends in pneumatic conveying systems has seen limited progress. Typically, the Geldart Group A type of fine powders have good air retention capabilities, such as fly ash, cement, pulverised coal, etc., and are conveyed in fluidised dense-phase mode (Pan 1999). Although fundamental modelling of granular flow (Kumaran, 2008; Maiti, Das, & Das, 2016; Reddy & Kumaran, 2007) can be achieved with relatively more success from the knowledge of particle-particle-wall mechanics, the same is far more difficult in case of fluidised flow (Das & Datta, 2016) of fine powders due to the highly turbulent and concentrated nature of flow. Highly concentrated aerated powder bed tend to exhibit an apparent viscosity (Gibilaro et al., 2007) that is far more challenging to be modelled with similar levels of accuracy as compared to the rheological studies carried out on various other non-Newtonian but single-phase fluids (Kumar & Shankar, 2005; Shankar, 2004). Therefore, many researchers followed the empirical modelling approach to predict the pressure loss for fine powders. This chapter includes the development of new empirical models for bend loss using dimensionless numbers and validation of the same. This chapter also shows the dependency “equivalent length” of a bend with mass flow rates of solids and air. The interdependencies of the predictions of straight-pipe and bend pressure drop models towards reliably estimating the total pipeline pressure drop has been assessed.

4.2 Development of the new validated empirical model

An empirical model for pressure drop in bends due pneumatic conveying of fine powders has been developed using the experimental data of 209 conveying trials including the data of 3 products, 2 different bend or pipeline diameters, 3 different radii of curvatures and 2 different locations of test bends; these tests were conducted in the 42/53 mm I.D. and 69 m long pipeline (see Chapter 2 for the details of experimental program). The expression for pressure drop through the bend is given by equation (4.1). This expression considers pressure drop due to the air and solids differently. The model for solids friction at the bend is given by equation (4.2). Air density and velocity values used in equations (4.1) and (4.2) correspond to that of exit to the bend. The model has been developed using the least square technique. Air density and velocity values used in the model correspond to that of exit to the bend. The ratio of air to particle density term in the model addresses the location of bends in the pipeline (air density decreases in the direction of flow) and the specific weight of the particles. The R_b/D term describes the effect of the radius of curvature of bend. The d_{50}/D term addresses the particle size effect on solids friction through the bend. The gas Froude number term describes the effect of conveying velocity on the particle-particle-wall friction at the bend. Mallick (2009)and Mallick & Wypych (2009)have shown that Froude number tends to track solids friction and minimum transport condition better as it seems to address the effect of scale-up of pipe diameter.

$$\Delta p_b = \left(\lambda_{bf} + m^* \lambda_{bs}\right) \cdot \frac{\rho_f {V_f}^2}{2} \tag{4.1}$$

$$\lambda_{bs} = 0.2462 \left(\frac{\rho_f}{\rho_s}\right)^{-0.9374} \left(\frac{R_b}{D}\right)^{-0.2933} \left(\frac{d_{50}}{D}\right)^{0.3217} (Fr)^{-0.4311} \tag{4.2}$$

The air only pressure loss was calculated using Itō (1960) correlation given below:

$$\lambda_{bf} = \frac{0.217\alpha}{Re^{0.2}}\left(\frac{2R_b}{D}\right)^{0.84} \text{ for } Re\left(\frac{D}{2R_b}\right)^2 > 91 \text{ and } \lambda_{bf} = \frac{0.248\alpha}{Re^{0.2}}\left(\frac{2R_b}{D}\right)^{0.9} \text{ for } Re\left(\frac{D}{2R_b}\right)^2 < 91 \quad (4.3)$$

where,

$$\alpha = 0.95 + 17.2\left(\frac{2R_b}{D}\right)^{-1.96} \qquad \text{for} \qquad \frac{2R_b}{D} < 19.7$$

$$\alpha = 1.0 \qquad \text{for} \qquad \frac{2R_b}{D} > 19.7$$

In the later stages of Ph.D., a new model for solids friction through the bend was developed. This model is given by equation (4.4). This model has been developed by replacing the particle density term of equation (4.2) to the bulk density of powders.

$$\lambda_{bs} = 0.215\left(\frac{\rho_f}{\rho_b}\right)^{-0.86}\left(\frac{R_b}{D}\right)^{-0.246}\left(\frac{d_{50}}{D}\right)^{0.189}(Fr)^{-0.38} \quad (4.4)$$

Referring to equations (4.2) and (4.4), negative exponent values of the ratio of gas density to particle and bulk density indicates that as the product density increases, there would be more solids friction in bends. The negative exponent value of the ratio of the radius of curvature of bend to pipe diameter indicates that for sharper bends, the solids friction through the bend would be more. The positive exponent value of the ratio of median particle diameter to pipe diameter indicates that for larger particles, the solids friction through the bend would be more. The negative exponent value of the Froude number indicates that when the gas velocity is high, the solids' friction through the bend would be less due to reduced particle-particle contact. It should be noted that in several existing models for bend pressure drop, the V^2 term has been only used to represent the basic framework in the existing models (just as V^2 term has been included in Darcy formula for air-only fluid). Therefore, with both V^2 and λ_{bs} in use, the effective exponent of velocity term (using Froude number term) has not been 2. Figure 4.1 shows a comparison of the solids' friction through bends predicted using equation (4.4) versus

the experimental finding. The standard deviation error of the pressure drop was found to be 9.6 % of the average value.

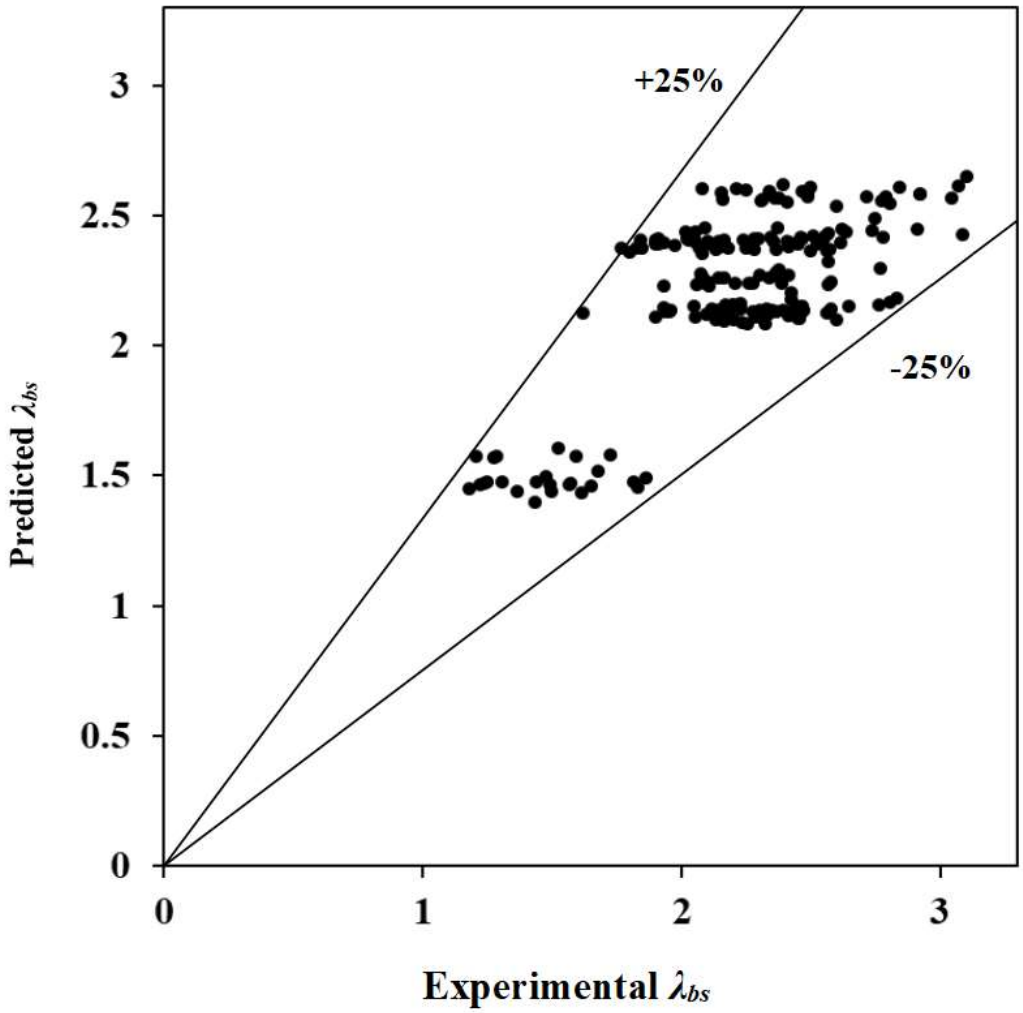

Figure 4.1: Experimental versus predicted values of solids friction factor through bends

While the model given by equation 4.2 is an improvement over the existing models, this model represents the losses in curvature and reacceleration (straight pipe) zones (following the bend) by a single power function terms. In reality, the pressure loss mechanisms in curvature and reacceleration zones differ considerably. This is the reason why equation 4.2 has provided partial improvements. In the later stages of thesis, this model has been further improved by introducing two different solids friction factor terms – one for the curvature zone and the other

for the reacceleration zone. Table 4.1 and 4.2 list the range of velocity values (before and after the bends) adopted in the experimental program from where the new bend loss models have been generated for low m* and high m* values respectively.

Table 4.1: Ranges of air velocity values before and after the bend at low m*

Case	$\mathbf{m_f\ (kg/m^3)}$	$\mathbf{m_s\ (kg/m^3)}$	$\mathbf{m^*}$	$\mathbf{V_i\ (m/s)}$	$\mathbf{V_o\ (m/s)}$
1	0.057	0.33	5.8	15.7	15.8
2	0.054	0.51	9.5	14.0	14.1
3	0.042	1.62	38.6	8.9	9.0
4	0.042	1.59	38.2	11.1	11.2
5	0.045	0.56	12.6	11.8	11.9
6	0.047	1.23	26.3	10.5	10.7
7	0.058	0.35	6.0	20.3	20.4

Table 4.2: Ranges of air velocity values before and after the bend at high m*

Case	$\mathbf{m_f\ (kg/m^3)}$	$\mathbf{m_s\ (kg/m^3)}$	$\mathbf{m^*}$	$\mathbf{V_i\ (m/s)}$	$\mathbf{V_o\ (m/s)}$
1	0.037	1.99	53.2	7.6	7.6
2	0.042	2.24	54.0	8.8	8.9
3	0.040	2.15	54.4	8.1	8.2
4	0.039	2.09	53.1	10.2	10.2
5	0.034	2.16	63.6	7.1	7.1
6	0.040	2.03	50.9	8.2	8.2
7	0.047	1.07	22.7	14.6	14.7

While several of the existing models were developed from limited experimental conditions, the new models (equations 4.2 and 4.4) have been developed from a range of data of different products, bend diameters, the radius of curvatures, and relative location of the bend in the total pipeline. The new model is therefore expected to be useful in estimating the pressure drop accurately due to bends for a range of fine powders, pipelines, and bend configurations. As an example, the new model given by equation (4.2) takes care of the effects of particle density, the radius of curvature of bend, bend diameter, the median size of particles, and gas velocity. The model developed in this study has a provision of using mean diameter only. However, it has been generally considered that a wider particle size distribution would make the powders more air retentive (hence more fluidised), causing reduced solids to solids and solids to pipe wall friction, thus overall reducing the losses in the bend. The model is particularly applicable to horizontal-to-horizontal bends, where the gravity effect may not be significant compared to the effect of pressure loss due to reacceleration. As the gas–solid mixture passes through the horizontal-vertical upward bend, gravity and flow directions become opposite in the vertical part of the bend. This causes an increase in the gravitational potential energy of the particles. To overcome this gravity effect, conveying gas will spend more energy to transport the particles as compared to a horizontal bend. In the case of a horizontal-vertical downward bend, gravity and flow directions are same Thus, the potential energy of particles can be used to accelerate solid particles and overcome flow resistance. Therefore, the conveying gas will spend less energy to transport the particles as compared to a horizontal bend.

Flow transition from dense to dilute-phase is characterised by the higher gas velocity at the inlet to the bend and lower solids volumetric concentration. Due to the aerated nature of fine powders, fluidised dense-phase type conveying will have smooth dense to dilute-phase transition. However, through the bend, the solids will be pushed at the outer periphery of the bend and slowed down to form a concentrated, dense bed of powders. Subsequently, the

powders will again get reaccelerated and attain its prevailing flow mode (dense or dilute). The model given by equation (4.2) has been further used to develop pneumatic conveying characteristics for bends for cement for different combinations of bend diameters (42 and 53 mm), radius of curvatures (1000 and 600 mm) and air densities at the exit to the bend (1.2 and 2.4 kg/m^3). Results are shown in Figures 4.2 to 4.5.

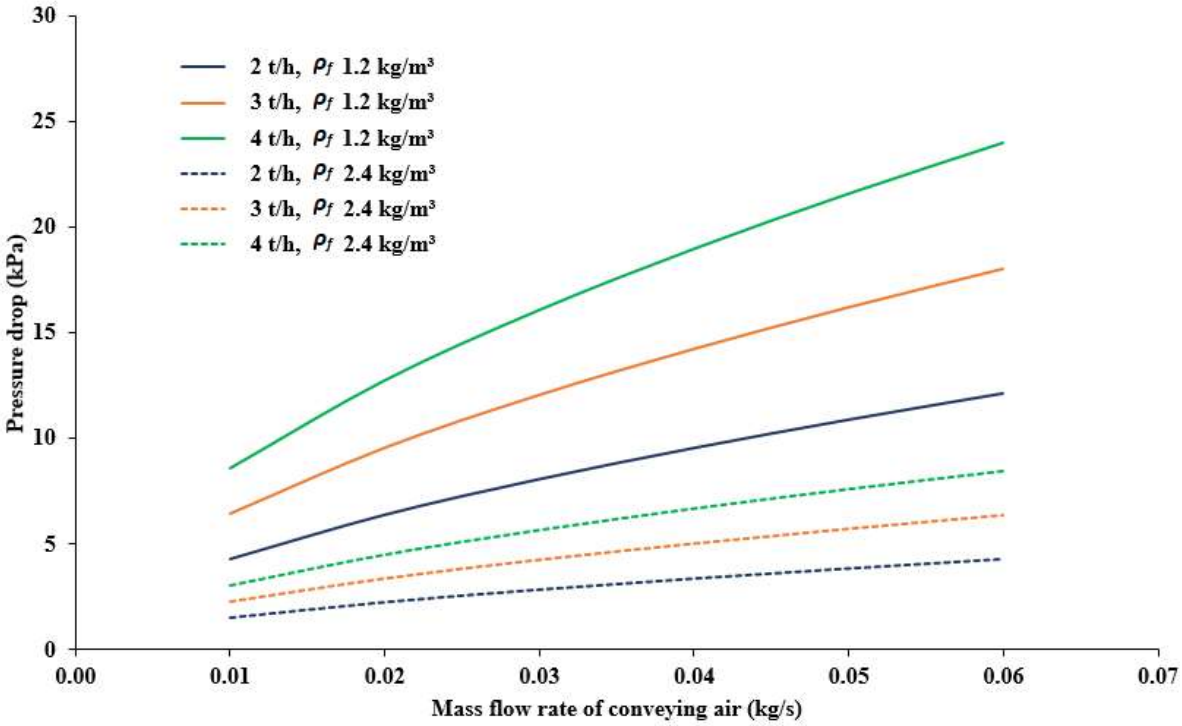

Figure 4.2: Predicted bend pressure loss characteristics for white Portland cement for R_b=1000 mm bend, I.D.= 53 mm with outlet air densities of 1.2 and 2.4 kg/m^3

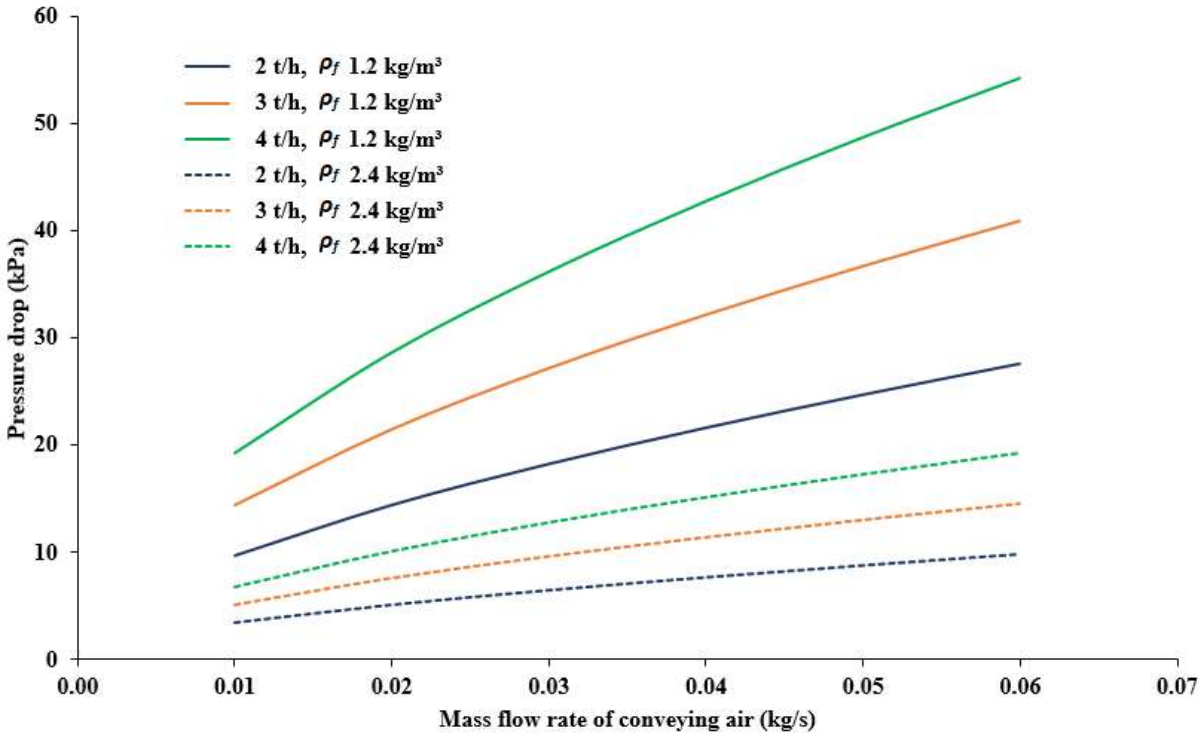

Figure 4.3: Predicted bend pressure loss characteristics for white Portland cement for R_b=1000 mm bend, I.D. = 42 mm with outlet air densities of 1.2 and 2.4 kg/m^3

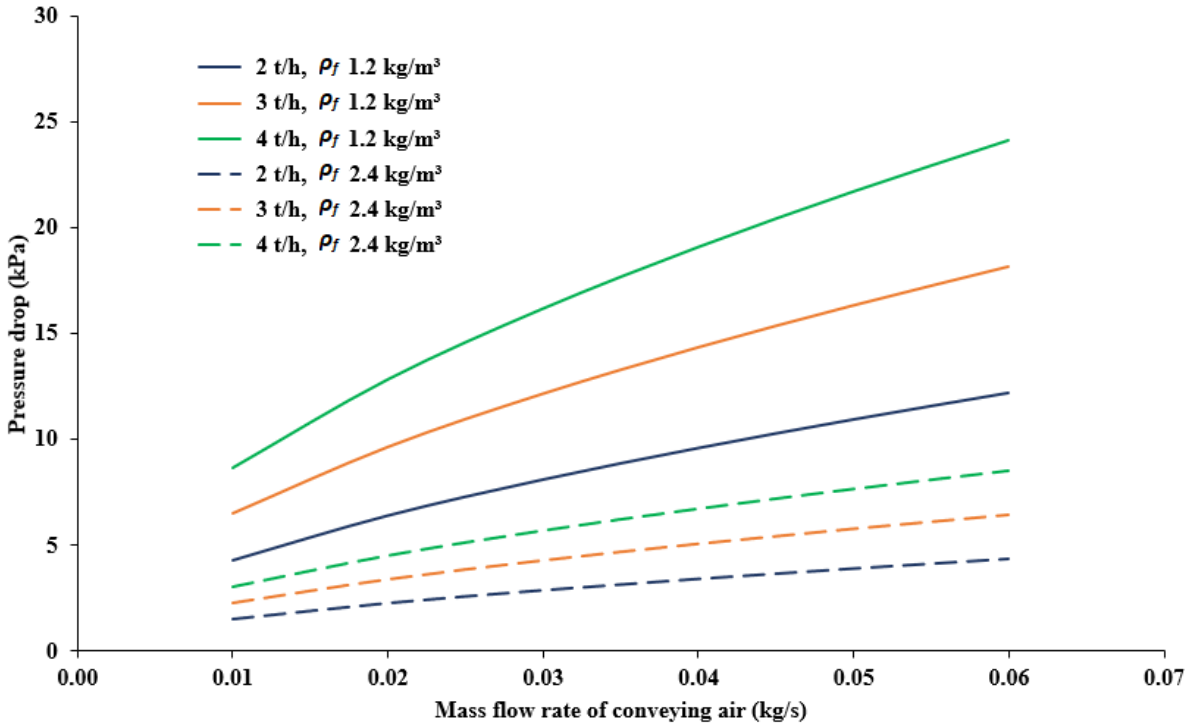

Figure 4.4: Predicted bend pressure loss characteristics for grey Portland cement for R_b=1000 mm bend, I.D.= 53 mm with outlet densities of 1.2 and 2.4 kg/m^3

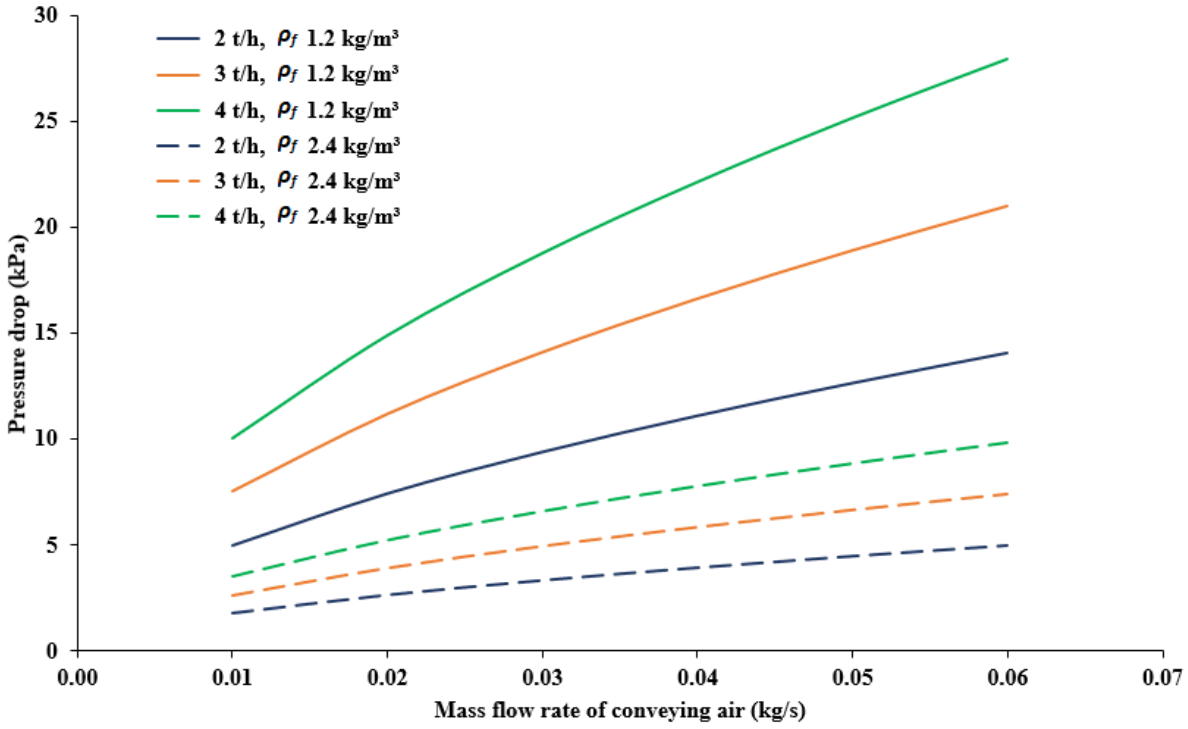

Figure 4.5: Predicted bend pressure loss characteristics for grey Portland cement for R_b=600 mm bend, I.D.= 53 mm with outlet densities of 1.2 and 2.4 kg/m^3

Figures 4.2 to 4.5 show that a decrease in the air density at the outlet of the bend by a factor of 2 can increase the pressure drop through the bend by a factor of 3 (approximately). This indicates that the pressure drop through a bend installed towards the end of a pipeline will be several times more than that through a bend near to the product feed point (towards the beginning of pipeline). This factor of enhancement seems to increase with the increase in material flow rate. A comparison between Figure 4.2 and Figure 4.3 shows that for a decrease in pipeline (or bend) diameter by about 25% has increased the pressure drop through the bend to 2 times. The factor of this change in magnitude is higher than what can be estimated for air or gas-only flows. A comparison between Figure 4.4 and Figure 4.5 shows that due to the reduction of the radius of curvature of bend from 1000 mm to 600 mm, the predicted pressure drop has increased by 15%. This seems to suggest that the effect of a sharp change in direction (and the associated drop of particle velocity at bend outlet and massive reacceleration loss)

dominates over the fact that in large radius bend, the particles have to travel through a long curvature length.

The new model (equation 4.2) was validated by using it to predict for bend losses for the experimental data provided in Pan (1992) and by comparing the predicted versus experimental values. Comparisons have been made between 4 different radii of curvatures of bends (100, 254, 450 and 1000 mm), 8 experimental conditions for fly ash (median size: 15 μm, particle density 2197 kg/m^3, loosed poured bulk density 634 kg/m^3) conveyed from fluidised dense to dilute-phase. The results are shown in Figure 4.6 and Figure 4.7.

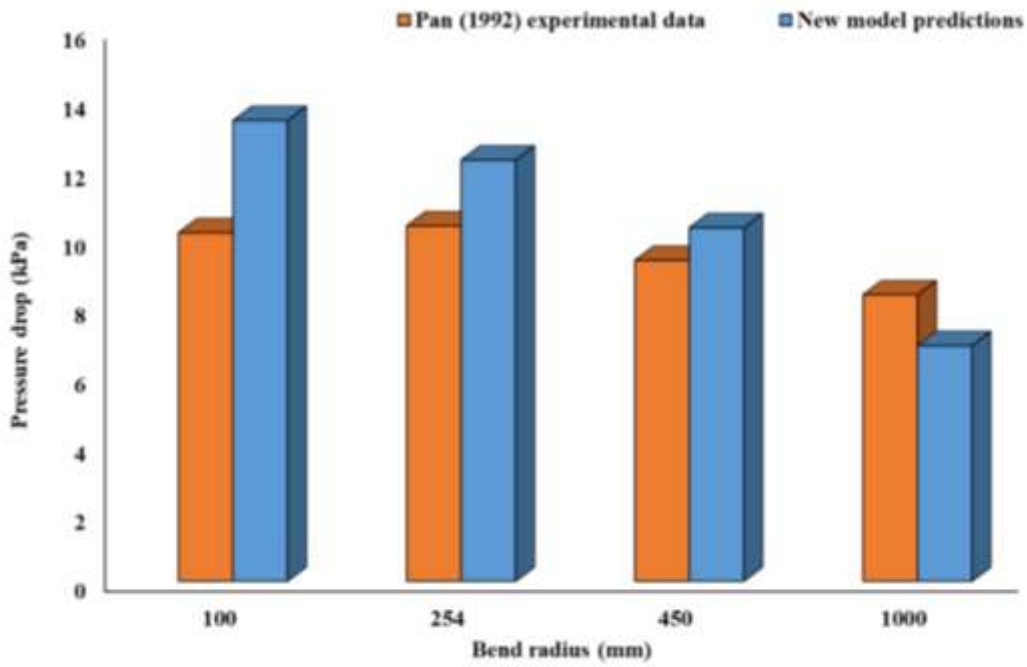

Figure 4.6: Comparison between Pan (1992) experimental data and predicted bend pressure drop using the new model (equation 4.2) for the different radius of curvature of bends at high solids flow rates and low superficial gas velocities (m*: 80 – 130)

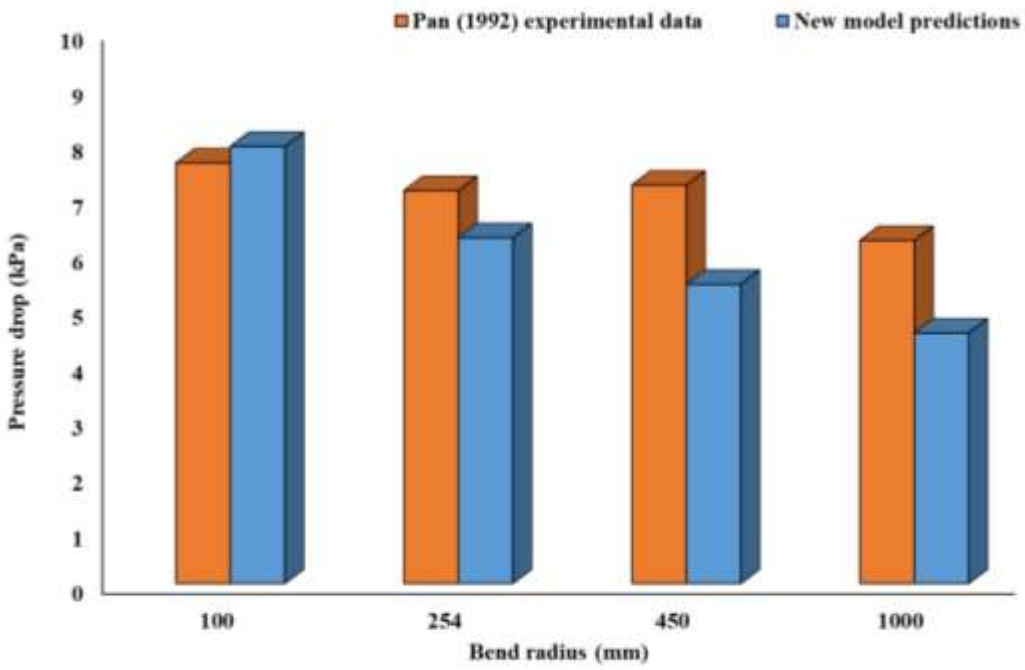

Figure 4.7: Comparison between Pan (1992) experimental data and predicted bend pressure drop using the new model (equation 4.2) for the different radius of curvature of bends at low solids flow rates and high superficial gas velocities (m*: 10-20)

Pan's (1992) data was considered to be suitable for validation because the data from which the new models were developed by the author and Pan, both belong to that of conveying of fine powders (fly ash and cement); i.e. both sets of powders/data sets represent fluidized dense-phase conveying. Table 4.3 provides the experimental conditions of those 8 tests and the absolute values of relative errors in percentage, calculated as [(experimental value – predicted value) / (experimental value)] × 100. Table 4.3 shows that the new model can predict the pressure loss in bend for fine powder consistently in the range of relative error of 4 to 32%. This seems to be an improvement compared to the performance of other models shown in Chapter 3.

Table 4.3: Experimental conditions for model (equation 4.2) validation tests and relative error in prediction

S.No	R_b (mm)	D (m)	R_b/D	m_s (kg/s)	m_f (kg/s)	Relative error in % (absolute)
1	100	0.0525	2	3.323	0.0271	32.25
2	254	0.0525	5	3.538	0.0409	18.55
3	450	0.0525	9	3.757	0.0282	10.19
4	1000	0.0525	19	3.366	0.0406	17.73
5	100	0.0525	2	1.012	0.0714	3.95
6	254	0.0525	5	1.001	0.0708	11.98
7	450	0.0525	9	1.008	0.0724	24.89
8	1000	0.0525	19	1.012	0.0714	26.97

In an attempt to find the performance of the new model (equation 4.4), Pan (1992) experimental data was further used to validate the predictions of this new model. The results are shown in Figure 4.8 and Figure 4.9.

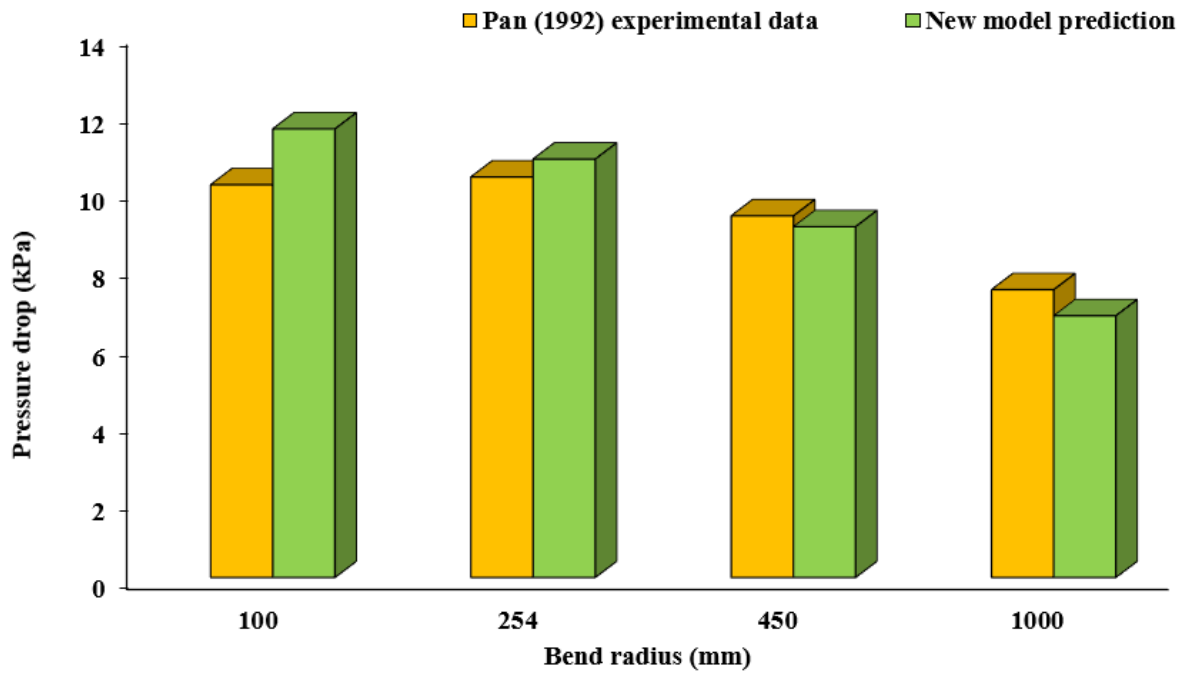

Figure 4.8: Comparison between Pan (1992) experimental data and predicted bend pressure drop using the new model (equation 4.4) for the different radius of curvature of bends at high solids flow rates and low superficial gas velocities (m*: 85 – 135)

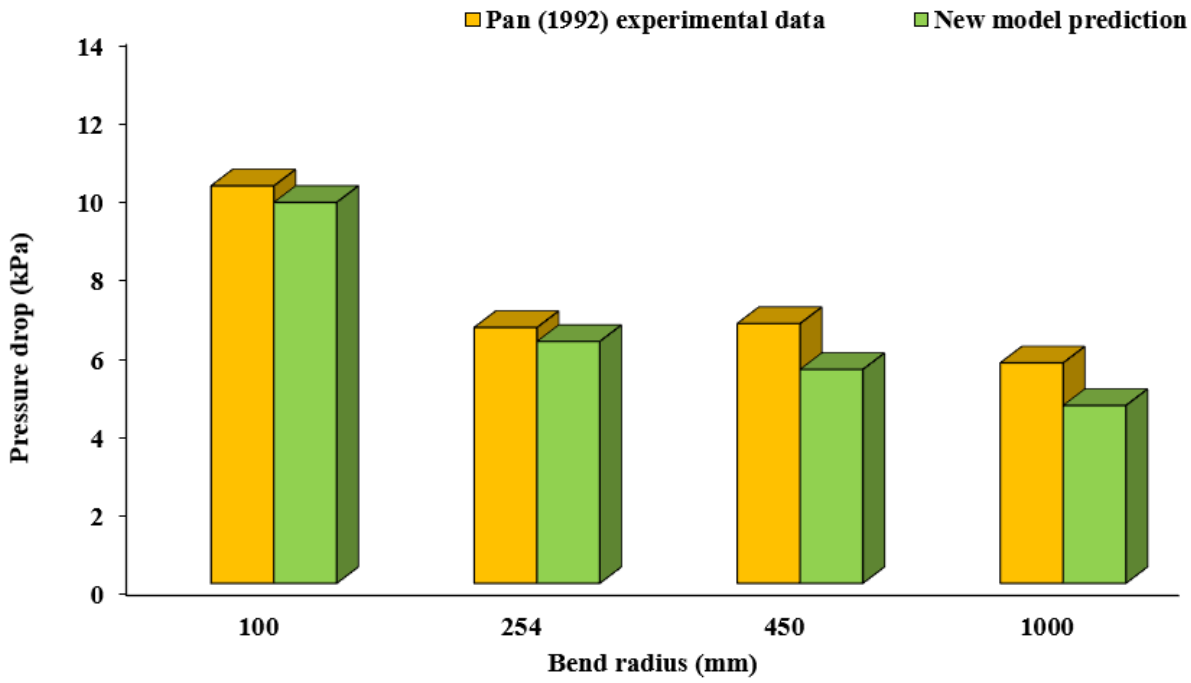

Figure 4.9: Comparison between Pan (1992) experimental data and predicted bend pressure drop using the new model (equation 4.4) for the different radius of curvature of bends at low solids flow rates and high superficial gas velocities (m*: 15-25)

Table 4.3 provides the sample experimental conditions and the absolute values of relative errors in percentage, calculated as [(experimental value – predicted value) / (experimental value)] × 100. Table 4.3 shows that the new model can predict the pressure loss in bends for fine powders consistently in the range of relative error of 3 to 19%. This seems to be an improvement as compared to the model in equation 4.2.

Table 4.4: Experimental conditions for new model (equation 4.4) validation tests and relative error in prediction

S.No	R_b (mm)	D (m)	R_b/D	m_s (kg/s)	m_f (kg/s)	Relative error in % (absolute)
1	100	0.0525	2	3.323	0.0271	14.2
2	254	0.0525	5	3.538	0.0409	4.5
3	450	0.0525	9	3.757	0.0282	3.0
4	1000	0.0525	19	3.565	0.0411	9.1
5	100	0.0525	2	1.7	0.0783	4.1
6	254	0.0525	5	1.233	0.0574	5.5
7	450	0.0525	9	1.238	0.0598	17.7
8	1000	0.0525	19	1.238	0.0583	19.3

Maximum and minimum values of error % are provided for a comparison purpose in the Table 4.4. It can be seen that the model equation 4.4 provide better results in the terms of providing a lower value of error % as compared with the model equation 4.2.

Table 4.5: Maximum and minimum values of error % for the new model equation 4.2 and new model equation 4.4.

Flow conditions	Error %	Model (equation 4.2)	Model (equation 4.4)
High m*	Maximum	32.2	14.2
Low m*		27.0	19.3
High m*	Minimum	10.2	3.0
Low m*		4.0	4.1

4.3 Interdependency of predictions of bend loss and straight-pipe pressure drop

In order to assess the interdependency of the predictions obtained from bend loss and straight pipe models, the following two exercises have been carried out: (a) a reliable, constant straight pipe model and various bend models (Chambers and Marcus 1986 to Cai et al. 2014) have been selected at a one-by-one basis. Total pipeline pressure drop conveying characteristics have been developed by adding the predicted pressure drop values obtained by using a reliable, constant straight pipe model and various bend models (a different bend model has been used each time); (b) two different straight pipe models have been used along with a constant bend model (Chambers & Marcus, 1986). Total pipeline pressure drop conveying characteristics have been developed by adding the predicted pressure drop values obtained using two different straight pipe models and a constant bend model (Chambers & Marcus, 1986). For both the above cases,

the fly ash conveying data (Mallick, 2009) of the University of Wollongong has been used (see Chapter 2).

Figure 4.10 to Figure 4.21 show the relative magnitudes of straight pipe to bend losses for the 69 mm I.D. and 168 m long pipeline and 105 mm I.D. and 168 m long pipelines for ash-flow rates of 19 t/h and 28 t/h, respectively for different existing bend models and that developed by the authors in this thesis (equation 4.4). To predict the pressure losses for the straight pipe, the two-layer model of Setia et al. (2016) has been used. The model has been provided by equation (4.5). This model has been provided in Chapter 3 but is being provided here again for completeness (and easy following of the reader). Relative magnitudes have been reported in terms of the percentage of total pipeline pressure drop. Losses due to verticals and initial acceleration (where the product is being fed into the pipeline by the blow tank) have been clubbed into the straight-pipe loss category.

$$\lambda_s = \tau_1 \left(8.04 \, (VLR)^{-0.22} \, (w_{fo}/V_f)^{1.48}\right) + \tau_2 \left(0.0043 \, C/V_f + 2(w_{f0}/V_f)/[(C/V_f) \, Fr^2]\right) \qquad (4.5)$$

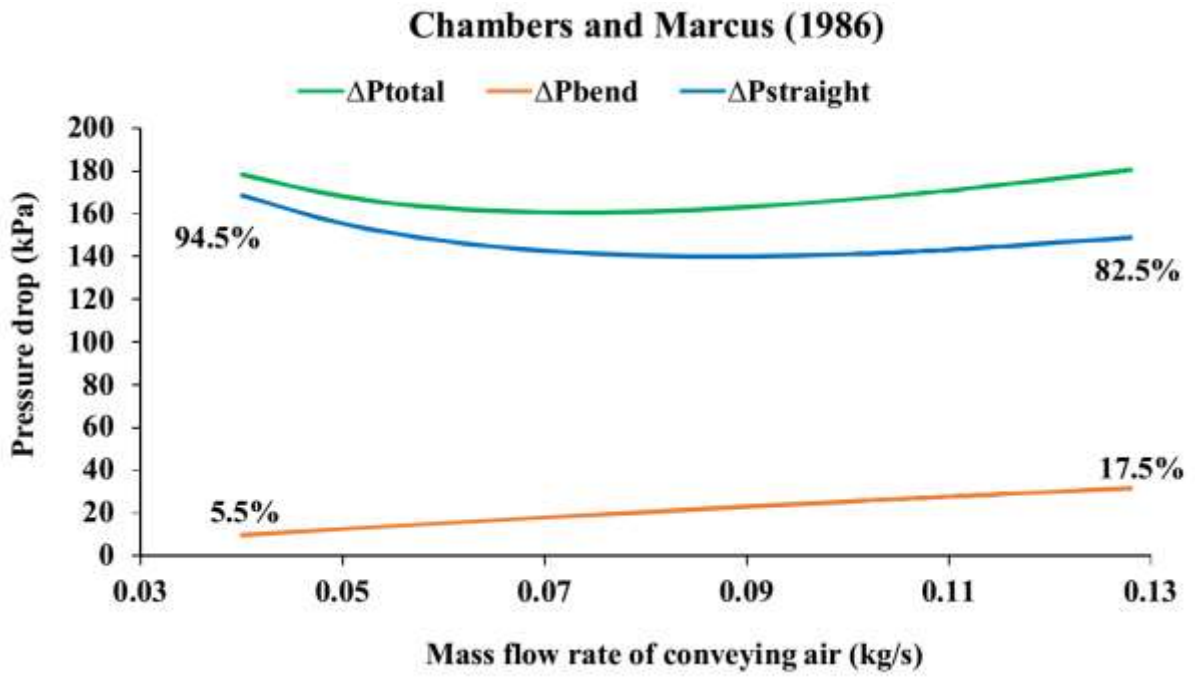

Figure 4.10: Trends of pressure drops in straight pipes versus bends predicted using Chambers and Marcus (1986) bend loss model (fly ash, D = 69 mm, L = 168 m, m_s = 19 t/h)

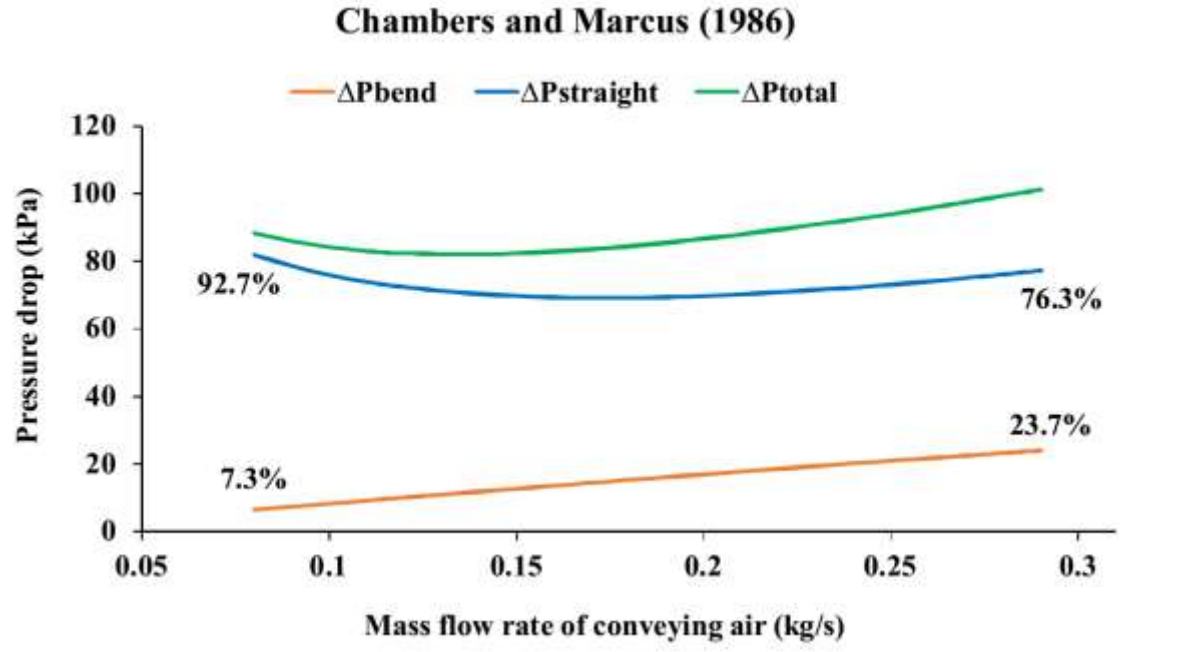

Figure 4.11: Trends of pressure drops in straight pipes versus bends predicted using Chambers and Marcus (1986) bend loss model (fly ash, D = 105 mm, L = 168 m, m_s = 28 t/h)

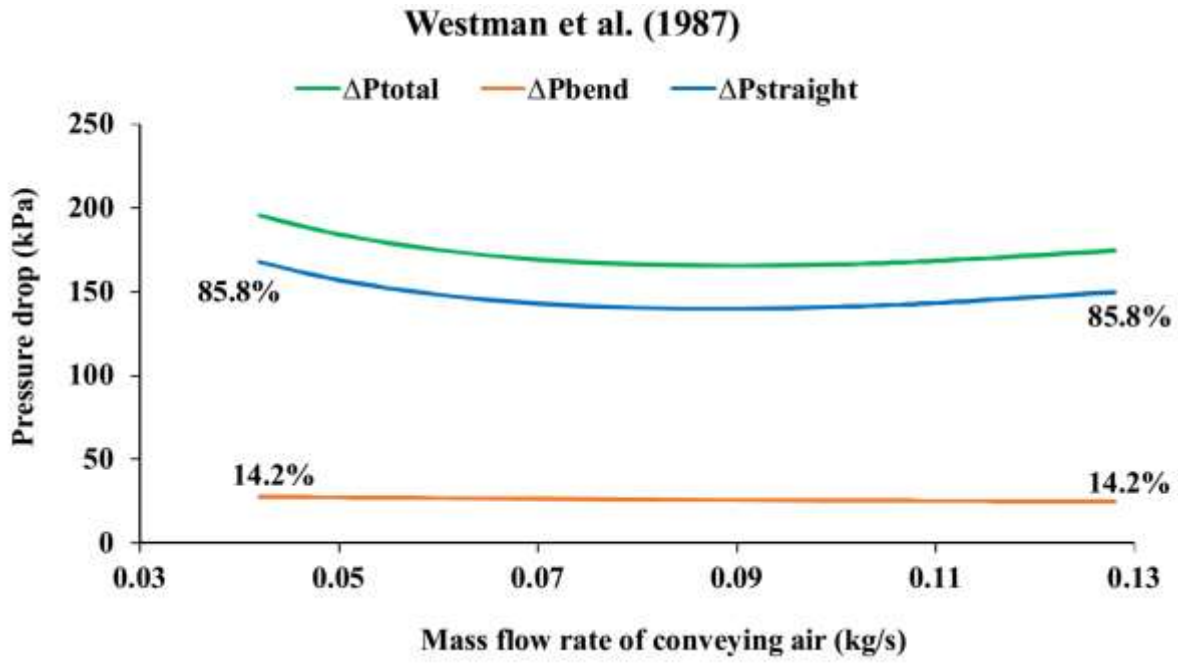

Figure 4.12: Trends of pressure drops in straight pipes versus bends predicted using Westman (1987) bend loss model (fly ash, D = 69 mm, L = 168 m, m_s = 19 t/h)

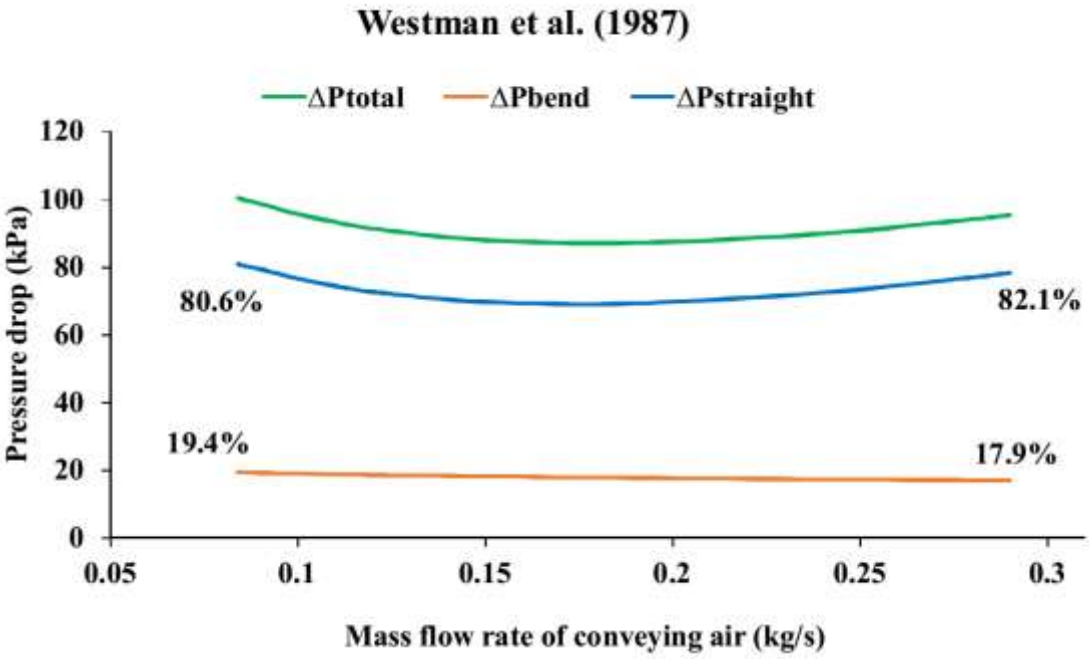

Figure 4.13: Trends of pressure drops in straight pipes versus bends predicted using Westman (1987) bend loss model (fly ash, D = 105 mm, L = 168 m, m_s = 28 t/h)

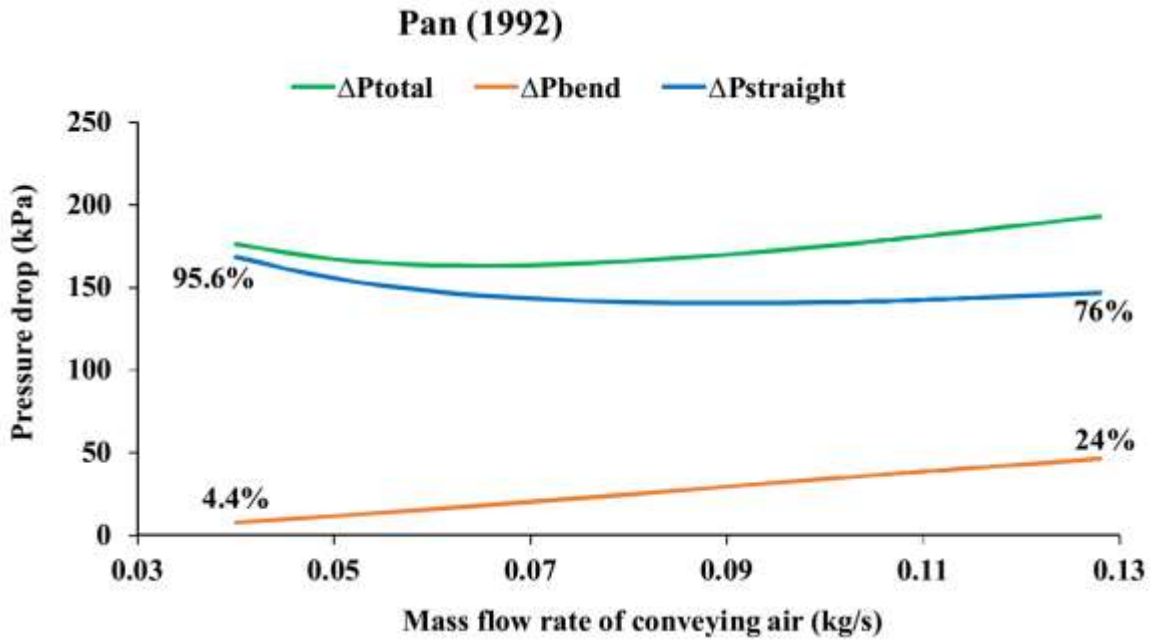

Figure 4.14: Trends of pressure drops in straight pipes versus bends predicted using Pan (1992) bend loss model (fly ash, D = 69 mm, L = 168 m, m_s = 19 t/h)

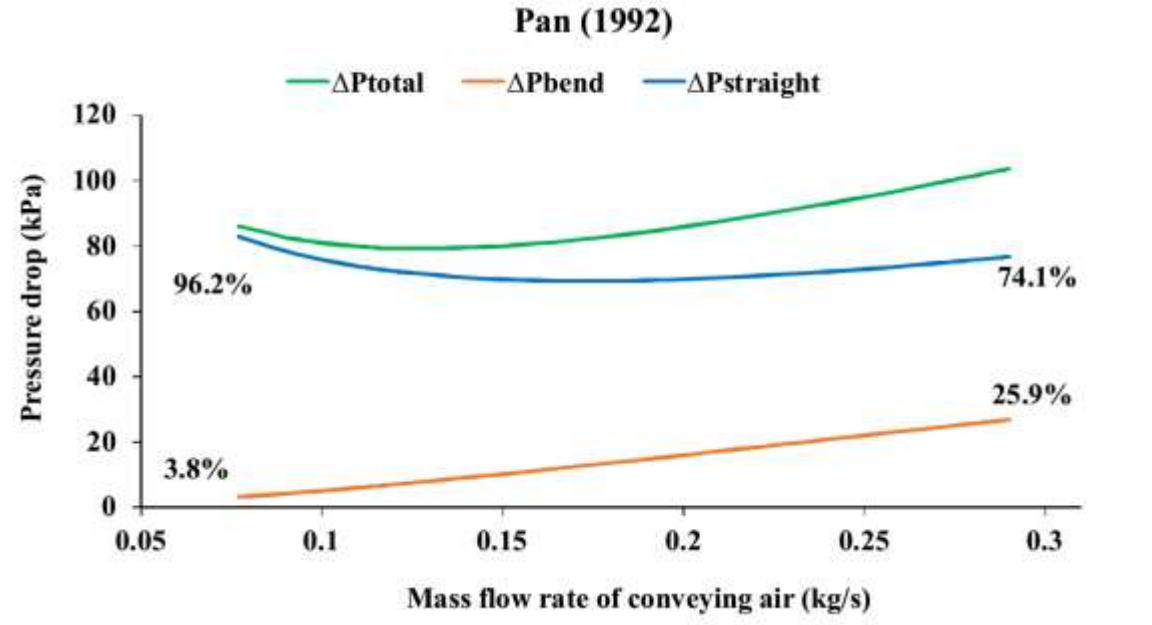

Figure 4.15: Trends of pressure drops in straight pipes versus bends predicted using Pan (1992) bend loss model (fly ash, D = 105 mm, L = 168 m, m_s = 28 t/h)

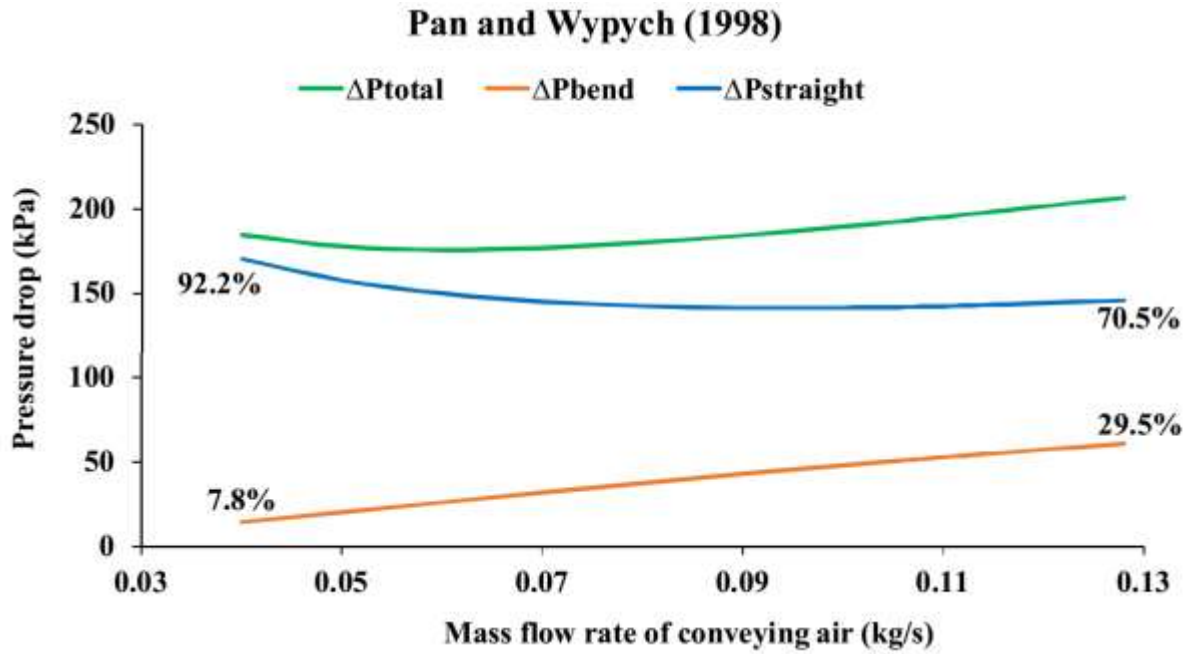

Figure 4.16: Trends of pressure drops in straight pipes versus bends predicted using Pan and Wypych (1998) bend loss model (fly ash, D = 69 mm, L = 168 m, m_s = 19 t/h)

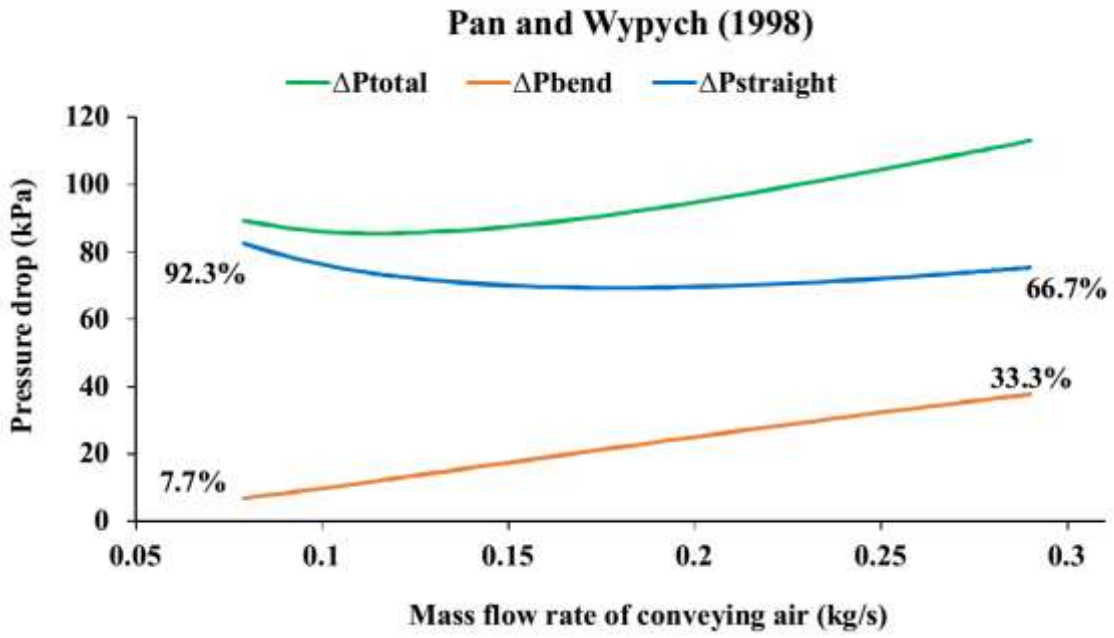

Figure 4.17: Trends of pressure drops in straight pipes versus bends predicted using Pan and Wypych (1998) bend loss model (fly ash, D = 105 mm, L = 168 m, m_s = 28 t/h)

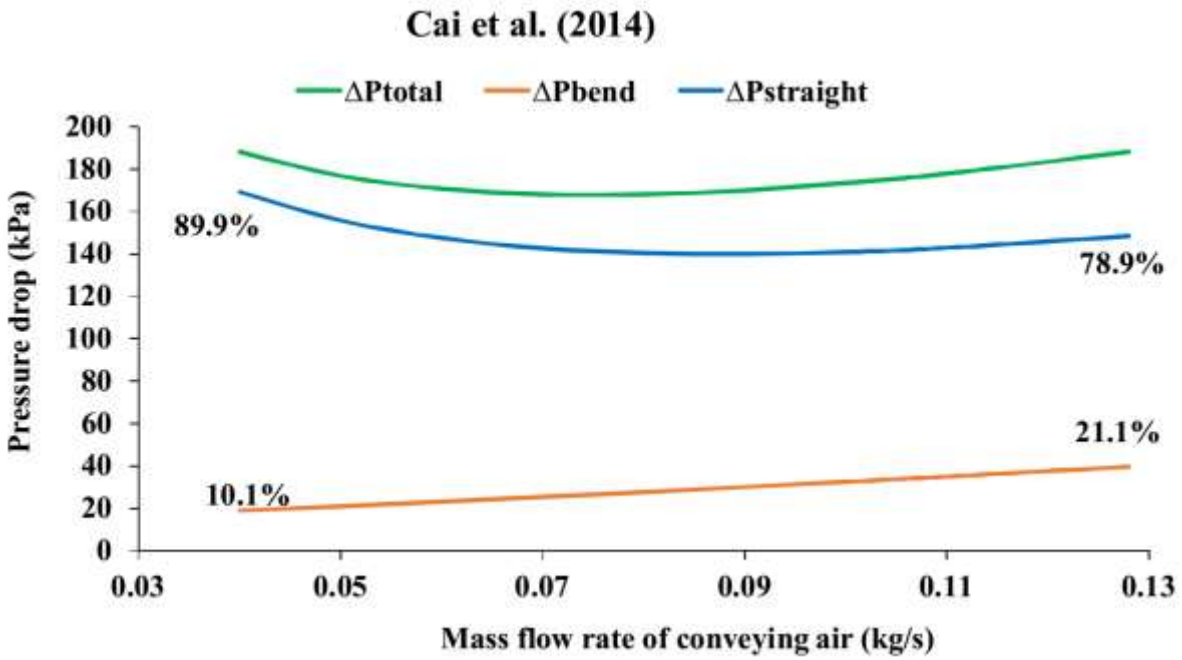

Figure 4.18: Trends of pressure drops in straight pipes versus bends predicted using Cai et al. (2014) bend loss model (fly ash, D = 69 mm, L = 168 m, m_s = 19 t/h)

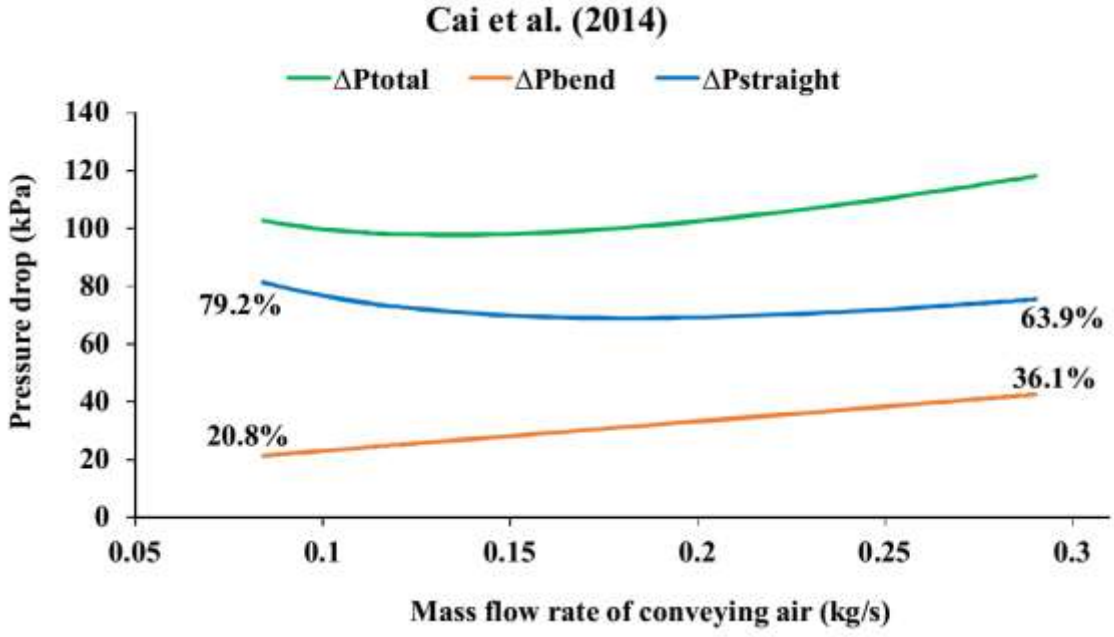

Figure 4.19: Trends of pressure drops in straight pipes versus bends predicted using Cai et al. (2014) bend loss model (fly ash, D = 105 mm, L = 168 m, m_s = 28 t/h)

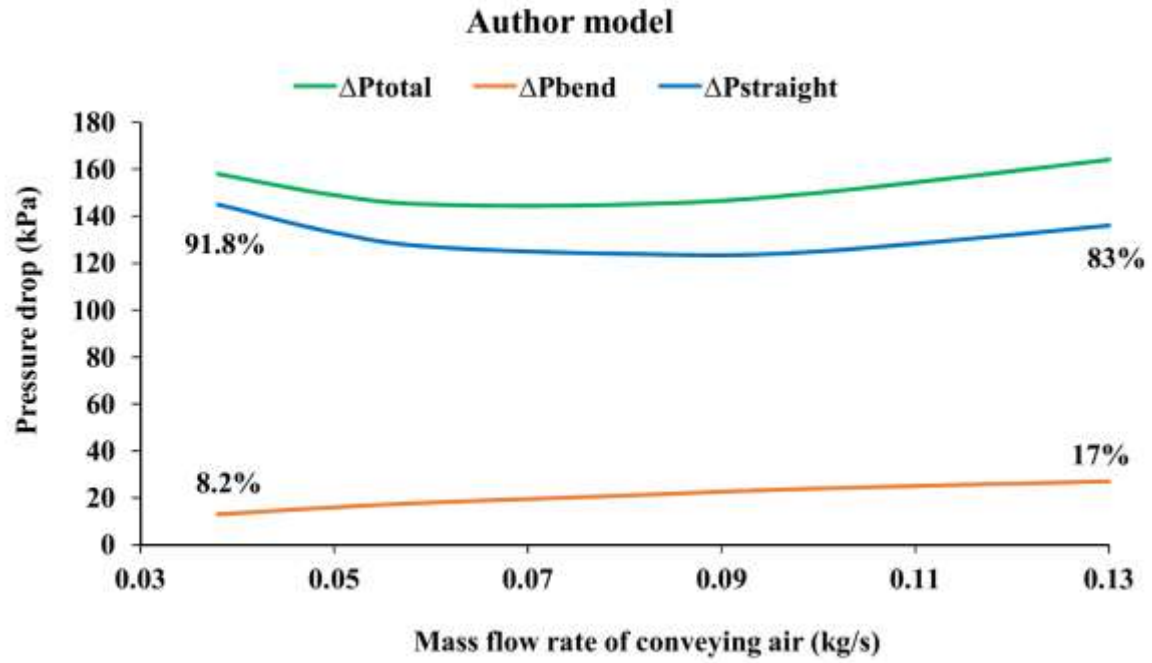

Figure 4.20: Trends of pressure drops in straight pipes versus bends predicted using author developed new bend loss model, equation 4.4 (fly ash, D = 69 mm, L = 168 m, m_s = 19 t/h)

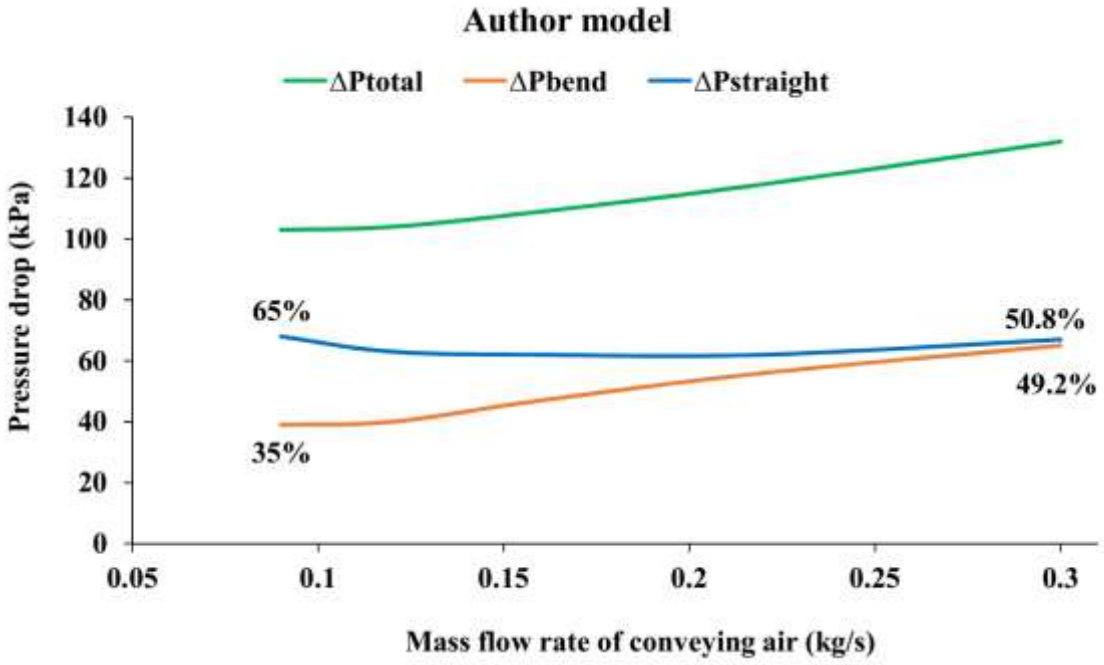

Figure 4.21: Trends of pressure drops in straight pipes versus bends predicted using author developed new bend loss model, equation 4.4 (fly ash, D = 105 mm, L = 168 m, m_s = 28 t/h)

A comparison amongst the figures (Figure 4.10 to Figure 4.21) shows that the percentage losses in the bends are more in case of the larger diameter pipe (i.e., the percentage of bend losses are more the 105 mm I.D. pipeline compared to the 69 mm pipe I.D.). Although the predicted straight pipe losses are less in the larger diameter pipeline, the relative magnitude of losses in bends is significantly higher compared to smaller diameter pipes (for the same number of bends). This validates that the mechanism of frictional losses in bends and straight pipes are quite different. Whereas all the models have shown an increase in pressure drop in bends with an increase in airflow rates, the bend loss predictions obtained using Westman et al. (1987) model show a different trend. Westman et al. (1987) model provide almost the same prediction in dense and dilute-phase. Except the Westman et al. (1987) model (which shows a trend contrary to all other models), the range of predicted bend loss in dense-phase varies from 4.4 to 10.1%, whereas the same in dilute-phase varies from 17 to 29.5% for the 69 mm I.D. and 168 m long pipeline; similar values in the 105 mm I.D. and 168 m long pipeline for the dense and dilute-phases are 3.8 to 35% and 23.7 to 49.2%, respectively. It is evident that the differences in the range of predictions get enhanced with an increase in pipe diameter.

Figure 4.22 and Figure 4.23 show the relative magnitudes of straight pipe and bend losses for the 69 mm I.D. and 168 m long pipeline with ash flow rates of 19 t/h by using Chambers and Marcus (1986) bend loss model. To predict the pressure losses for the straight pipe, the two different straight pipe pressure drop models have been used, i.e., the two-layer model of Setia et al. (2016) (see equation 4.5) and uniform flow model Setia et al. (2017). The uniform flow model of Setia et al. (2017) has been provided by equation (4.6).

$$\lambda_s = 7.94\ (VLR)^{-0.26}\ (w_{fo}/V_f)^{1.51} \qquad (4.6)$$

Relative magnitudes have been reported in terms of the percentage of total pipeline pressure drop. Losses due to verticals and initial acceleration (where the product is being fed into the pipeline by the blow tank) have been clubbed into the straight-pipe loss category.

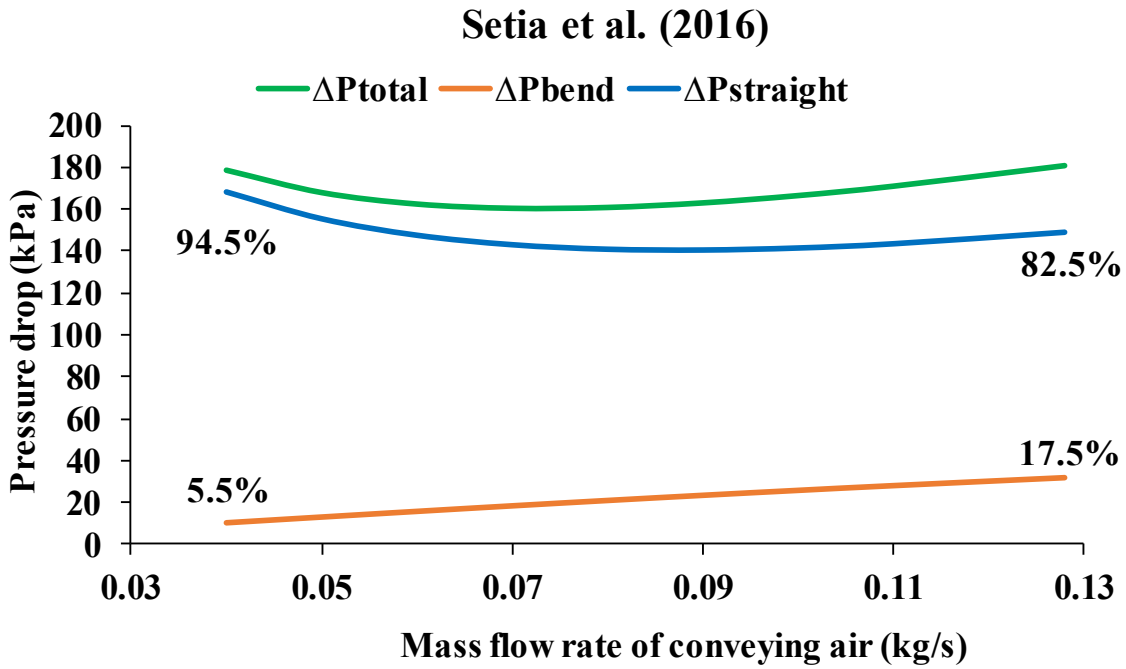

Figure 4.22: Trends of pressure drops in straight pipes versus bends predicted using Setia et al. (2016) straight pipe model and Chambers and Marcus (1986) bend model (fly ash, D = 69 mm, L = 168 m, m_s = 19 t/h)

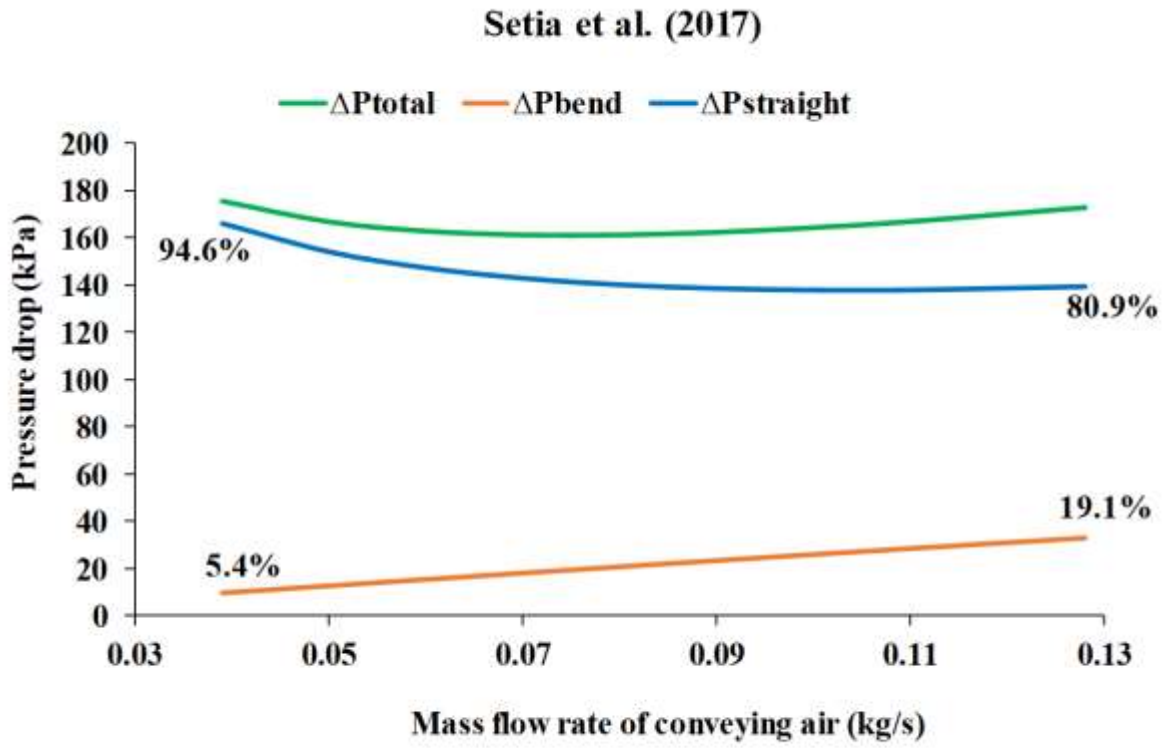

Figure 4.23: Trends of pressure drops in straight pipes versus bends predicted using Setia et al. (2017) straight pipe model and Chambers and Marcus (1986) bend model (fly ash, D = 69 mm, L = 168 m, m_s = 19 t/h)

The results show that while selection of different bend loss model (with a constant straight pipe model) significantly alters the trends of pneumatic conveying characteristics (Figure 4.10 to Figure 4.21), the opposite situation (i.e., where the bend model is the same, but the straight pipe models are different) do not result in any appreciable changes in the relative share of predicted bend and straight pipe losses.

CHAPTER 5

MODELLING BEND PRESSURE DROP IN CURVATURE AND REACCELERATION ZONE

5.1 Introduction

While the use of bends in pneumatic conveying systems adds to the flexibility of routing the pipelines and add to the system compactness, bends are also known to result in a substantial amount of pressure drop due to the flow of solids and air through them (Molerus, 1996; Wypych, 1999). The existing empirical models provide reliable predictions for bend pressure drop when used with the researchers' data, but they have not been adequately accurate for different products and setup conditions (Tripathi et al. 2018). Moreover, existing models for solids friction factor through bends use a combined bend loss factor (or solids friction through bends) for the curvature and reacceleration zones, i.e. these models do not differentiate between losses occurring in the curvature and reacceleration zones (straight pipe section just following the bend). In the curvature zone, the pressure drop is attributed to the change of momentum (due to change of direction of flow) and particle-particle-air-wall frictions of solids and air flowing through the bend. After the solid particles exit the bend, the particles get reaccelerated to their steady-state velocities by absorbing energy from the gas stream (Pan and Wypych 1998; Chunhui et al. 2012; Cai et al. 2014). As the mechanisms of pressure losses in the curvature and reacceleration zones are significantly different, it would be appropriate to develop a bend pressure drop model that would consider each of the pressure loss components separately. This chapter describes the different components of total bend pressure drop through the bend and their trends with respect to other conveying parameters. This chapter also includes a new expression for total pressure drop through the bend having separate models for different bend loss components.

5.2 Pressure drop through curvature, primary and secondary reacceleration zones

In an attempt to enhance the understanding of the effect of particle properties, bend and pipeline configurations on the pressure drop through the bends, the following five areas of concerns were unidentified where it was considered necessary to carry out a detailed experimental study with the objectives of (a) relative share of pressure losses within the bend (curvature zone) and after the bend (reacceleration zone); (b) effect of change of powder properties on the pressure drop of bends; (c) effect of different radius of curvature on bend pressure drop; (d) effect of different pipe diameter on bend pressure drop; (e) effect of conveying velocity on bend pressure drop. Figures 5.1 and 5.2 show the distribution of total bend loss within the bend and at the reacceleration zone (straight pipe portion after the bend) for higher and lower ranges of solids loading ratio for different combinations of pipe diameters, product properties, pipeline diameters, radius of curvature of bends and bend locations in test rig. In this section of the study, higher and lower solids loading ratios have been considered to be in the ranges of 63 to 19 and 43 to 10, respectively. Tables 5.1 and 5.2 show the experimental conditions for these cases of higher and lower loading ratio ranges. Figures 5.1 and 5.2 show the measured static pressures just before and after bends (refer to Figure 2.1 for the location of pressure tapping points). For the first test bend location (B1), P3 to P4 zone (on a straight pipe section) has been termed as the reacceleration zone 1 (primary reacceleration zone), and P4 to P6 zone has been termed as the reacceleration zone 2 (secondary reacceleration zone). The pressure drop between P2 to P3 corresponds to the loss occurring in the curvature zone of the bend. Similar categories have been made for the second test bend location (B4) with P7 to P11 tapping point locations. The pressure drop in the curvature zone is contributed by the change in momentum (due to change of direction of flow) and particle-particle-air-wall frictions of solids and air flowing through the bend. It should be remembered that particles are likely to be pushed outward to the surface of bend while going through the curvature, thus possibly generating a zone of closely

spaced “rope” of particles having enhanced particle to particle friction (Pan and Wypych 1998; Chunhui et al. 2012; Cai et al. 2014). In the primary and secondary reacceleration zones, the pressure drop is caused by the combined effects of particle reacceleration and particle-particle-air-wall friction (Tripathi et al. 2018). Reacceleration loss is attributed due to the slip velocity between the gas and solids phases at the exit to the bend. Just at exit to the bend, the slip velocity is maximum due to the slowing down of particles in the curvature zone of bends (due to the increased solids-solids-wall interactions in a concentrated zone along the outer radius of the bend). Therefore, the initial reacceleration loss is more. As the powders continue to accelerate, the slip velocity and the requirement of energy recovery reduces. Therefore, in the second part of reacceleration zone, the reacceleration loss is relatively less. At the exit of the bend, the particles are slowed down due to the change in momentum through the bend and enhanced particle-wall friction (Pan and Wypych 1998). Subsequently, the particles get reaccelerated to their steady-state velocities by absorbing energy from the gas stream. It is suspected that in the reacceleration zone, the pressure drop caused by the reacceleration of particles is much higher compared to that caused by particle-particle-air-wall friction (Pan and Wypych 1998; Chunhui et al. 2012; Cai et al. 2014). The pi-charts in Figures 5.1 and 5.2 show the percentage of total bend pressure loss (sum of losses occurring in the curvature and reacceleration zones) occurring in the curvature, reacceleration zones 1 and 2.

Table 5.1: Selected experimental condition for an investigation into pressure drop distribution for higher solids loading ratio range (63 to 19)

Case no.	**Product**	**R (mm)**	**D (mm)**	**R/D**	**Location**	**m_f (kg/s)**	**m_s (kg/s)**
1	Grey Portland cement	600	53	11	B1	0.039	2.15
4	Grey Portland cement	1000	53	19	B4	0.041	2.16
5	Fly ash	1000	53	19	B1	0.034	2.13
7	White Portland cement	1000	42	24	B1	0.048	0.89

Table 5.2: Selected experimental condition for an investigation into pressure drop distribution for lower solids loading ratio range (43 to 10)

Case no.	**Product**	**R (mm)**	**D (mm)**	**R/D**	**Location**	**m_f (kg/s)**	**m_s (kg/s)**
1	Grey Portland cement	600	53	11	B1	0.048	0.72
4	Grey Portland cement	1000	53	19	B4	0.039	1.69
5	Fly ash	1000	53	19	B1	0.043	0.79
7	White Portland cement	1000	42	24	B1	0.048	0.042

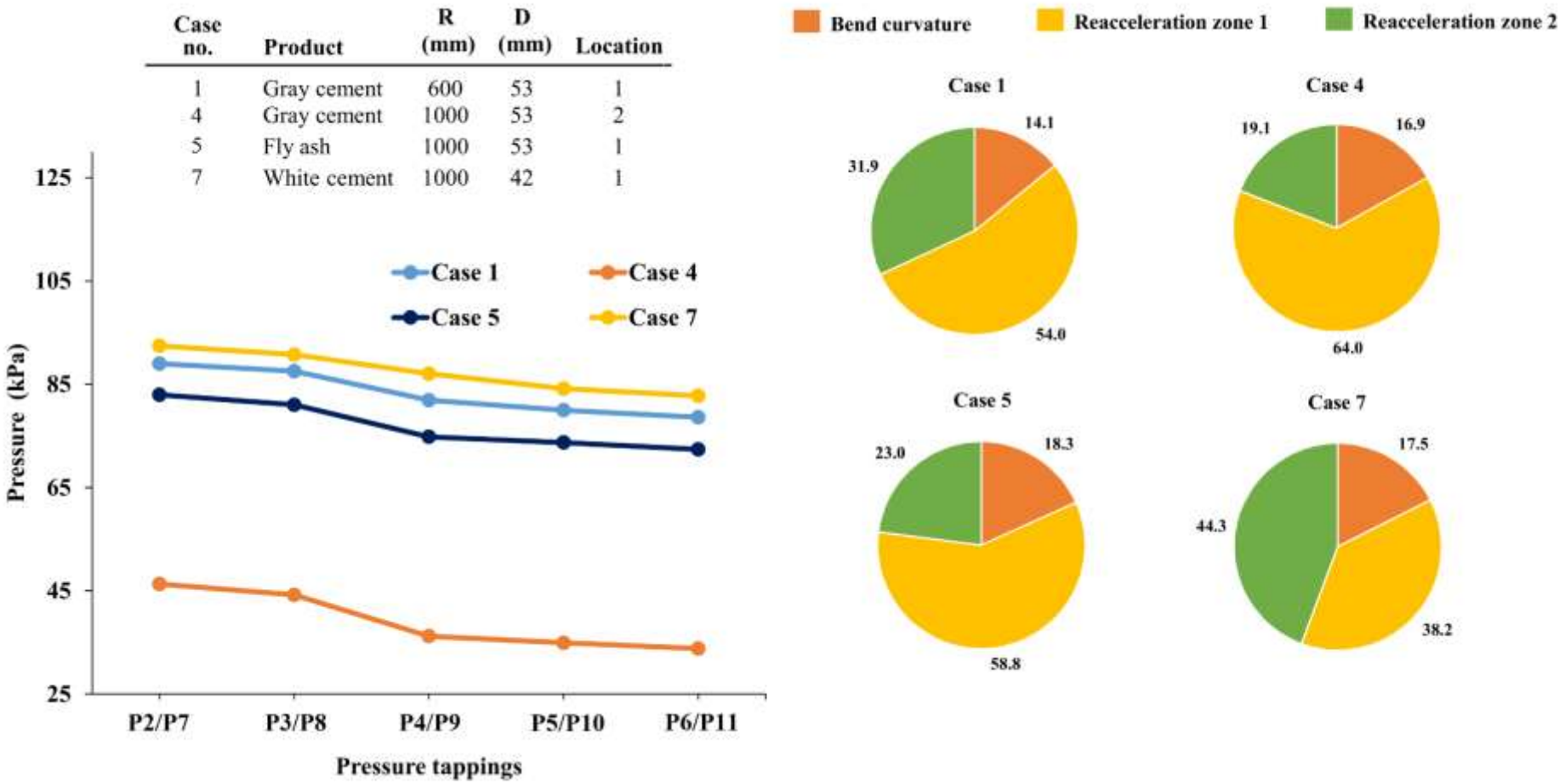

Figure 5.1: Pressure drop percentages in the bend curvature, primary reacceleration zone, and secondary reacceleration zone for different products, pipeline diameters, bend radius of curvatures and locations for high solids flow rates and low superficial gas velocities (m*: 63 to 19)

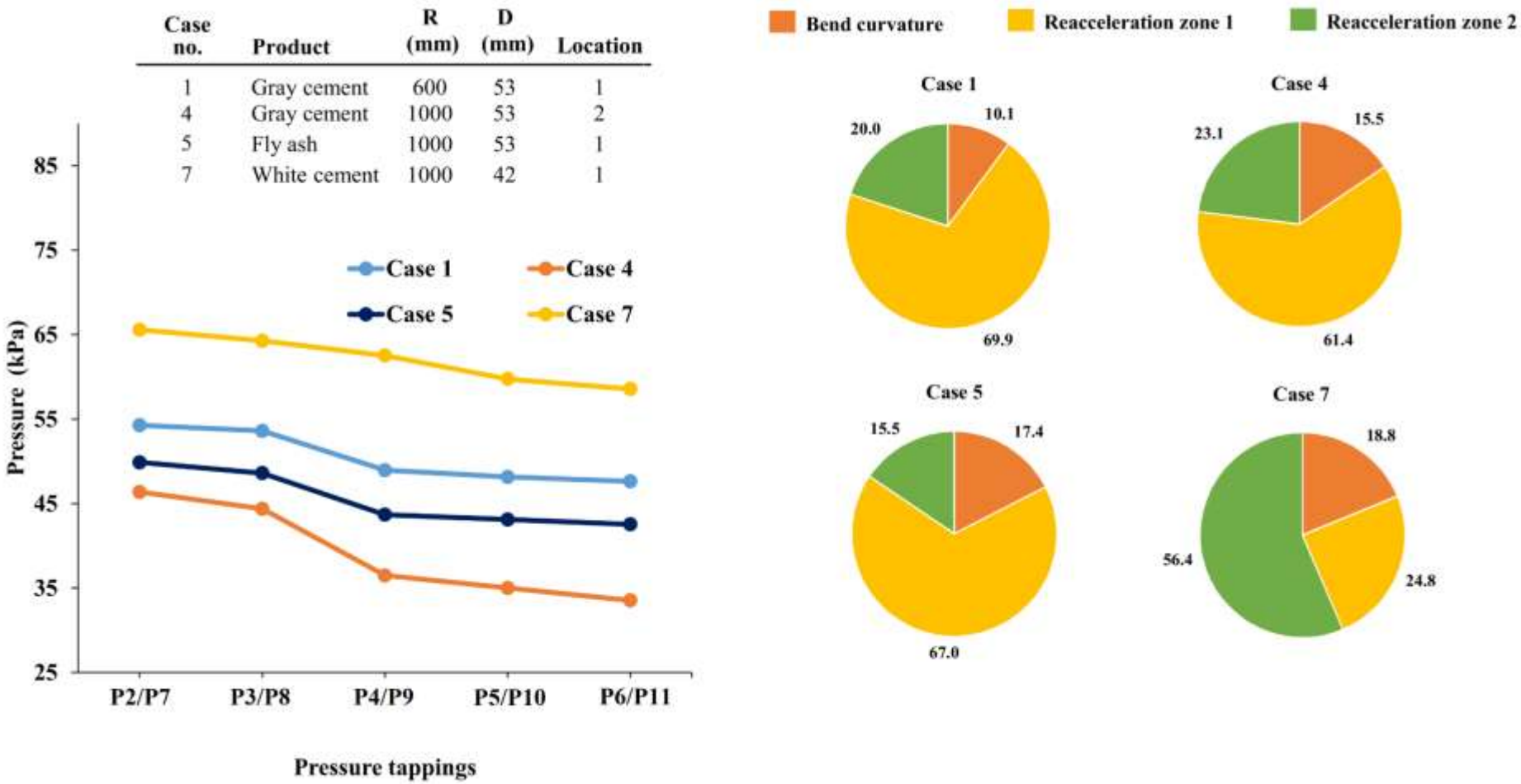

Figure 5.2: Pressure drop percentages in the bend curvature, primary reacceleration zone, and secondary reacceleration zone for different products, pipeline diameters, bend radius of curvatures and locations for low solids flow rates and high superficial gas velocities (m*: 43 to 10)

Figures 5.1 and 5.2 show that for high solids loading ratio, the losses in the curvature portion range from 14.1 to 18.3%. The same for lower solids loading ratio is in the range of 10.1 to 18.8%. Therefore, the pressure drop in the curvature portion remains almost similar irrespective of the regime of the solids loading ratio. For the cases of 1, 4, and 5, the losses in the primary reacceleration zone vary from 54 to 64% in Figure 5.1, whereas the same is from 61.4 to 69.9% in Figure 5.2. For these cases, the losses in the secondary reacceleration zone vary from 19.1 to 31.9% in Figure 5.1, whereas the same is from 15.5 to 23.1% in Figure 5.2. This shows that for both higher and lower solids loading ratio for these cases, the losses in the primary acceleration zone is much more significant than that occurring in the secondary acceleration zone. The relative percentage losses in the secondary reacceleration zone have increased with a decrease in solids loading ratio for these cases. For the cases of bend loss through a smaller pipe (case 7, where the pipe internal diameter is 42 mm compared to 53 mm in case numbers 1, 4 and 5), the secondary reacceleration losses are quite substantial compared to the primary reacceleration losses; in fact, the pressure drop is more in the secondary reacceleration zone compared to the primary acceleration zone. Nonetheless, overall, the combined losses occurring in the primary and secondary reacceleration zones have been found to be typically 4 to 8 times more than that occurring in the curvature zones. Results provided in Figure 5.1 and Figure 5.2 show certain typical characteristics; similar results were obtained in several other conveying trials.

5.3 New bend model development by separately addressing different pressure drop components

In this section, the effects of different powders, the radius of curvature of bends, pipeline diameters, and conveying velocities on the overall pressure drop through the bend (combining losses in the curvature and acceleration zones) have been studied. Experimental results for

different cases have been compared. For a comprehensive evaluation, experimental results of total bend losses have been first compared, followed by an investigation into the bend loss characteristics. To develop the bend loss characteristics, experimental data of pressure drop through the bends were modelled. For the modelling of pressure drop through the bends, the following format has been often used by previous researchers (Pan and Wypych 1998; Chunhui et al. 2012; Cai et al. 2014), as given by equation (5.1). Air density and velocity values used in the model correspond to that prevailing at the exit to the bend. The model considers pressure drops due to the air and solids differently.

$$\Delta p_b = \left(\lambda_{bf} + m^* \lambda_{bs}\right) \cdot \frac{\rho_f {V_f}^2}{2} \tag{5.1}$$

Existing models for solids friction factor through bends do not differentiate between losses occurring in the curvature and reacceleration zones (straight pipe section just following the bend). In the curvature zone, the pressure drop is attributed to the change of momentum (due to change of direction of flow) and particle-particle-air-wall frictions of solids and air flowing through the bend. Due to this friction, the velocity of the solid particles gets decelerated while going through the bend, and at the exit, this velocity becomes much lower than their steady-state velocity. Subsequently, after the solid particles exit the bend, the particles get reaccelerated to their steady-state velocities by absorbing energy from the gas stream (Pan and Wypych 1998; Chunhui et al. 2012; Cai et al. 2014). Also, there would be particle-particle-air-wall friction in the reacceleration zone (Tripathi et al. 2015), though it is generally reported that the particle reacceleration is the leading cause of bend pressure drop in the reacceleration zone (Pan and Wypych 1998; Chunhui et al. 2012; Cai et al. 2014). It is evident that the mechanisms of pressure losses in the curvature and reacceleration zones are significantly different. Therefore, it would not be appropriate to combine the pressure drops in these two regimes (with very different flow mechanisms) into a single solids' friction factor term. With

this consideration, two different solids friction factor terms or models have been introduced in this study – one for the curvature zone and one for the reacceleration zone, as given by equations (5.2) and (5.3), respectively. Models were developed using the test data of 209 number of experiments. Air density and velocity values used in the model correspond to that of exit to the bend. The ratio of air density term in the model addresses the location of bends in the pipeline (air density decreases in the direction of flow). The R/D term describes the effect of the radius of curvature of bend. The d_{50}/D term addresses the particle size effect on solids friction and reacceleration. The gas Froude number term describes the effect of conveying velocity on the particle-particle-wall friction and reacceleration velocity requirement. Figure 5.3 shows a comparison between the experimental versus predicted pressure drop.

Curvature zone: $\lambda_{bsc} = 10^{-2.012} \left(\frac{\rho_f}{\rho_s}\right)^{-1.028} \left(\frac{R}{D}\right)^{0.629} \left(\frac{d_{50}}{D}\right)^{0.273} (Fr)^{-1.261}$ (5.2)

Reacceleration zone: $\lambda_{bsr} = 10^{-4.675} \left(\frac{\rho_f}{\rho_s}\right)^{-1.817} \left(\frac{d_{50}}{D}\right)^{0.444} (Fr)^{-1.119}$ (5.3)

Where, $\lambda_{bs} = \lambda_{bsc} + \lambda_{bsr}$ (5.4)

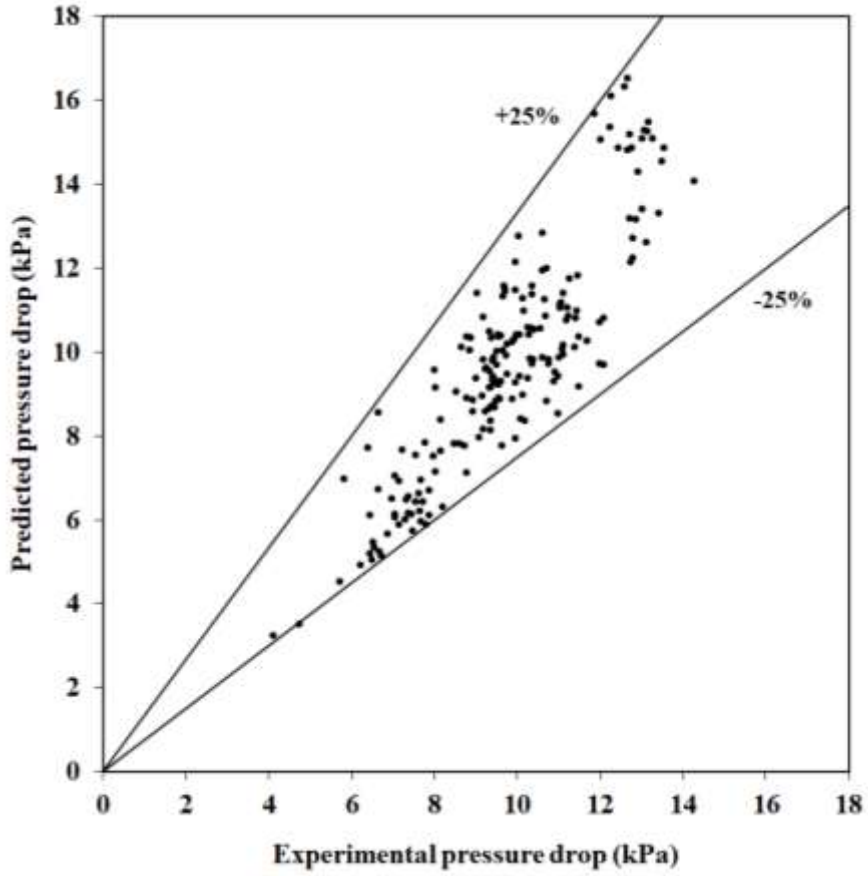

Figure 5.3: Comparison of model prediction versus experimental pressure drop through bends

Using these models (equations 5.2 and 5.3), predictions of pressure drops at the curvature and reacceleration zones have been estimated for different powders, the radius of curvature of bends, pipeline diameters, and gas velocities. Individual pressure drops estimated for curvature, and reacceleration zones have been added to develop plots for total bend loss. These estimated plots are provided in Figures 5.5, 5.7, 5.9, and 5.10. Experimental plots are provided in Figures 5.4, 5.6, and 5.8. Figure 5.4 shows the experimental plots for grey cement, white cement, and fly ash conveyed through 53 mm internal diameter of pipeline and bend radius of curvature of 1000 mm. Experiment data were selected, having similar values of solids and flow rates and solids loading ratio for the ease of comparison. Figure 5.5 shows the estimated bend loss

characteristics for a range of mass flow rates of air and 4 t/h of product flow rates (using the models provided by equations 5.2 and 5.3) for 53 mm internal diameter of pipeline and bend radius of curvature of 1000 mm.

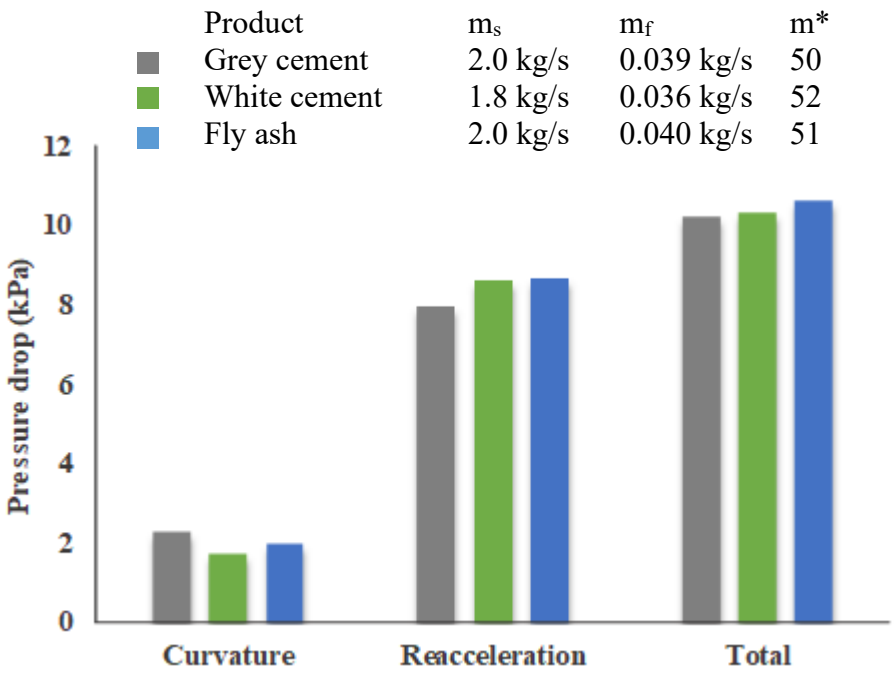

Figure 5.4: Comparison of the bend pressure drop for grey cement, fly ash and white cement for 53 mm internal diameter of pipeline and bend radius of curvature of 1000 mm

Results (Figure 5.4) show that the losses in the reacceleration zone are about four times higher than that occurring in the curvature zone. Total bend loss is lowest for the case of grey cement and highest for the case of fly ash. This could be due to the larger particle size of fly ash compared to cement powders.

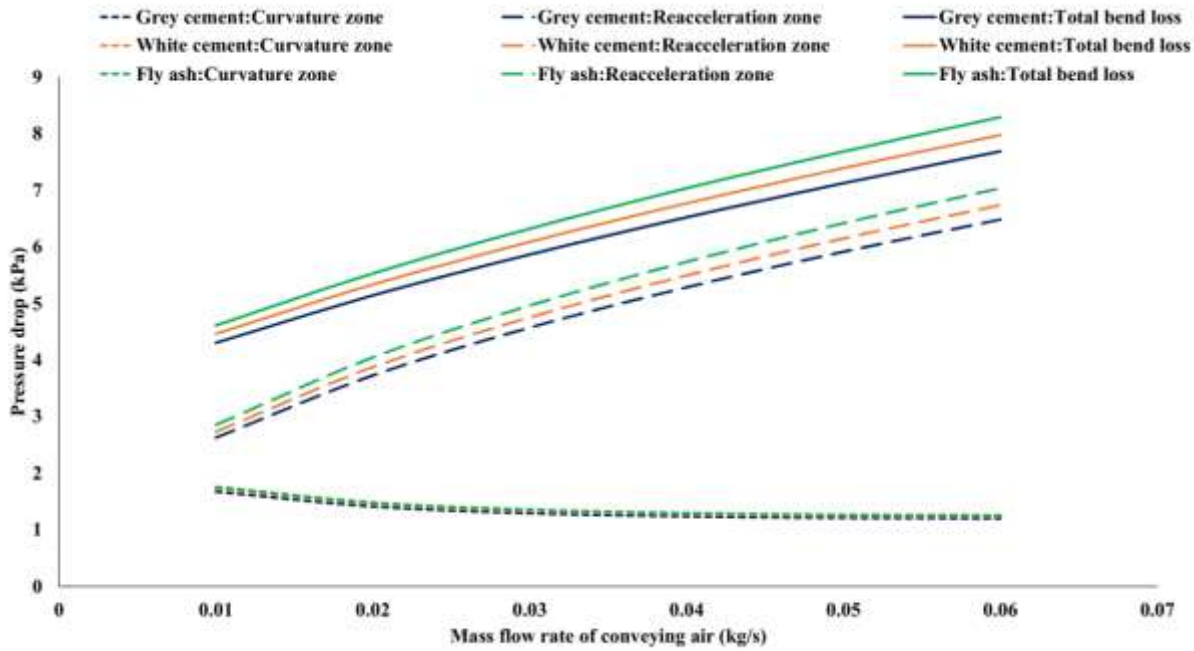

Figure 5.5: Comparison of the estimated bend pressure drops for grey cement, fly ash and white cement for a product flow rate of 4/h for 53 mm internal diameter of pipeline and bend radius of curvature of 1000 mm

Figure 5.5 shows that with an increase in airflow rates, there is a slight decrease in pressure drop characteristics in the curvature zone. There is a very slight difference between the plots of different powders in this zone. However, the pressure drop characteristics in the reacceleration zone for different powders have a sharply rising characteristic, with an increase in air mass flow rates. The reason for this sharp rising characteristics could be that for higher conveying air mass flow rates (i.e., higher steady-state air and solids velocities), the particles would require massive amount of energy to make up for the higher differences of particle velocities between their steady-state values and that just at the exit to the bend curvature (where the particles have got slowed down due to large solids to wall friction drop along the curvature of bend). There are considerable differences between the plots of reacceleration pressure drops for different powders. Fly ash and grey cement have shown pressure drop characteristics with

the highest and lowest values, respectively. It can be seen that the rising pressure drop characteristics of the reacceleration zone dominate over the mildly drooping characteristics of the pressure drop of the curvature zones. As a result, the overall characteristics of the total bend pressure drop shows a rising characteristic with an increase in air mass flow rates. Figure 5.6 shows the experimental plots for grey cement and 53 mm pipeline internal diameter for three different radii of curvature of bends: 600, 800, and 1000 mm. Experiments were selected, having similar values of solids and flow rates and solids loading ratio for the ease of comparison. Figure 5.7 shows the estimated bend loss characteristics for a range of mass flow rates of air and 4 t/h of product flow rates (using the models provided by equations 5.2 and 5.3) for 600, 800 and 1000 mm radius of curvature of bends for grey cement and 53 mm pipeline internal diameter.

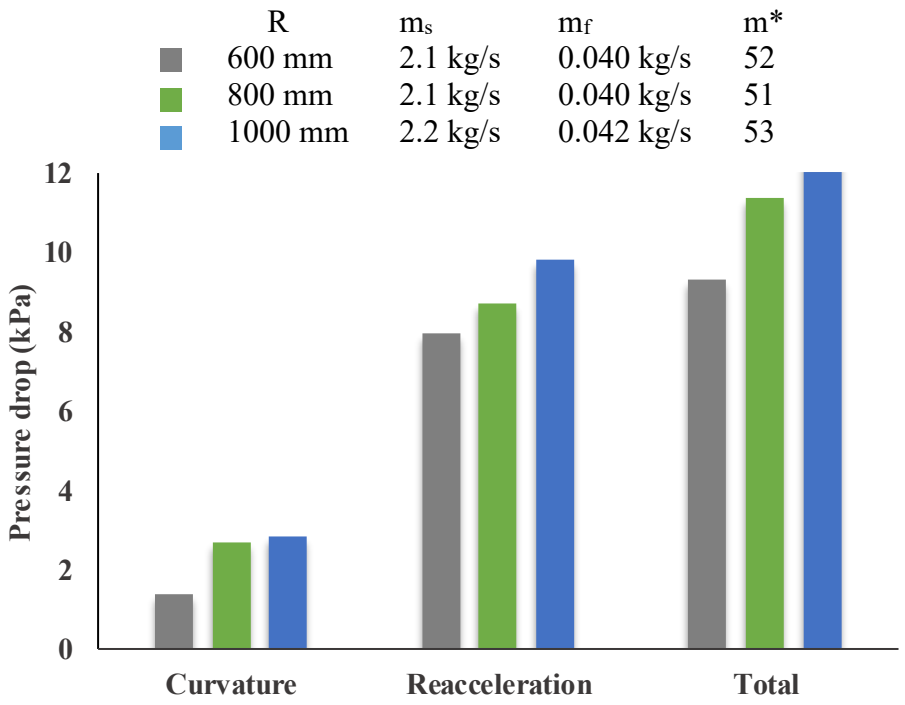

Figure 5.6: Comparison of bend pressure drops for the bend radius of curvatures of 600, 800 and mm 1000 mm for grey cement and 53 mm internal diameter of the pipeline

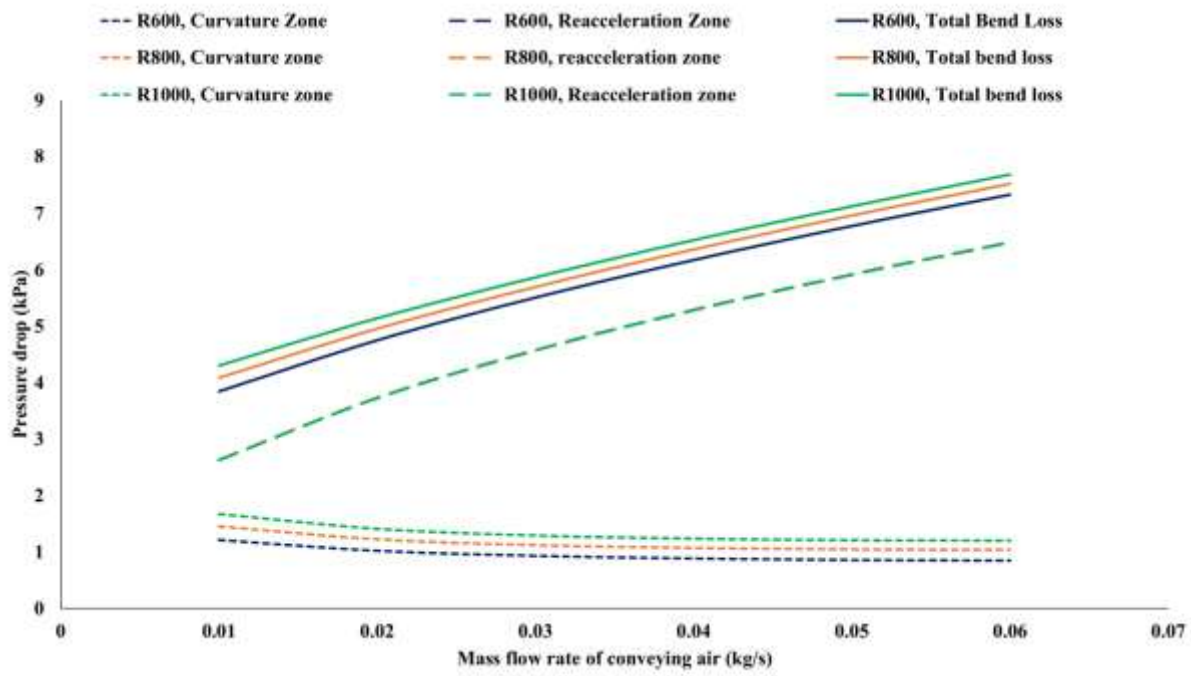

Figure 5.7: Comparison of estimated bend pressure drops for the bend radius of curvatures of 600, 800 and mm 1000 mm for grey cement and 53 mm internal diameter of pipeline and 4 t/h of product flow rate

Results (Figure 5.6) show that the losses in the reacceleration zone are about four times higher than that occurring in the curvature zone. Total bend loss is lowest for the case of a 600 mm radius of curvature of bend and highest for a 1000 mm radius of curvature of bend. This could be because with a larger radius of curvature; the particles could be travelling through a much longer arc distance in the curvature, thus resulting in a prolonged stay inside the bend and associated additional friction with the bend wall. Figure 5.7 shows that with an increase in air mass flow rates, there is a slight decrease in pressure drop characteristics in the curvature zone. Once again, the pressure drop in the curvature zone increases with an increase in the radius of curvature of bends. The pressure drop characteristics in the reacceleration zone show a sharply rising characteristic with an increase in air mass flow rates. Since the model for reacceleration pressure drop is independent of the radius of curvature of the bend, hence identical predictions have been obtained for pressure drop in the reacceleration zone for all the three combinations

of the radius of curvature of bends. Once again, rising pressure drop characteristics of the reacceleration zone dominate over the mildly drooping characteristics of the curvature zone. Due to this, the overall characteristics of the total bend pressure drop shows a rising characteristic with an increase in air mass flow rates. Figure 5.8 shows the experimental plots for grey cement and 1000 mm pipeline internal diameter for two different pipeline diameters: 53 mm and 42 mm. Once again, experiments were selected, having similar values of solids and flow rates and solids loading ratio for the ease of comparison. Figure 5.9 shows the estimated bend loss characteristics for a range of mass flow rates of air and 4 t/h of product flow rates (using the models provided by equations 5.2 and 5.3) for 53 and 42 mm pipeline internal diameters for 1000 mm radius of curvature of bends for grey cement.

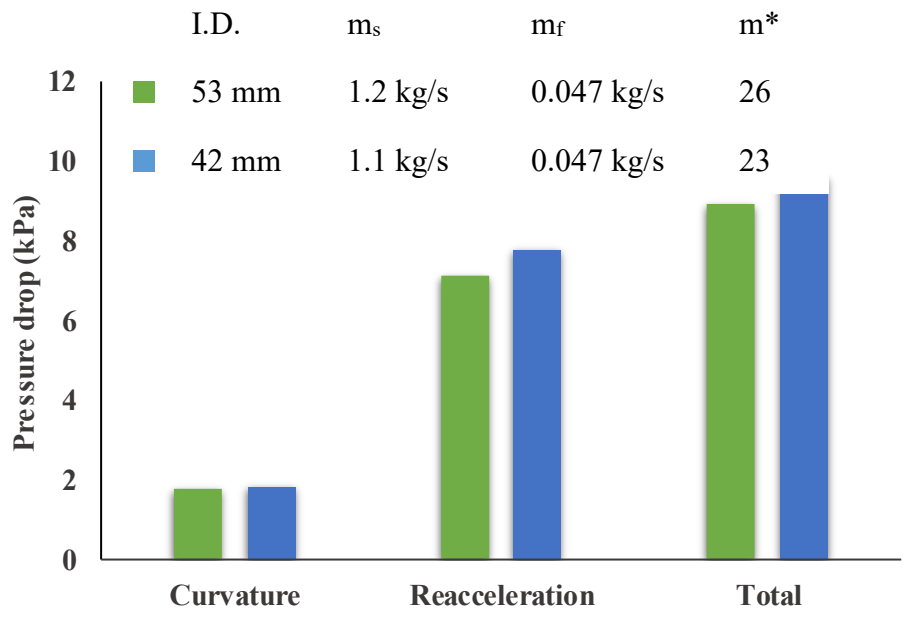

Figure 5.8: Comparison of bend pressure drops for 53 mm and 42 mm pipe internal diameters for the bend radius of curvatures of 1000 mm for grey cement

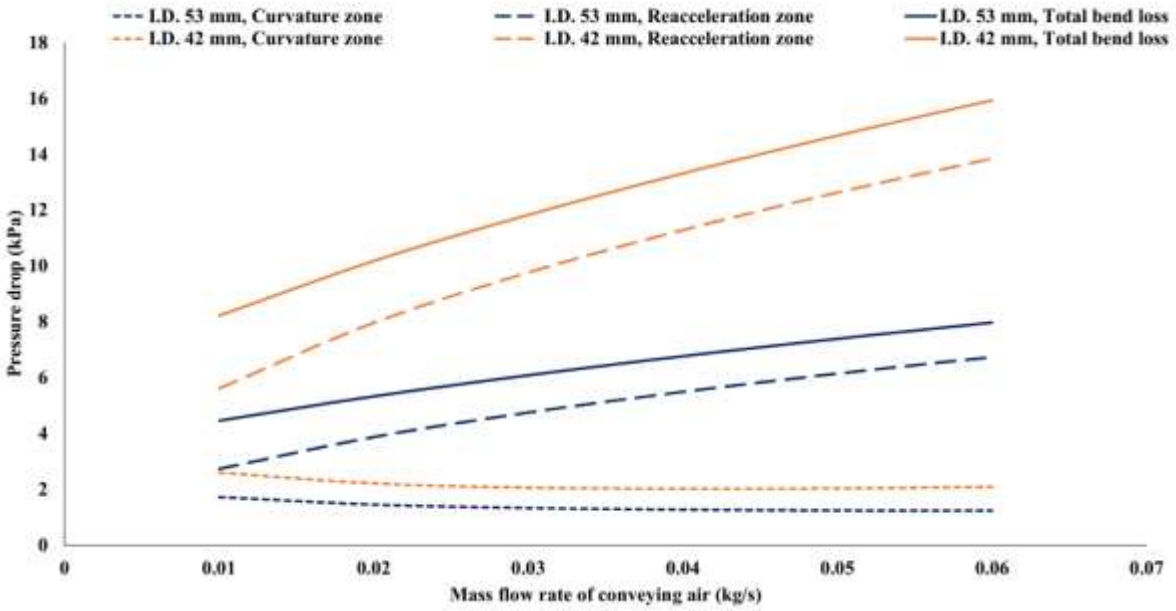

Figure 5.9: Comparison of estimated bend pressure drop for 53 mm and 42 mm pipeline internal diameters for grey cement and solids flow rate of 4 t/h for the bend radius of curvatures of 1000 mm

Results (Figure 5.8) show that the total pressure drop through the bend is more for the smaller pipeline diameter. Once again, losses in the reacceleration zone are about four times that were occurring in the curvature zone. Figure 5.9 shows that there are mildly drooping pressure drop characteristics in the curvature zone with an increase in air mass flow rate with higher pressure drop occurring for the 42 mm pipeline internal diameter compared to the 53 mm internal diameter pipeline. The pressure drop in the reacceleration zone shows a sharply rising characteristic with an increase in air mass flow rates. As a result, the overall nature of the bend loss characteristics is a rising one, with an increase in air mass flow rates. Figure 5.12 shows the estimated bend loss characteristics for a range of mass flow rates of air and 4 t/h of product flow rates (using the models provided by equations 5.2 and 5.3) for 4, 8 and 12 m/s superficial air velocity at the outlet of bend for 53 pipeline internal diameter with 1000 mm radius of curvature of bend and grey cement.

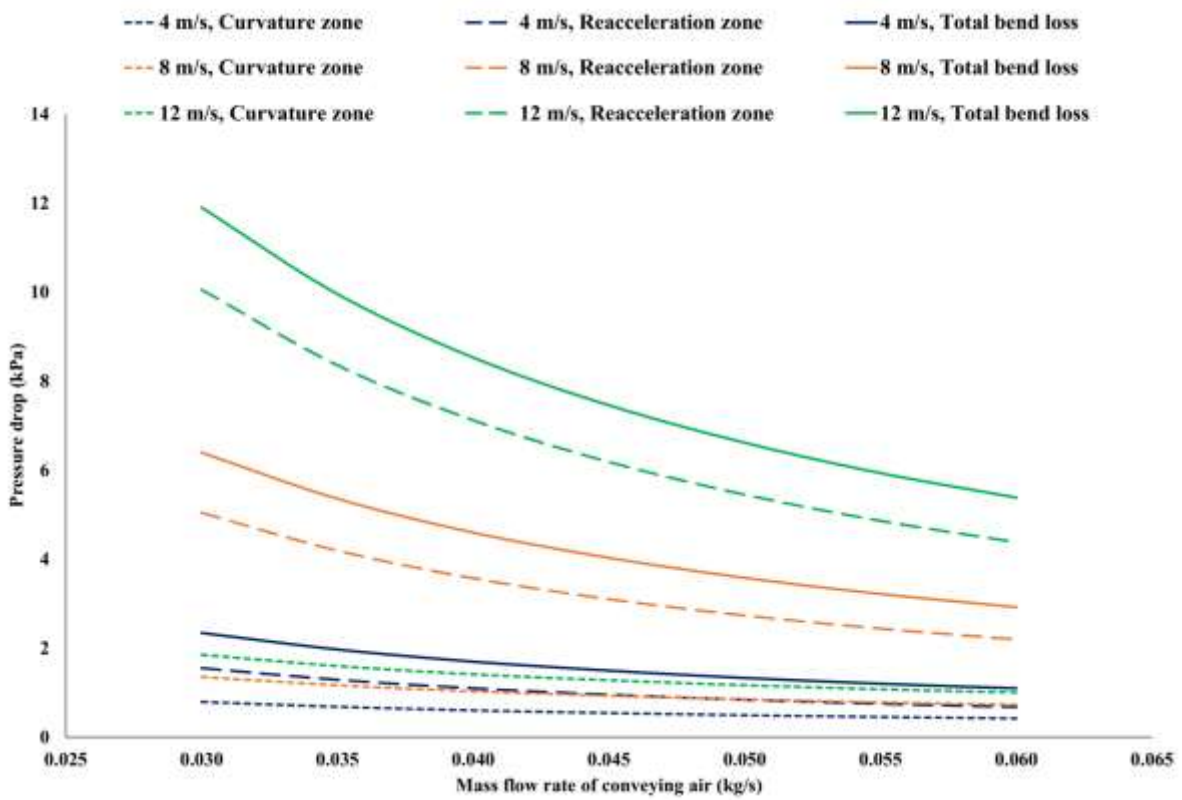

Figure 5.10: Comparison of estimated bend pressure drop for 4, 8 and 12 m/s superficial air velocity at the outlet of bend for 53 mm pipeline internal diameter with 1000 mm radius of curvature of bend and grey cement conveyed at 4 t/h

Results (Figure 5.10) show that for a specific mass flow rate of air, an increase in conveying velocity increases the total bend loss at a sharp rate. The difference between total bend loss due to the difference in conveying velocities is more in lower mass flow rates of air. With an increase in mass flow rates of air, the differences between pressure drop characteristics (for constant superficial air velocity) gradually reduces.

The models provided from equations (5.1) to (5.4) have been further validated for their utility and applicability by using them to predict the overall bend for the 105 mm I.D. × 168 m long pipeline and 69 mm I.D. × 554 m long pipeline for fly ash (based on the data of University of Wollongong, refer to section 2.4). To predict the losses occurring in the straight pipe section,

the model of Setia et al. (2016) (refer to equation 4.5) has been used. In the original work of Setia et al. (2016), the model of Chambers and Marcus (1986) was used to predict the losses in the bends. Predictions have been made for a higher and lower mass flow rates of solids.

Figures 5.11 and 5.12 show a comparison of experimental versus predicted conveying characteristics for fly ash for 105 mm I.D. × 168 m long pipeline, and 69 mm I.D. × 554 m long pipeline respectively.

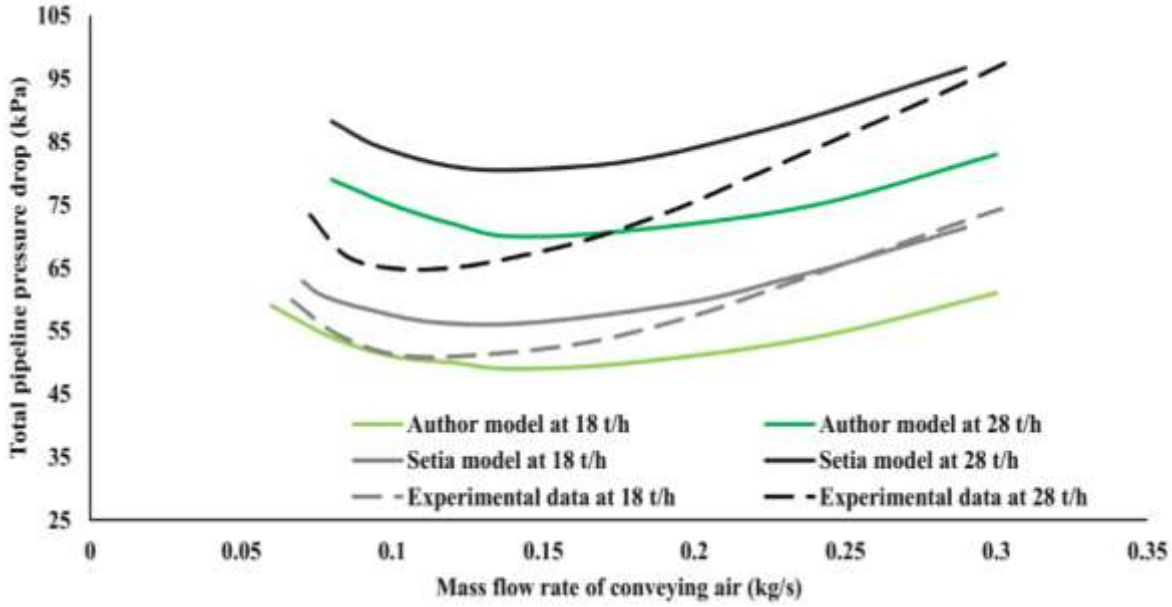

Figure 5.11: Comparison of experimental versus predicted pneumatic conveying characteristics for fly ash, 105 mm I.D. × 168 m long pipeline

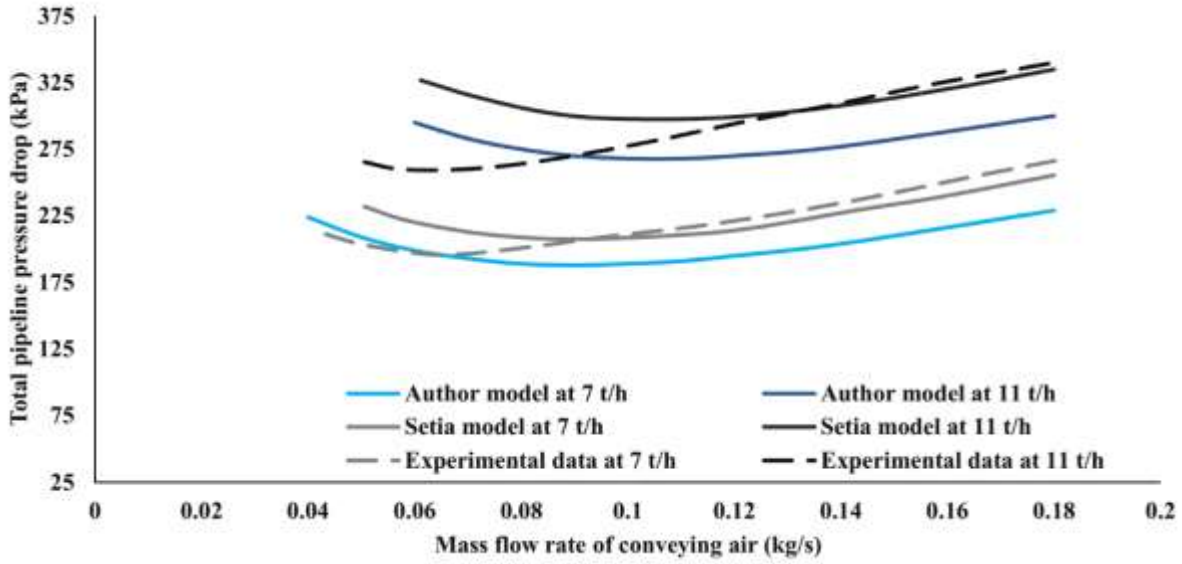

Figure 5.12: Comparison of experimental versus predicted pneumatic conveying characteristics for fly ash, 69 mm I.D. × 554 m long pipeline

Figures 5.11 and 5.12 show that use of the new bend model has resulted in more accurate predictions of total pipeline pressure drop values, i.e., the experimental and predicted pneumatic conveying characteristics obtained using the combinations of Setia et al. (2016) straight pipe model with the newly developed bend model (equations 5.1 to 5.4) are more closer to each other in the low velocity (or dense-phase) conveying regime compared to that obtained using the combination of Setia et al. (2016) straight pipe model with Chambers and Marcus (1986) bend model. While the new bend model results in much-improved predictions in dense-phase, the new model provides some under-predictions in dilute-phase. The results also show that significant improvement in total pipeline pressure drop prediction is possible by addressing bend pressure drop issues.

5.4 Development of semi-empirical bend loss model

Figure 5.13 shows the conceptual framework of the new approach to modelling bend loss. The bend curvature is between tapping point no. 2 to point no. 3 of Figure 2.1. Subsequently, the reacceleration zone extends up to tapping point 6 of Figure 2.1 (thus, the straight length between points 3 and 6 marks the reacceleration zone). The corresponding superficial air and particle velocities are V_2, C_2 at tapping point 2; V_3, C_3 at tapping point 3; and V_6, C_6 at tapping point 6. In the new approach of modelling, the total pressure drop through the bend has been divided into five components: (a) change in momentum of solids due to directional charge of solids going through the curvature zone of bend (corresponding change in velocity of solids is from C_2 to C_3); (b) change momentum of air due to directional charge of air going through the curvature zone of bend; (c) friction of solids and air (particle-particle-wall-air friction) going through the curvature zone of bend; (d) friction of solids and air (particle-particle-wall-air friction) going through the reacceleration zone (straight pipe section after the bend); (e) reacceleration of particles from C_3 to C_6 in the reacceleration zone (straight pipe section after the bend). In this study, the contributions coming from (c) and (d) have been clubbed together by adding the arc length of the curvature zone to the straight pipe length of the reacceleration zone.

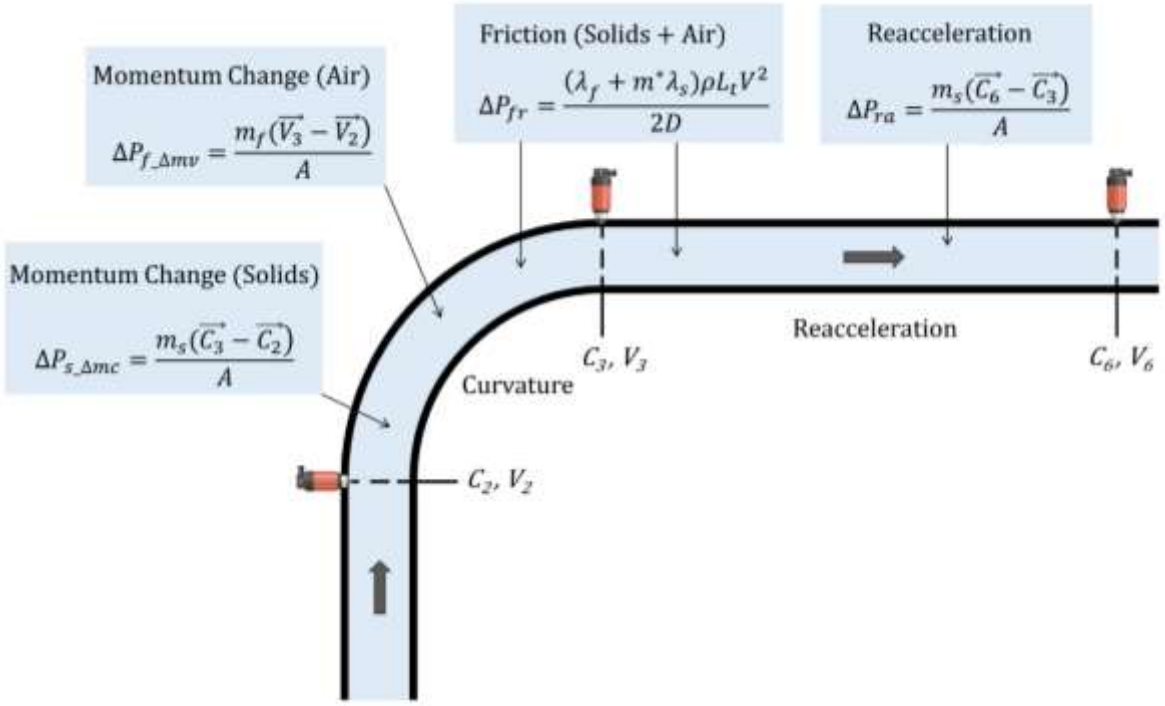

Figure 5.13: Different pressure drop components in curvature and reacceleration zone of a bend

Pressure drop due to the momentum change of solids in the curvature zone is given by equation (5.5):

$$\Delta P_{s\_\Delta mc} = \frac{m_s(\overrightarrow{C_3} - \overrightarrow{C_2})}{A} \tag{5.5}$$

Pressure drop due to momentum change of air in the curvature zone is given by equation (5.6):

$$\Delta P_{f\_\Delta mv} = \frac{m_f(\overrightarrow{V_3} - \overrightarrow{V_2})}{A} \tag{5.6}$$

Pressure drop due to air and solids friction in the curvature and reacceleration zone is given by equation (5.7):

$$\Delta P_{fr} = \frac{(\lambda_f + m^*\lambda_s)\rho L_t V^2}{2D} \tag{5.7}$$

Where, λ_s was found using straight pipe pressure drop model, as given by Weber (1981):

$$\lambda_s = 2.1 m^{*-0.3} Fr^{-2} Fr_s^{0.5} \left(\frac{D}{d_s}\right)^{0.1} \quad (5.8)$$

$$Fr = \left(\frac{V_f}{\sqrt{gD}}\right) \quad (5.9)$$

$$Fr_s = \left(\frac{w_{fo}}{\sqrt{gD}}\right) \quad (5.10)$$

λ_f was found using the Swamee and Jain (1976) model, as given by:

$$\lambda_a = \frac{1.325}{\left[ln\left(\frac{\varepsilon}{3.7D} + \frac{5.74}{Re^{0.9}}\right)\right]^2} \quad (5.11)$$

Pressure drop due to acceleration of the solids in the reacceleration zone is given as (Tripathi et al. 2018):

$$\Delta P_{ra} = \frac{m_s(\overrightarrow{C_6} - \overrightarrow{C_3})}{A} \quad (5.12)$$

In order to determine pressure drop as per equations (5.5), (5.6), and (5.12), it is essential to determine the values of particle velocity at the tapping points 2, 3, and 6 (i.e., C_2, C_3, and C_6). Majority of the attempts have been made towards the estimation of particle velocity considering the coarser particles (i.e., applicable for dilute phase mode) and very little work has been reported so far in the area of measurement of particle velocity for fine powders due to challenges, such as fine powders have high turbulent nature of flow, and it is difficult to analyse the structure (i.e., movement) of the dunes between the sensors; fine powders tend to coat the sight glass thus making it difficult to see through the glass. Table 5.3 shows the various particle velocity correlations for pneumatic conveying.

Table 5.3: Particle velocity correlations for pneumatic conveying

Author	**Empirical correlations**	**Data range**
Hinkle (1953)	$C = \mathrm{U}_a\left(1 - 0.1344{\mathrm{d}_{50}}^{0.3}{\rho_\mathrm{s}}^{0.5}\right)$	0.36 mm $< d_{50} <$ 8.38 mm 1048 kg/m^3 $< \rho_s <$ 1808 kg/m^3
Arastoopour et al. (1979)	$C = \mathrm{U}_a\left(1 - 0.044{\mathrm{d}_{50}}^{0.3}{\rho_\mathrm{s}}^{0.5}\right)$	Same as Hinkle (1953)
IGT (reported in Klinzing et al. 1987)	$C = \mathrm{U}_a\left(1 - 0.68{\mathrm{d}_{50}}^{0.92}{\rho_\mathrm{s}}^{0.5}{\rho_f}^{-0.2}\, D^{-0.54}\right)$	Not given
Klinzing et al. (1989)	$C = \left(\mathrm{U}_a - {w_{fo}}^{0.71}\right)D^{0.019}$	67 µm $< d_{50} <$ 900 µm 2395 kg/m^3 $< \rho_s <$ 5004 kg/m^3
Hong and Shen (1994)	$C = \mathrm{U}_a\left[1 - 0.533\left(\frac{1000\rho_f}{\rho_s}\right)^{1.093}\left(\frac{D}{100 d_{50}}\right)^{-0.721}\right]$	High solid-gas ratio, fine powder
Tripathi et al. (2018)	$\frac{C}{\mathrm{U}_a} = 1 - 0.072\left[Ar\left(\frac{\rho_s - \rho_f}{\rho_f}\right)\right]^{0.091}$	0.23 mm $< d_{50} <$ 4 mm 940 kg/m^3 $< \rho_s <$ 3794 kg/m^3
Santo et al. (2018)	$\frac{C}{\mathrm{U}_a} = 1 - 0.02\left[Ar\left(\frac{\rho_s - \rho_f}{\rho_f}\right)\left(\frac{D}{d_{50}}\right)^{-2}\right]^{0.14}$	0.06 mm $< d_{50} <$ 4 mm 940 kg/m^3 $< \rho_s <$ 5800 kg/m^3

Out of the several models presented in Table 5.3, the Hong and Shen (1994) model has been used in the present study to determine the particle velocities in the steady-state zones (i.e., at tapping point locations 2 and 4, ref. to Figure 2.1), i.e., where the gas velocities are presumably in the steady-state zone. This is because only the Hong and Shen (1994) model has been reported to work for fine powders and under dense-phase flow conditions. From the knowledge of C_6 values, C_3 values (particle velocity at the exit to the curvature) has been estimated using equation (5.13). Figures 5.14 to 5.20 show the particle velocity values (C_2, C_3, and C_6) for three different conditions of products, pipeline diameters, and bend radius of curvature at different tapping point locations (just before and after the bend and at the end of reacceleration zone).

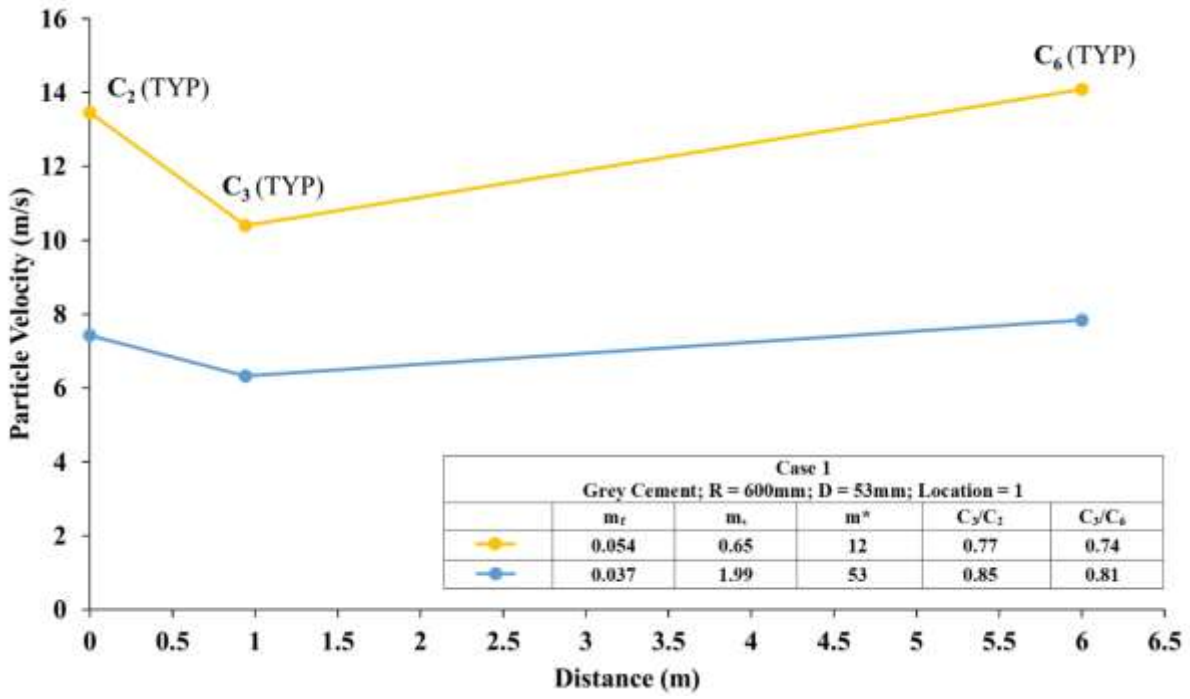

Figure 5.14: Particle velocity values at bend inlet, outlet and after reacceleration for grey cement, 600 mm radius of curvature of bends and 53 mm pipeline diameter

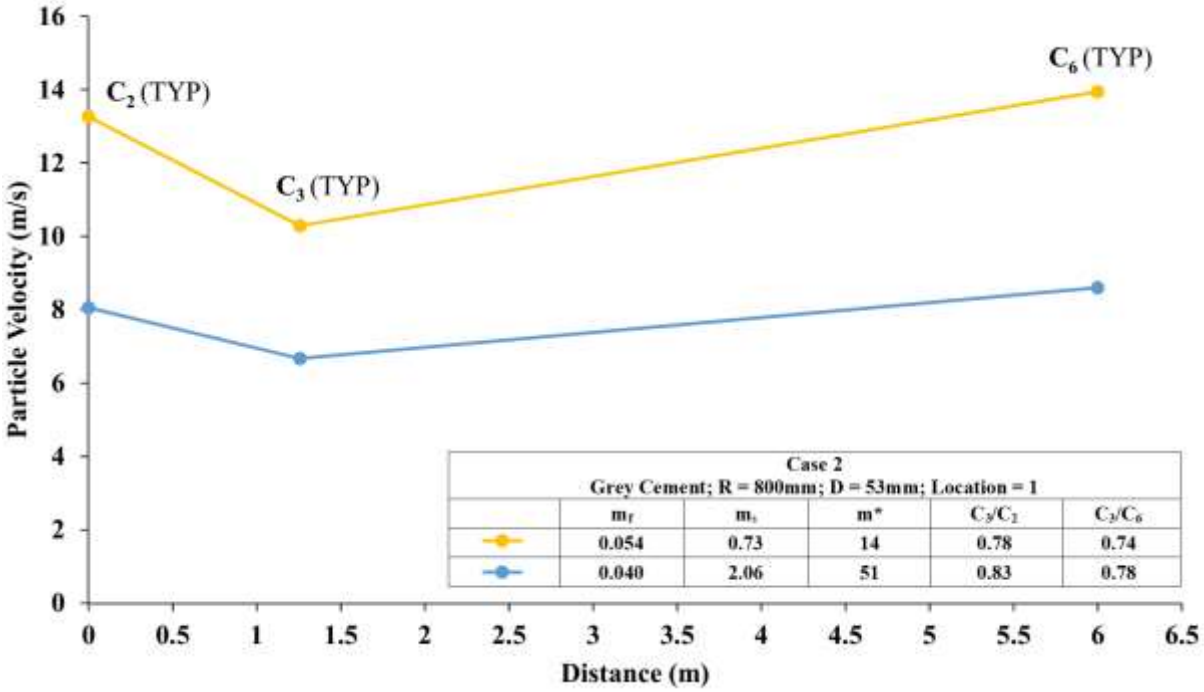

Figure 5.15: Particle velocity values at bend inlet, outlet and after reacceleration for grey cement, 800 mm radius of curvature of bends and 53 mm pipeline diameter

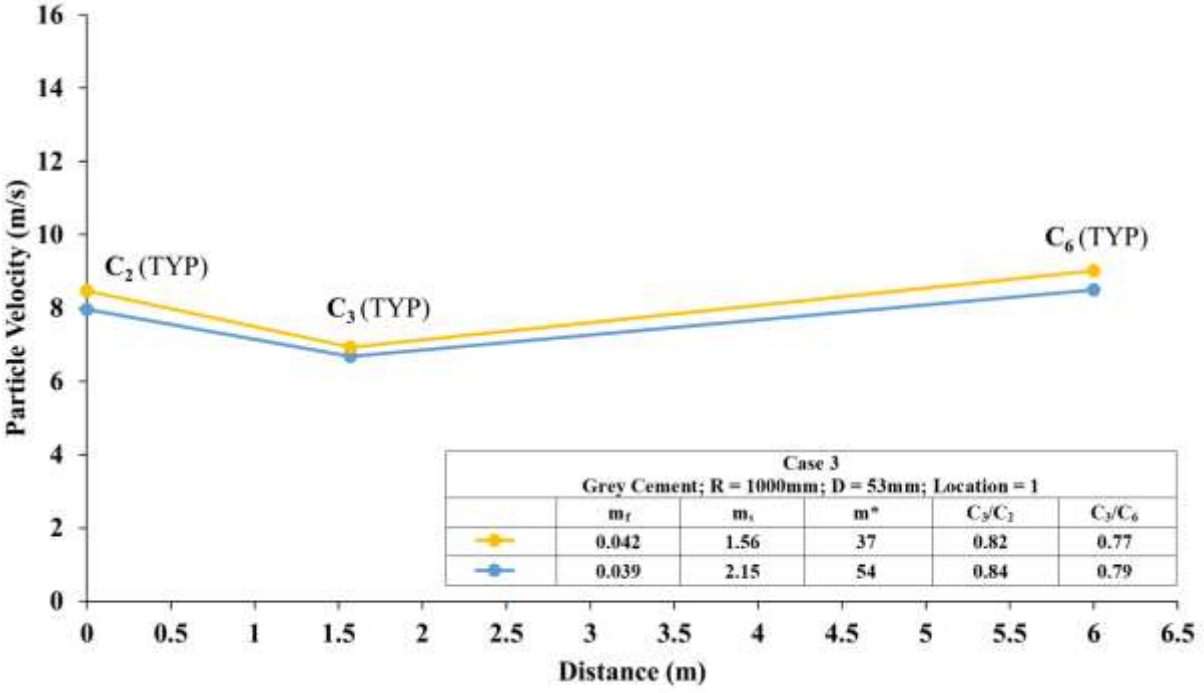

Figure 5.16: Particle velocity values at bend inlet, outlet and after reacceleration for grey cement, 1000 mm radius of curvature of bends and 53 mm pipeline diameter

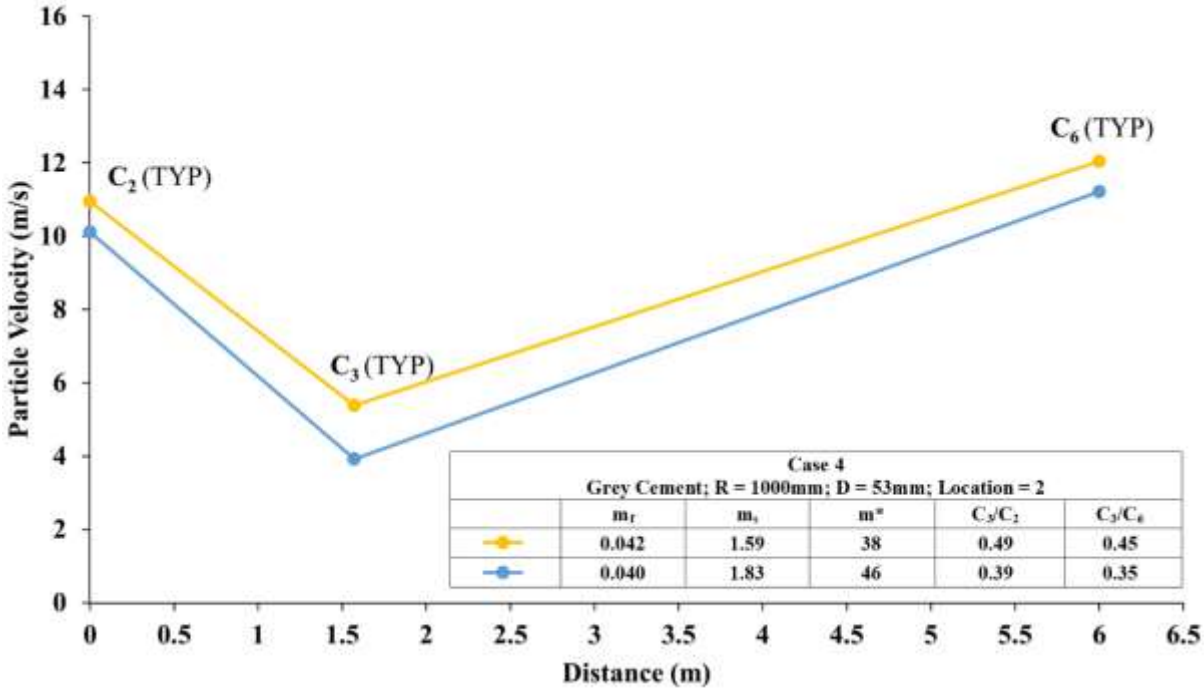

Figure 5.17: Particle velocity values at bend inlet, outlet and after reacceleration for grey cement, 1000 mm radius of curvature of bend, 53 mm pipeline diameter at location 2

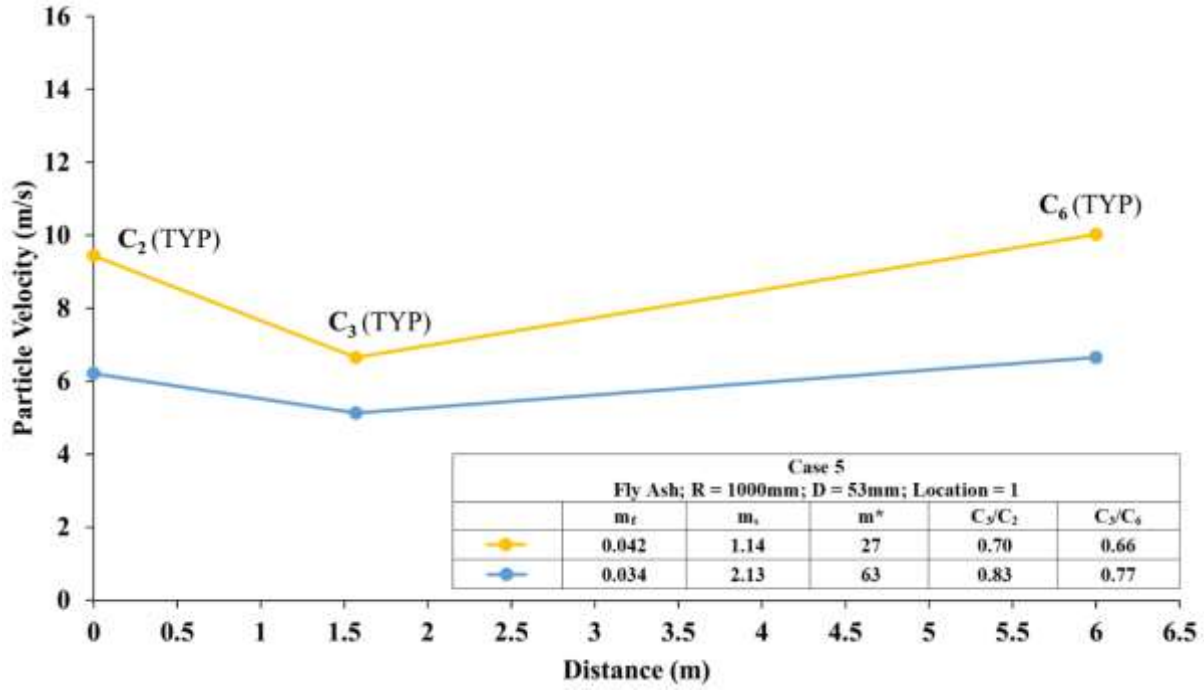

Figure 5.18: Particle velocity values at bend inlet, outlet and after reacceleration for fly ash, 1000 mm radius of curvature of bends and 53 mm pipeline diameter

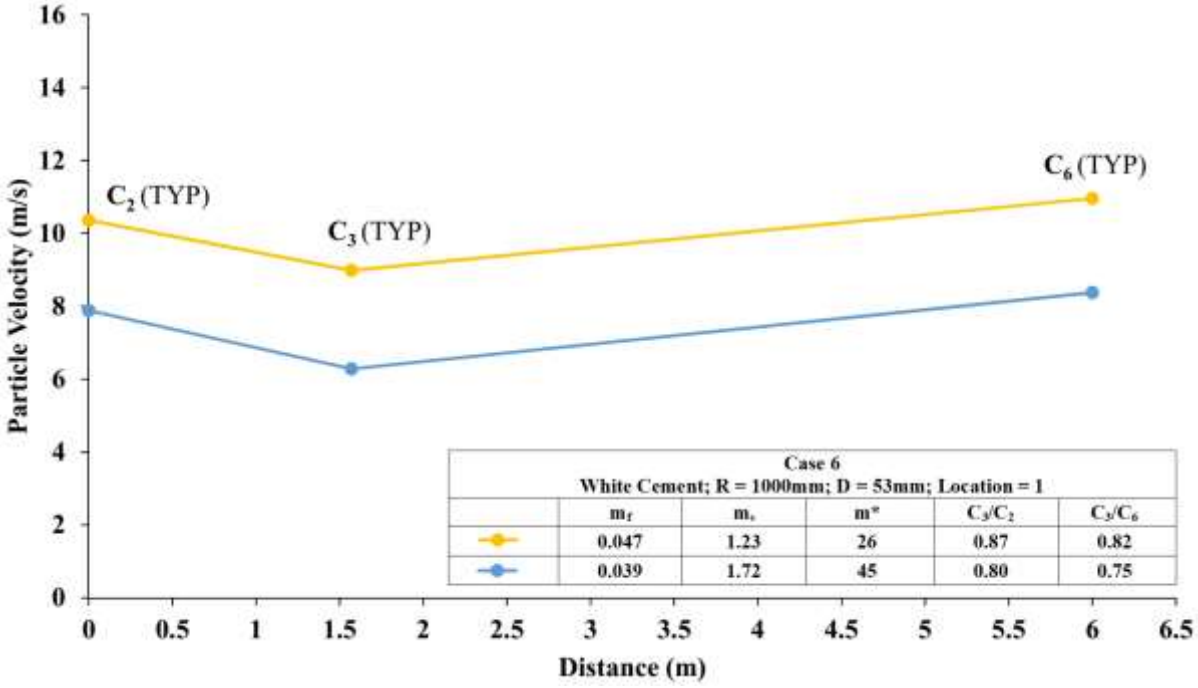

Figure 5.19: Particle velocity values at bend inlet, outlet and after reacceleration for white cement, 1000 mm radius of curvature of bends and 53 mm pipeline diameter

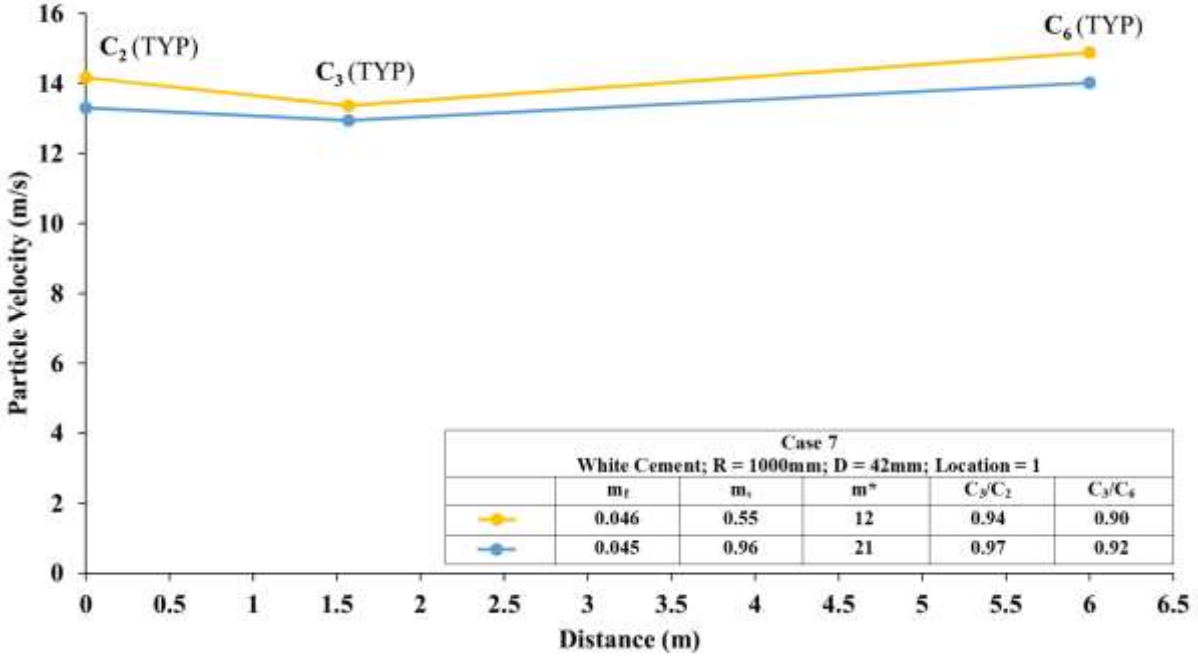

Figure 5.20: Particle velocity values at bend inlet, outlet and after reacceleration for white cement, 1000 mm radius of curvature of bends and 42 mm pipeline diameter

Figure 5.14 to 5.20 show that there is a reduction of particle velocity just at the exit to the bend. Subsequently, the particle velocity is picked up in the reacceleration zone. Experiments with lower values of solids loading ratio showed a higher amount of dip in values of particle velocities at the exit to the bend with the subsequent requirement of a higher rise of particle velocity to achieve the steady-state velocity. As the extent of this reacceleration is related to pressure drop due to reacceleration of particles, hence this category of loss would be more significant in dilute-phase conveying compared to dense-phase transport. Table 5.4 lists the different values of the ratio of particle velocities around the bends.

Table 5.4: Ratio of particle velocities around the bends

Case	**Description**	**m***	**C_3/C_2**	**C_2/C_6**
1	Grey Cement R_b = 600 mm D = 53 mm Location = 1	12	0.77	0.74
		18	0.77	0.73
		44	0.59	0.55
		53	0.85	0.81
2	Grey Cement R_b = 800 mm D = 53 mm Location = 1	14	0.78	0.74
		19	0.84	0.80
		44	0.76	0.71
		51	0.83	0.78
3	Grey Cement R_b = 1000 mm D = 53 mm	37	0.82	0.77
		42	0.70	0.65
		49	0.82	0.77

	Location = 1	54	0.84	0.79
4	Grey Cement R_b = 1000 mm D = 53 mm Location = 2	38	0.49	0.45
		44	0.49	0.44
		49	0.73	0.67
		53	0.65	0.60
5	Fly Ash R_b = 1000 mm D = 53 mm Location = 1	16	0.47	0.45
		18	0.50	0.48
		55	0.94	0.89
		64	0.89	0.84
6	White Cement R_b = 1000 mm D = 53 mm Location = 1	26	0.87	0.82
		32	0.92	0.87
		44	1.03	0.98
		51	0.90	0.85
7	White Cement R_b = 1000 mm D = 42 mm Location = 1	14	0.86	0.81
		15	0.87	0.83
		19	0.97	0.92
		22	0.97	0.91

Based on the data of 209 experiments, the average values of C_3/C_2 and C_3/C_6 are 0.774 and 0.737, respectively. The respective values of standard deviations were found to be 0.157 and

0.153, respectively. Combining all the five different components of pressure drop, the consolidated model for bend loss is represented as:

$$\Delta p_b = k_1(\Delta p_{s\_\Delta mc} + \Delta p_{f\_\Delta mv}) + k_2(\Delta p_{fr}) + k_3(\Delta p_{ra}) \quad (5.13)$$

Where k_1, k_2, and k_3 are empirical constants. These constants have been introduced considering the highly complex nature of the flow, where not all particles would flow with the same particle velocity. Using a method of minimising the sum of the square of differences between experimental and predicted pressure drop values for 209 experiments, the values of k_1, k_2, and k_3 have been obtained as k_1 = 0.04, k_2 = 0.495 and k_3 = 2.623. Based on the data of 209 experiments, the average absolute error between model predictions and experimental results is 27%. In order to validate the new model for the high solids flow rate, the new model was validated for different experimental conditions for fly ash (Table 5.5 and Table 5.6) and in the new pilot plant (Figure 2.7). The results of the validation are provided in Figure 5.21 and Figure 5.22. A comparison of the experimental data and predicted results (Figure 5.21 and Figure 5.22) shows that the new model could improve prediction accuracy with the relative error percentage mostly less than 12.2% for high m* range and 19.6% for low m* range, which has been considered to be acceptable.

Table 5.5: Experimental conditions for fly ash in 105 mm I.D. × 128 m long pipeline for high solids loading ratio

Sl. No.	m_f (kg/s)	m_s (kg/s)	m*
1	0.120	6.2	51
2	0.118	9.7	82
3	0.112	9.8	88
4	0.110	10.9	99
5	0.099	12.0	121
6	0.091	15.4	170

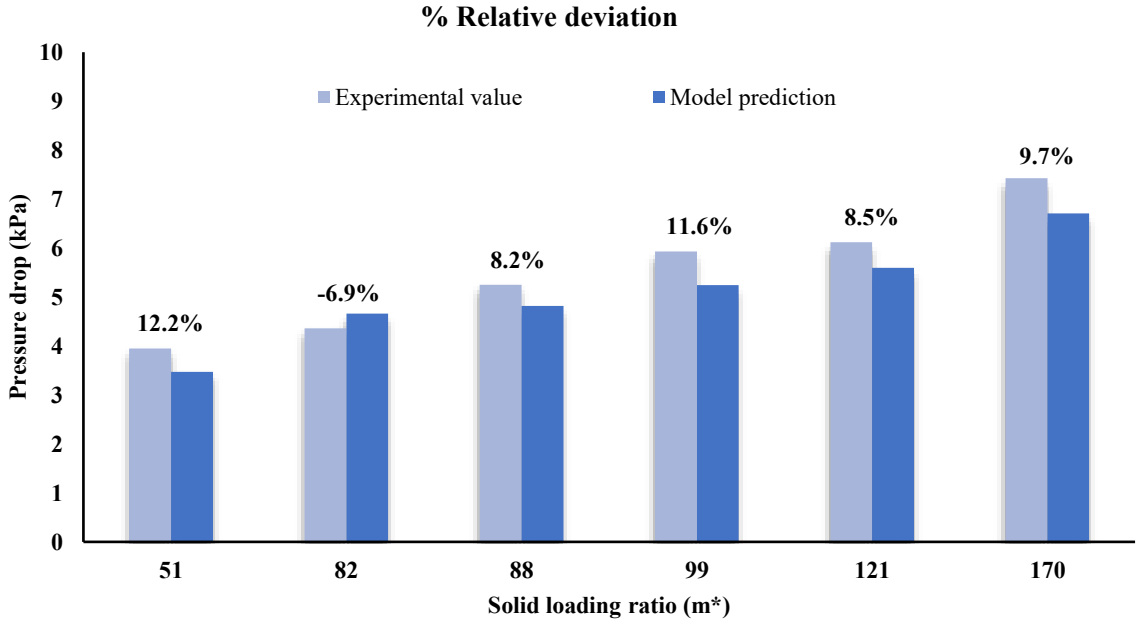

Figure 5.21: Model prediction using new bend loss model versus experimental bend pressure drop for high solids loading ratio

Table 5.6: Experimental conditions for fly ash in 105 mm I.D. × 128 m long pipeline for low solids loading ratio

Sl. No.	m_f (kg/s)	m_s (kg/s)	m*
1	0.147	3.3	22
2	0.141	3.4	24
3	0.135	3.7	27
4	0.123	3.5	28
5	0.138	4	29

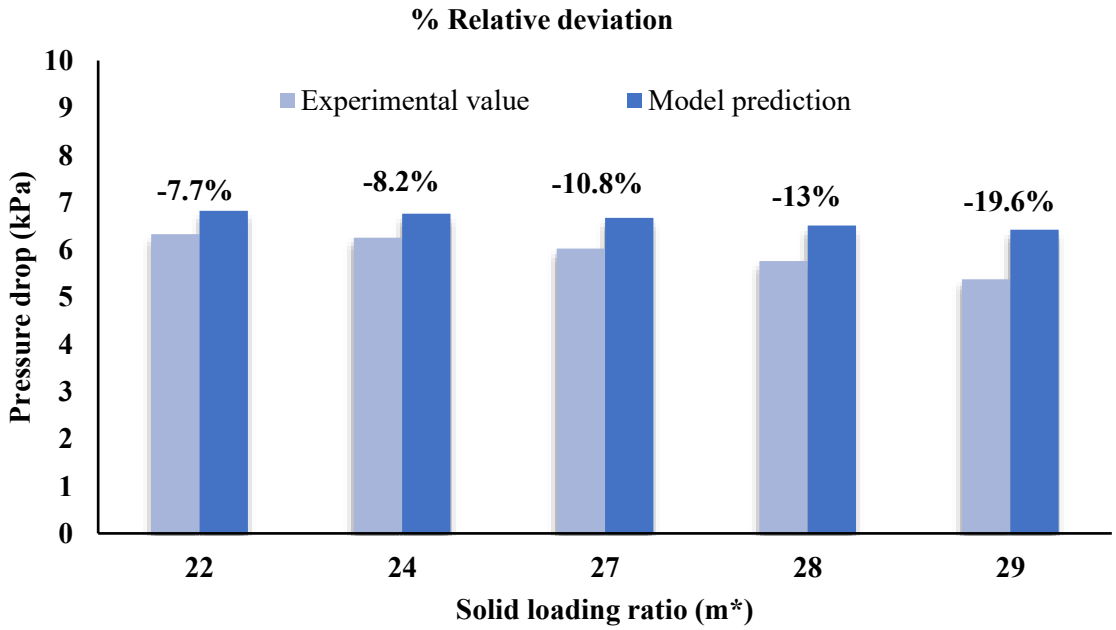

Figure 5.22: Model prediction using new bend loss model versus experimental bend pressure drop for low solids loading ratio

CHAPTER 6

CONCLUSION AND FUTURE SCOPE OF WORK

6.1 Conclusion

The estimation of bend pressure drop can have a considerable impact on correctly predicting the total pressure loss in a pneumatic conveying system. The predicted pneumatic conveying characteristics obtained using different bend loss models are found to be significantly different, in terms of both predicted values and overall trends, thus signifying the requirement of correctly selecting an appropriate bend model towards reliably predicting total pipeline pressure drop. In this thesis, the effects of different powders, the radius of curvatures of bend, pipeline diameters, and conveying velocities on the pressure drop through bends have been studied. Specific conclusions from this study include:

- It is concluded that the losses in the reacceleration zone are typically 4 to 8 times larger than that occurs in the curvature zone. The pressure drop characteristics in the curvature zone show a slightly drooping characteristic with an increase in airflow rates. However, pressure drop characteristics rise rather sharply in the reacceleration zone and as a result, the overall plot of bend pressure loss with respect to an increase in air mass flow rate is a rising one.
- Based on the products tested, the product with the largest particle size provided the highest pressure drop compared to the other products. With an increase in the radius of curvature of bends, the bend pressure drop values were found to have increased. Bend pressure drop was found to sharply increase with an increase in conveying air velocity at the outlet of bend and with a decrease in pipeline diameter.
- It has been found that the average ratio of particle velocities between that just before the curvature zone and to that just at the outlet curvature zone is 0.77 and the average ratio of particle velocities between that just at the outlet of the curvature zone and to that at the end of the reacceleration zone is 0.73.

- A new semi-fundamental model has been developed by considering the different components of the total pressure drop due to the bend, such as due to change in momentum of solids and air through the curvature zone, frictional pressure drop due to solids and air flows through the curvature zone and straight section of pipe (reacceleration zone) after the curvature zone and reacceleration of slow-moving particles at the end of curvature zone to their steady-state velocities. This model has been used to predict bend loss for solids loading ratio of in the range of 51 to 170 (very dense-phase) and 22 to 29 (dilute phase). The new model provided better predictions with the relative errors percentage mostly less than 12.2% for dense phase and mostly less than 19.6% for the dilute phase.
- Models provided in Chapter 4 are more suitable for designing a system where the contribution of bend losses is not significant (e.g. long distance and/or dense-phase conveying) as these models are simpler (but somewhat conservative). For cases where there are too many bends in pipeline (especially for a short distance conveying) and/or dilute-phase conveying, where accuracy of prediction of bend loss is of significant importance, model provided in Chapter 5 should be used (as this model is more accurate, although the calculation process is somewhat tedious). The novelty of the model provided in Chapter 5 is that it considers/models different components of the losses separately, which seems to better address the actual flow mechanism.

6.2 Future scope

Even though the models proposed under the present study have shown improved prediction results, there are still many aspects of the bend pressure loss that have not been fully addressed. There are some areas where further research can improve the understanding of the complex

nature of gas solids flow of fine powders through bends. A few suggestions for further studies follow:

- The bends considered in this study were placed in the horizontal-horizontal orientation. The industry also uses horizontal-vertical and vertical-horizontal bends in the pneumatic conveying loops. Therefore, more research is required to study the effect of bend orientations.

- More fine powders having different physical properties should be tested to obtain the improved exponents for the solid friction factor. An investigation on the use of particle size distribution data instead of d_{50} in the pressure drop model can also be carried out to improve the model accuracy.

- The biggest pipeline diameter used to develop the models was 53 mm. However, the diameter of 150-300 mm is commonly used for pneumatic transport in a variety of industries/plants. Therefore, further study should be carried out to investigate the scale-up validation of the models on a plant scale.

- In the present study, an existing particle velocity model has been used in the bend model to predict the pressure loss. It is expected that the use of actual (measured) particle velocity data will improve the prediction accuracy of the bend model. Therefore, more research is required to investigate the accuracy of the model prediction by incorporating actual particle velocity data.

- It is suggested that further studies should be made for the applicability of numerical based fundamental models to simulate gas-solids flow through the bends.

REFERENCES

Akilli, H., Levy, E. K., & Sahin, B. (2001). Gas-solid flow behavior in a horizontal pipe after a 90° vertical-to-horizontal elbow. *Powder Technology*, *116*(1), 43–52. https://doi.org/10.1016/S0032-5910(00)00360-0

Arastoopour, H., Modi, M. V, Punwani, D. V, & Talwalkar, A. T. (1979). *Review of design equations for dilute phase gas-solids horizontal conveying systems for coal and related materials*. Institute of Gas Technology, Chicago, IL, Chicago, IL.

Bansal, A. (2012). *Investigation into Straight Pipe Pressure Drop and Flow-Mode Transition Criteria for Fludised Dense-Phase Pneumatic Conveying Systems*.

Barth, W. (1954). Strömungstechnische Probleme der Verfahrenstechnik. *Chemie Ingenieur Technik*, *26*(1), 29–34.

Bilirgen, H., & Levy, E. K. (2001). Mixing and dispersion of particle ropes in lean phase pneumatic conveying. *Powder Technology*, *119*(2–3), 134–152. https://doi.org/10.1016/S0032-5910(00)00413-7

Bradley, M. S A, Farnish, R. J., Hyder, L. M., & Reed, A. R. (2001). A novel analytical model for the acceleration of particles following bends in pneumatic conveying systems. In *Handbook of Powder Technology* (Vol. 10). https://doi.org/10.1016/S0167-3785(01)80043-9

Bradley, M S A, Hyder, L. M., Famish, R. J., & Reed, A. R. (2001). Latest development of the direct technique for measurement of the pneumatic conveying characteristics of bulk materials. In *Handbook of Powder Technology* (Vol. 10, pp. 319–328). Elsevier.

Bradley, Michael S A. (1990). *Prediction of pressure losses in pneumatic conveying pipelines*.

Thames Polytechnic.

Cai, L., Liu, S., Pan, X., Guiling, X., Gaoyang, Y., Xiaoping, C., & Changsui, Z. (2014). Comparison of pressure drops through different bends in dense-phase pneumatic conveying system at high pressure. *Experimental Thermal and Fluid Science*, *57*, 11–19. https://doi.org/10.1016/j.expthermflusci.2014.03.016

Chambers, A. J., & Marcus, R. D. (1986). Pneumatic conveying calculations. *Second International Conference on Bulk Materials Storage, Handling and Transportation: 1986; Preprints of Papers*, 49. Institution of Engineers, Australia.

Das, B., & Datta, A. (2016). Modeling of hydrodynamics in a bubbling fluidized-bed gasifier and evaluation of the inter-phase gas exchange rate under different operating conditions. *Particuology*, *25*, 151–158. https://doi.org/10.1016/j.partic.2015.05.009

Dhodapkar, S., Solt, P., & Klinzing, G. (2009). Understanding bends in pneumatic conveying systems. *Chemical Engineering*, *116*(4), 46–52.

Ebrahimi, M., Crapper, M., & Ooi, J. Y. (2014). Experimental and simulation studies of dilute horizontal pneumatic conveying. *Particulate Science and Technology*, *32*(2), 206–213. https://doi.org/10.1080/02726351.2013.851133

Frye, L., & Peukert, W. (2004). Transfer of fracture mechanical concepts to bulk solids attrition in pneumatic conveying. *International Journal of Mineral Processing*, *74*(SUPPL.). https://doi.org/10.1016/j.minpro.2004.08.001

Gibilaro, L. G., Gallucci, K., Di Felice, R., Pagliai, P., Felice, R. Di, & Pagliai, P. (2007). On the apparent viscosity of a fluidized bed. *Chemical Engineering Science*, *62*(1–2), 294–

300. https://doi.org/10.1016/j.ces.2006.08.030

Guan, Q., Liu, Z., Fang, X., Liu, B., Peng, B., Feng, Z., … Li, W. (2017). Experimental study on dense-phase pneumatic conveying of coal powder at high pressures. *Clean Energy*, *1*(1), 50–67. https://doi.org/10.1093/ce/zkx007

Hall, S. (2012). *Rules of Thumb for Chemical Engineers* (5th ed.). https://doi.org/10.1016/C2010-0-65782-8

Hastie, D. B., Pan, R., Wypych, P. W., & Guiney, P. R. (2001). Handbook of Conveying and Handling of Particulate Solids. *Handbook of Powder Technology*, *10*, 379–386. https://doi.org/10.1016/S0167-3785(01)80039-7

He, C., Chen, X., Wang, J., Ni, H., Xu, Y., Zhou, H., … Xianglin, S. (2012). Conveying characteristics and resistance characteristics in dense phase pneumatic conveying of rice husk and blendings of rice husk and coal at high pressure. *Powder Technology*, *227*, 51–60. https://doi.org/10.1016/j.powtec.2012.02.014

Hettiaratchi, K., Woodhead, S. R., & Reed, A. R. (1998). Comparison between pressure drop in horizontal and vertical pneumatic conveying pipelines. *Powder Technology*, *95*(1), 67–73. https://doi.org/10.1016/S0032-5910(97)03318-4

Hinkle, B. L. (1953). *Acceleration of particles and pressure drops encountered in horizontal pneumatic conveying*. Georgia Institute of Technology.

Hong, J., & Shen, Y. S. (1994). Flow characteristics of high density continuous conveying of solids. *Engineering Chemistry and Metallurgy*, *15*, 122–128.

Hyder, L. M., Bradley, M. S. A., Reed, A. R., & Hettiaratchi, K. (2000). An investigation into the effect of particle size on straight-pipe pressure gradients in lean-phase conveying. *Powder Technology*, *112*(3), 235–243.

Itō, H. (1960). Pressure Losses in Smooth Pipe Bends. *Journal of Basic Engineering*, *82*(1), 131. https://doi.org/10.1115/1.3662501

Klinzing, George E., Farid Rizk, R. Marcus, and L. S. L. (2010). *Pneumatic conveying of solids: a theoretical and practical approach* (3rd ed.). New York: Springer.

Klinzing, G. E., Myler, C. A., Zaltash, A., & Dhodapkar, S. (1989). A simplified correlation for solids friction factor in horizontal conveying systems based on Yang's unified theory. *Powder Technology*, *58*(3), 187–193.

Klinzing, G. E., Rohatgi, N. D., Zaltash, A., & Myler, C. A. (1987). Pneumatic transport—a review (generalized phase diagram approach to pneumatic transport). *Powder Technology*, *51*(2), 135–149.

Kumar, A. S., & Shankar, V. (2005). Instability of high-frequency modes in viscoelastic plane Couette flow past a deformable wall at low and finite Reynolds number. *Journal of Non-Newtonian Fluid Mechanics*, *125*(2–3), 121–141. https://doi.org/10.1016/j.jnnfm.2004.09.010

Kumaran, V. (2008). Dense granular flow down an inclined plane: From kinetic theory to granular dynamics. *Journal of Fluid Mechanics*, *599*, 121–168. https://doi.org/10.1017/S002211200700002X

Laín, S., & Sommerfeld, M. (2013). Characterisation of pneumatic conveying systems using

the Euler/Lagrange approach. *Powder Technology*, *235*, 764–782. https://doi.org/10.1016/j.powtec.2012.11.029

Maiti, R., Das, G., & Das, P. K. (2016). Experiments on eccentric granular discharge from a quasi-two-dimensional silo. *Powder Technology*, *301*, 1054–1066.

Mallick, S. S. (2009). *Modelling of fluidised dense-phase pneumatic conveying of powders*. University of Wollongong.

Mallick, S. S., & Wypych, P. W. (2009). Minimum transport boundaries for pneumatic conveying of powders. *Powder Technology*, *194*(3), 181–186. https://doi.org/10.1016/j.powtec.2009.04.003

Maynard, E. (2006). Designing pneumatic conveying systems. *Chemical Engineering Progress*, *102*(5), 23–33.

Meloy, J. R., & Hoff, A. S. (2002). *Effect of Close-Coupled Bends in Pneumatic Conveying*. 253–266. https://doi.org/10.1080/02726350290058119

Molerus, O. (1996). Overview: Pneumatic transport of solids. *Powder Technology*, *88*, 309–321.

Pan, R. (1999). Material properties and flow modes in pneumatic conveying. *Powder Technology*, *104*(2), 157–163. https://doi.org/10.1016/S0032-5910(99)00044-3

Pan, R., & Wypych, P. W. (1997). Pressure drop and slug velocity in low-velocity pneumatic conveying of bulk solids. *Powder Technology*, *94*(2), 123–132. https://doi.org/10.1016/S0032-5910(97)03290-7

Pan, R, & Wypych, P. W. (1998). Dilute and dense phase pneumatic conveying of fly ash. *Proceedings of the 6th International Conference on Bulk Materials Storage and Transportation, Wollongong, NSW, Australia*, 183–189.

Pan, Renhu. (1992). *Improving scale-up procedures for the design of pneumatic conveying systems*.

Reddy, K. A., & Kumaran, V. (2007). Applicability of constitutive relations from kinetic theory for dense granular flows. *Physical Review E - Statistical, Nonlinear, and Soft Matter Physics*, *76*(6), 1–9. https://doi.org/10.1103/PhysRevE.76.061305

Rossetti, S. J. (1983). Concepts and criteria for gas-solids flow. In *Handbook of fluids in motion*. Boston: Ann Arbor Science Publishers.

Santo, N., Portnikov, D., Eshel, I., Taranto, R., & Kalman, H. (2018). Experimental study on particle steady state velocity distribution in horizontal dilute phase pneumatic conveying. *Chemical Engineering Science*, *187*, 354–366.

Schuchart, P. (1968). Widerstandsgesetze beim pneumatischen Transport in Rohrkrümmern. *Chemie Ingenieur Technik*, *40*(21-22), 1060–1067.

Setia, G., Mallick, S. S., Pan, R., & Wypych, P. W. (2016). Modeling solids friction factor for fluidized dense-phase pneumatic transport of powders using two layer flow theory. *Powder Technology*, *294*, 80–92. https://doi.org/10.1016/j.powtec.2016.02.006

Setia, G, Mallick, S. S., Pan, R., & Wypych, P. W. (2017). An experimental investigation into modeling solids friction for fluidized dense-phase pneumatic transport of powders. *Particuology*, *30*, 83–91.

Setia, Gautam. (2016). *Improving Scale-Up Procedures for Solids Friction and Minimum Transport Boundary for Fluidized Dense-Phase Pneumatic Conveying Systems*.

Shankar, V. (2004). Stability of two-layer viscoelastic plane Couette flow past a deformable solid layer. *Journal of Non-Newtonian Fluid Mechanics*, *117*(2–3), 163–182. https://doi.org/10.1016/j.jnnfm.2004.01.009

Singh, B., & Wolfe, R. R. (1972). Pressure losses due to bends in pneumatic forage handling. *Transactions of the ASAE*, *15*(2), 246–248.

Swamee, P. K., & Jain, A. K. (1976). Explicit Equations for Pipe Flow Problems. *ASCE J Hydraul Div*, *102*(5), 657–664.

Tripathi, N. M., Levy, A., & Kalman, H. (2018). Acceleration pressure drop analysis in horizontal dilute phase pneumatic conveying system. *Powder Technology*, *327*, 43–56. https://doi.org/10.1016/j.powtec.2017.12.045

Tripathi, N., Sharma, A., Mallick, S. S., & Wypych, P. W. (2015). Energy loss at bends in the pneumatic conveying of fly ash. *Particuology*, *21*, 65–73. https://doi.org/10.1016/j.partic.2014.09.003

Vásquez, N., Jacob, K., Cocco, R., Dhodapkar, S., & Klinzing, G. E. (2008). Visual analysis of particle bouncing and its effect on pressure drop in dilute phase pneumatic conveying. *Powder Technology*, *179*(3), 170–175. https://doi.org/10.1016/j.powtec.2007.06.015

Venkatasubramanian, S., Tashiro, H., Klinzing, G. E., & Mykelbust, K. (2000). Solids flow behavior in bends: Assessing fine solids buildup. *Powder Technology*, *113*(1–2), 124–131. https://doi.org/10.1016/S0032-5910(00)00217-5

Weber, M. (1981). Principles of hydraulic and pneumatic conveying in pipes. *Bulk Solids Handling*, *1*(1), 57–63.

Westman, M. A., Michaelides, E. E., & Thomson, F. M. (1987). Pressure losses due to bends in pneumatic conveying. *Journal of Pipelines*, *7*(1), 15–20.

Wypych, P. W. (1999). Pneumatic conveying of powders over long distances and at large capacities. *Powder Technology*, *104*(3), 278–286. https://doi.org/10.1016/S0032-5910(99)00105-9

Yan, Y., Byrne, B., & Coulthard, J. (1994). Radiometric determination of dilute inhomogeneous solids loading in pneumatic conveying systems. *Measurement Science and Technology*, *5*(2), 110–119. https://doi.org/10.1088/0957-0233/5/2/006

LIST OF PUBLICATIONS DURING COURSE OF PhD

Referred SCI journal papers published – 2Nos.

Sr. No.	Title of paper	Authors' Names	Journal	Volume, Year, Page no.	Impact factor
1.	Modelling pressure drop in bends for pneumatic conveying of fine powders	**Atul Sharma,** S.S. Mallick,	**Powder Technology** (Elsevier)	356, 2019, 273-283	4.142
2.	An investigation into pressure drop through bends in pneumatic conveying systems	**Atul Sharma,** S.S. Mallick,	**Particulate Science and Technology** (Taylor & Francis)	Online 19 Dec 2019	1.619